All-Fiber Acousto-Optical Tunable Filtering Technology for Optical Communication

Li Hao

School of Electrical & Electronic Engineering

A thesis submitted to the Nanyang Technological University
in fulfillment of the requirement for the degree of
Doctor of Philosophy

2006

To my parents, my siblings and my friends
for their encouragement and love.

Acknowledgements

I would like to show the deepest gratitude to my supervisor, Associated Professor Wen Changyun, who has given me invaluable supervision, motivation and advice.

Specially, I would like to express my deepest gratitude to my co-supervisor, Doctor Zhang Ying for his patient, assiduous and heuristic instruction, continuous encouragement and invaluable advice throughout this project. Without his patient guidance, I would not be able to complete my work.

I would specially thanks to Professor Soh Yeng Chai for his kindly advice and help during the course of this project.

Special thanks are dedicated to Mr.Kok Shaw Wei, Mr.Wang Qijie and all other members of the optical measurement group in Singapore Institute of Manufacturing and Technology for the technical help and support rendered in the course of the project.

Table of Contents

List of Figures

List of Tables

Summary

All-optical tunable filter has attracted more and more attentions in the field of optical communication recently. The interests arose from the all-optical feature of the next generation optical networks. In such optical networks, all dynamic processes such as signal modulation, switching and routing will be implemented in all-optical manners to avoid the electro-optical bottleneck and in turn the fiber bandwidth is more sufficiently utilized. To support the dynamic processes in all-optical domain, optical tunable filter plays a key role and it has become one of the enabling technologies for the future dynamic all-optical networks. Therefore, various all-optical tunable filter technologies have been developed, among which all-fiber acousto-optic tunable filter (AF-AOTF) has scored the most promising all-optical tunable filter technology because of its attractive features such as small insertion loss, wide tuning range, fast tuning speed, simple electronic control mechanism and excellent compatibility with fiber-based networks.

This thesis systematically studies the design, optimization, implementation and applications of using several AF-AOTF to obtain a tunable optical filter with pre-specified complex transmissions for different dynamic functions required by all-optical communication networks. As each stage of AF-AOTF only contributes a notch transmission, a desired complex transmission is formed by superposition of several shifted notch transmissions. Therefore, the challenge of achieving high performance tunable optical filter is the design of the tuning mechanism of each notch

filter to maintain the pre-specified spectrum while it is being tuned. The tuning mechanism must be as simple as possible from the practical point of view. To design such tuning mechanism with pre-specifications, the concept of tunability of a complex transmission and a quantitative measure of the tunability are for the first time formulated in the thesis. This advancement enables us to quantify the capability of a composite transmission being maintained while its position is tuned from one wavelength to another.

Using the proposed tunability measure, a strain control scheme is proposed and systematically developed to obtain tunable optical tunable filters with specified complex transmissions by using multi-stage AF-AOTF. This scheme is first developed based on the traditional multi-stage AF-AOTF design which cascades multiple AO interaction stages subject to frequency difference control scheme. In this design, the desired complex transmission profile is achieved by applying different frequency RF signals on each AO interaction stage where axial strain is applied as well. The shifting the composite transmission is achieved through adding an identical increment on the RF signal frequency of all AO interaction stages. The axial strain effect on the system tunability is modelled and analyzed for the first time. It is shown in theory that by applying a fixed axial strain on each AO fiber in the cascaded AF-AOTFs, the tunability of the resultant composite transmission can be enhanced.

Secondly, to further improve the tunability of multi-stage AF-AOTF, a strain difference control scheme is developed. In this scheme, the desired composite transmission profile is realized by introducing different fixed strains on different AO interaction stages in a calibration stage. All AO interaction stages are driven by the RF signals with same frequency. The transmission is tuned simply by tuning this RF signal frequency as tuning a single-stage of AO-AOTF. This simplicity gives advantage over the traditional frequency difference control scheme. Through theoretical analysis, it is shown that multi-stage AF-AOTF subject to strain difference control has better

tunability than the multi-stage AF-AOTF subject to frequency difference control scheme when they are used to deliver same complex transmission profile. The theoretical analysis are justified by both simulation studies and experimental studies where the desired complex transmission is a maximally flat stopband transmission.

Besides the tuning schemes, the improvement of the tunability is studied from practical perspective by addressing the implementation issues of multi-stage AF-AOTF. In traditional multi-stage AF-AOTF, each AF-AOTF is driven by individual piezoelectric transducer (PZT). The characteristics of the PZTs deviate one from others. To avoid the synchronizing problems between different AO interaction stages in the system, a novel loop structure AF-AOTF is proposed in the thesis to avoid the system tunability degradation due to the mismatch between acoustic bandwidths of different PZT in the cascading structure AF-AOTF. Enhanced notch filter using the proposed loop structure is demonstrated to solve the weak AO coupling efficiency problem of single mode fiber based AF-AOTF. Tunable bandstop filter is used as a study case to demonstrate the superiority of proposed loop structure on the synchronization of different AO interaction stages. The characteristics of different AF-AOTF integration structures are compared and their advantages and disadvantages of them in different applications are also analyzed.

To demonstrate the performance improvement of multi-stage AF-AOTF and its applications in all-optical communication networks, several typical and important applications of the proposed AF-AOTFs design are investigated in the thesis as well. First, a loop structure multi-stage AF-AOTF subject to strain difference control design is used to obtain a dynamic optical wavelength add/drop multiplexing filter over a broadband. As the filter can be designed with high roll-off factor, the channel crosstalk and signal distortion in multiplexing is greatly reduced. Next, the proposed design is used to design filters for gain control of erbium-doped fiber amplifiers in two typical applications. The first application is EDFA gain equalization based

on multi-stage AF-AOTF. An improved genetic algorithm is proposed to on-line tune the control parameters of multi-stage AF-AOTF to equalize the dynamic gain of EDFA. The second application is the EDFA gain clamping. A novel all-optical EDFA gain clamping scheme with dynamic optical feedback level control using AF-AOTF is proposed. In the design, the dynamic model taking into account the AF-AOTF dynamics is derived first, based on which poles placement method is applied to obtain the tuning rules of AF-AOTF. It is shown that the EDFA transmission penalty due to the relaxation oscillation transient is strongly suppressed by the proposed scheme.

Chapter 1

Introduction

1.1 Motivation

In 1835, Morse and Vail in the United States, developed the telegraph, and the truly meaning communications technology was born. In the following two centuries, promoted by the ever-increasing demand on large volume data transmission, new communication technologies are successively invented and developed, which include electronic communication, wireless communication, optical communication, wireless over fiber communication, and so on. These communication technologies directly affect the progress of human civilization. They make the earth become unbelievable smaller than what it looks like in the past centuries. People living toady can directly hear, watch and talk with anyone else in any corner of the planet, no matter they are on the highest top of huge mountain or in the deepest bottom of the pacific ocean, whether in the middle of the Sahara desert or on the floating ice in the Arctic Ocean.

Among different communication technologies, optical communication is out of question the most important and powerful one. Its huge volume data transmission ability makes it to occupy quickly and continuously most territory of conventional electric

communication technology. This can be seen from that the optical fiber has steadily overtaken copper cables as the medium of choice for modern-day networks after its invention in 1977. Today, most parts of this planet, no matter it is on which continents and oceans or belong to which countries, states and areas, are connected by this slight and tiny glass wire. With the rapidly growing demands of the internet on the transmission bandwidth, it is a clear trend that the customers continually require more efficient, rapid and higher quality information collection and exchange ability. As a result, optical communication technology becomes more and more important to develop the great potential of light on the information transmission capacity.

To fully utilize the ultra-broad 30THz bandwidth of optical fiber as much as possible, wavelength division multiplexing (WDM) is developed [1, 2]. It soon attracted many attentions and had become the most hopeful multiplexing technology for high speed optical networks. Before the invention of WDM technology, there are some other multiplexing technologies such as frequency division multiplexing (FDM), a standard technique in analog transmission systems, and time division multiplexing (TDM), a standard technique in digital transmission systems. WDM works on the same principles except that the channel discriminator is wavelength not frequency or time. WDM technique can multiple the capacity of optical fiber strands through creating virtual channels and unlocking the full bandwidth potential of fiber. Multiple channels are transmitted over the same fiber while there is no performance degradation or specific protocol requirements because light waves of different wavelengths do not interfere with one another during transmission. Whereas, it introduces some troubles and limitations on the dynamic control, modulation and management of the communication channels in the networks. Recently, with the speed of WDM optical network has extended to several tens of gigabit, these dynamic limitations have become more and more important and serious.

In conventional WDM optical networks, there are many Optical-Electrical (OE) conversion joints in network nodes where the data need to exchange. At these joints, the data are converted from the optical form to the electronic form firstly. Then, the dynamic functions such as modulation, management and control are implemented by electronic means. Finally, the data is converted back to the optical form and transmitted through the fiber to next nodes of the network. Since the bandwidth of electric signal is much smaller than that of optical signal, these OE/EO joints greatly limit the bandwidth of the whole network. Electro-optic bottleneck problem has become the primary shackle on the service quality improvement of optical WDM networks. Therefore, high-speed all-optical dynamic WDM network comes into picture and has been recognized as the future trend of optical communication technology. In all-optical network, the transmitted data remains in the optical form throughout the whole optical link [3, 4, 5, 6]. All dynamic functions such as dynamic routing, channel add/drop multiplexing, channel switching are directly implemented on the optical link layer to enable some more efficient upper-level protocol such as IP over WDM [7, 8, 9, 10, 11, 12].

Clearly, the realization of high-speed all-optical dynamic WDM network relies on whether all dynamic functions for all-optical network can be implemented by all-optical means. From the technical point of view, the key challenge lies in how to implement a tunable complex transmission using all-optical or more preferably all-fiber methods. This is because optical WDM networks use wavelength as the channel discriminator and all the dynamic functions are essentially based on modulation of the wavelength spectrum by using a filter with certain transmission. Therefore, if the tunable complex transmission can be obtained by an all-optical filter, the all-optical implementations of all the dynamic functions required by all-optical network would be involuntary.

One of the needs on tunable complex transmission in modern optical communication

is the optical add/drop multiplexing which is one of the enabling technologies for WDM networks with multiple communication links share the same physical link. It means to control isolation or gain of the wavelength signals passing through a node in all-optical WDM networks. To achieve this function, optical tunable filter with a transmission profile including multiple stopbands and passbands are clearly indispensable, and their transmission profile should satisfy several requirements. First, there should be clear partition between different channels to avoid the unwanted crosstalk problem. This demands the transmission profile have fast roll factor. Second, because the optical channels adding and dropping are arbitrary in practical applications, the stopband or passband transmissions should be tuned to any wavelength quickly.

Another important need on tunable complex transmission is related to Erbium-doped fiber amplifier (EDFA) which has played an enabling role in optical communication. EDFA is used to amplify and regenerate the severely impaired optical signal after long distance transmission. However, EDFA is troubled by two problems in real application. The first one is that the gain of EDFA is not equal for all wavelengths. When the optical signals in multiple wavelengths pass through an EDFA, some channels are over amplified while the weak signals are amplified. This will cause serious transmission errors at the receiving end. The second problem is that EDFA gain profile continuously fluctuates with the random variation of total input power. Thus, if some existing channels are dropped suddenly or some new channels are added, the signals in the rest channels will be disturbed and high bit error rate will be resulted in for these channels. To solve these problems, it requires an optical tunable filter with complex transmission profile that can dynamically compensate the fluctuating and complex transmission of EDFA.

The needs of tunable complex transmission are not limited to this. They are needed in signal generator, signal modulation, and signal detection. They are also needed

to form a feedback channel filter for the tunable single or multiple wavelength ring laser. In some high level network operations, they are used in optical routing, optical channel management and dynamic network reconfiguration. To entertain these needs, many optical filtering technologies have been developed to design optical tunable filters to deliver complex transmissions. However, with the advancement of optical dense WDM (DWDM) technology where the channel spacing is getting smaller and smaller, the requirement on the tunable complex transmission becomes more and more stringent. The desired high performance tunable complex transmission profile requires wide tuning range, fast tuning speed, low insertion loss, high band isolation, simple tuning scheme, and easy configurability and controllability. This has imposed challenges on the design of optical tunable filters.

To see the challenges in the implementation and realization of tunable complex transmission, the state of art of the optical filtering technology is briefly reviewed. Currently available optical tunable filter technologies include Fabry Perot interferometer tunable filters (FFP) [13, 14, 15], cascaded Mach-Zehnder interferometer based filters (CMZI) [16, 17, 18, 19], Fiber Bragg Gratings based filters (FBG) [20, 21, 22, 23, 24], acousto-optic tunable filters (AOTF) [25, 26, 27, 28, 29], electro-optic tunable filters (EOTF) [30, 31], ferroelectric liquid crystal Fabry-Perot filters (LCFP) [32], arrayed waveguide grating tunable filters (AWGC) [33, 34, 35, 36, 37, 38], ring resonator tunable filters (RRTF) [39, 40, 41, 42] and active filters (AF) [43].

These optical filters are summarized in Table.1.1 and their performance are compared in terms of insertion loss, isolation, bandwidth, tuning range, tuning speed and tuning mechanism [44].

From the comparison in the Table.1.1, the following conclusions can be reached. The FFP filters are limited by the slow tuning speed and narrow tunable range. Thus, they are not suitable for dynamic optical system. Similarly, the tuning speed of

Table 1.1: Comparison of different optical tunable filers

Type	Insertion loss	isolation	Bandwidth	Tuning range	Tuning speed	Tuning mechanism
FFP	2dB	2nm/30dB	0.5nm	10nm	ms	PZT
LCFP	3dB	2nm/30dB	0.5nm	50nm	100μ s	Crystal orientation
MFP	1dB	2nm/30dB	0.5nm	60nm	100μ s	Micro-machine
CMZI	1dB	0.4nm/22dB	0.2nm	4nm	50ns	electro-optic
FBG	0.1dB	1.6nm/30dB	0.2nm	10nm	2ms	Stretching
AOTF	4dB	4nm/30dB	2nm	100nm	μ s	Acousto-optic
EOTF	4dB	4nm/25dB	2nm	50nm	ns	Electro-optic
AWGC	8dB	0.8nm/30dB	0.2nm	40nm	10ms	Thermo-optic
AF		0.1nm/30dB	5nm	10nm	ns	Current injection
RRTF	3dB	2nm/30dB	0.2nm	25nm	ms	Temperature

LCFP and MFP still need to be improved. Although CMZI filters have good tuning accuracy and high tuning speed, the narrow tunable range limits their applications. Moreover, since CMZI uses several nanometers length difference between its two arms, its tuning mechanism is very difficult to implement in practice. The FBG filters can attain small insertion loss and narrow linewidth, but the problems of small tunable range and slow tuning speed need to be resolved before FBG filters can be widely applied in WDM system. EOTF filters seem not bad only except for the limited tunable range and the large voltages (about 100 volts) requirement. AWGC and RRTF are too slow and AF suffers from their wide linewidth.

Among all optical filter technologies, the acousto-optic tunable filters have a unique combination of following desirable properties.

- They offer a broadband tunability in the range of interest for guided wave optics including both L band and C band. The tuning range reaches a hundred nanometers and it is only limited by the acoustic transducer's fractional bandwidth.

- They have a moderate switch speed of few micro-seconds. The tuning speed of AOTF is only limited by the propagation speed of the acoustic wave. It is faster than those of most optical tunable filters.

- They have narrow-band filter characteristics with a full width at half maximum bandwidth (FWHM) less than 2 nm.

- They are convenient to be configured to deliver complex transmission.

- They are capable of performing parallel channel processing on multiple wavelengths by driving the filter with multiple RF frequencies simultaneously. Thus, more flexible network design can be implemented using AOTFs.

- The acousto-optic tunable filters require low electrical driving power about several tens mW.

These attractive properties, especially the large tunable range and simple electronic controllability, make the acousto-optic tunable filter (AOTF) the most potential and promising tunable filter technology for the future high speed dynamic WDM communication systems [44, 45, 46, 47, 48, 49].

However, conventional AOTF is based on the bulk optical technology or optical waveguide technology. The interaction between acoustic wave and optical beam performs through a crystal block or planar optical waveguide. It is connected to the optical networks through fiber pigtails. The material absorption and pigtails attenuation make the devices to suffer a high insertion loss ($5 - 7dB$ according to Table.1.1). To reduce the high insertion loss and increase the compatibility

with the optical networks, all-fiber based or fiber compatible AO interaction devices find their niches [50]. The potential of the fiber based AOTF was theoretically appreciated by Taylor [51]. Initial prototypes of fiber based acousto-optical devices were developed by Nosu in 1983 [52, 53] and by Risk in 1984 [54], respectively. Later, Kim and Blake developed in 1986 the first all-fiber acousto-optical tunable filter (AF-AOTF) that uses special designed acousto-optic transducer [55]. Birks and Russell further studied AO interaction in fiber and provided basic design rule for single-stage all-fiber acousto-optical devices [56]. After that, many all-optical acousto-optical devices were proposed and AF-AOTF technology was born [57, 58, 59, 60, 61, 62, 63, 64, 65, 66, 67, 68, 69, 70, 71].

In the past several tens of years, R&D efforts pushed the all-fiber acousto-optical tunable filter technology to advance progressively. When AF-AOTF was invented in 1983, the most urgent and observable problem for AF-AOTF was low power conversion efficiency, unsatisfied noise performance and the limitation on the transmission profile modulation. Therefore, the conventional researches were focused on efficiency improvement, noise ripple suppression and transmission profile modulation of single-stage AF-AOTF. Several schemes such as chemical etching and mechanical taping were proposed to solve these problems. Soon, AF-AOTFs with high power conversion efficiency, low side ripple level, ultra-broad and ultra-narrow bandwidth were implemented early or later. Now, AF-AOTF has been made much more efficient, small, flexible and low-cost than its first prototype in 1983. Continuous technical advancement makes AF-AOTF technology exhibit great potential to be employed in future all-optical WDM networks to implement different kinds of dynamic functions.

The basic transmission of an AF-AOTF is a notch. It can be directly used in optical switching. But more frequently and widely used optical tunable filter in optical networks are those with complex transmission profiles such as tunable bandstop, bandpass filter and EDFA gain compensation filter. To this end, multiple AO inter-

action stages are cascaded in line. Each AO interaction stage is controlled to deliver a notch transmission at certain wavelength with certain gain. The desired complex transmission is formed by composing the notch transmissions. The tuning of the composite transmission is implemented by synchronically tuning and controlling all AO interaction stages. The inaccuracy in the synchronous tuning would results in distortion of the complex transmission. Therefore, the design, synchronization control, realization and implementation of multiple AF-AOTFs in these applications must be optimized to reduce the distortion while attaining a fast tuning speed. It gives rise to the tunability of multi-stage AF-AOTF. The tunability defines the capability of a composite transmission being maintained while its position is tuned from one wavelength to another. It is an important factor that directly affect the system dynamic performance in most applications of multi-stage AF-AOTF in optical WDM networks. However, the tunability of the multiple AF-AOTF have not been addressed and it is an open but important issue.

1.2 Objectives

In this thesis, we address the tunability of multi-stage AF-AOTF quantitatively and systematically study the design, optimization, implementation and applications of using several AF-AOTF to obtain a tunable optical filter with pre-specified complex transmissions for different dynamic functions required by all-optical communication networks. To this end, the tunability is first formulated, based on which a strain control scheme is developed to improve tunability of multi-stage AF-AOTF. Then, pilot studies on some applications of multi-stage AF-AOTF in the dynamic all-optical WDM networks are explored. The primary objectives of this thesis are listed as follows:

- Quantitative formulation of the tunability of tunable complex transmission profile produced by multiple AO interactions.
- Quantitative assessment of strain effect and strain control on the tunability improvement of tunable complex transmission profile.
- Study of formalized design approach to improve the tunability of complex transmission profile produced by multiple AO interactions.
- Study of efficient implementation structure of optical tunable filters with improved tunability.
- Study on the design and control of multi-stage AF-AOTF in the important application of dynamic optical Add/Drop multiplexing.
- Study on the design and control of Multi-stage AF-AOTF in the important application of EDFA gain equalization and gain clamping.

1.3 Major Contributions

This thesis systematically studies the design, optimization, implementation and applications of using multiple AF-AOTF to obtain a tunable optical filter with pre-specified complex transmissions for different dynamic functions required by all-optical communication networks. In this thesis, the following major contributions have been made to the AF-AOTF design and its applications.

- For the first time, we address the tunability of the tunable complex transmission produced by multiple AF-AOTF. The quantitative measure of the tunability is proposed and used to design the tuning mechanism and the implementation structure of multiple AF-AOTFs. Using the measure, tunability improvement schemes are developed for multi-stage AF-AOTF.

- A strain control scheme is proposed to improve the tunability of the complex transmission delivered by traditional cascading AF-AOTFs. It analytically shows that applying the axial strain on the AO interaction sections of the cascading AF-AOTFs can help to improve the tunability of the resultant complex transmission.

- A strain difference control scheme is proposed to deliver a tunable complex transmission by using multi-stage AF-AOTF. It is shown analytically and experimentally that using the strain difference control scheme can obtain more improved tunability than that of using the traditional frequency difference control scheme. Moreover, the proposed scheme can help to simplify the tuning mechanism of the multi-stage AF-AOTF and in turn increase the system reliability.

- The tunability improvement is investigated by considering some key practical issues. The PZT synchronization problems, acoustic bandwidth limitation and acoustic interaction effect are studied and analyzed from view point of the system structure optimization. A loop structure AF-AOTF, which has particular superiority in practical implementation and can greatly improve the reliability of multi-stage AF-AOTF, is proposed and demonstrated in theory and experiment.

- As an application of the proposed schemes for AF-AOTF tunability improvement, a dynamic optical Add/Drop multiplexing filter using the multi-stage AF-AOTF is demonstrated with wide tunable range and specified roll off factor.

- As an application of the proposed schemes for AF-AOTF tunability improvement, an intelligent dynamic EDFA gain equalization filter is demonstrated by using multi-stage AF-AOTF.

- As an application of the proposed schemes for AF-AOTF tunability improvement, a dynamic EDFA gain clamping scheme is proposed and demonstrated, which can greatly suppress the relaxation transient of EDFA.

1.4 Organization of the Thesis

The rest of this thesis is organized as follows:

Chapter 2 addresses the tunability of the complex transmission delivered by multi-stage AF-AOTF. It starts with the operation principle of AF-AOTF where the transmission model of single AF-AOTF is given. Then, the state of art of AF-AOTF technology and its application issues for optical communication are reviewed, from which we see the potential of the multi-stage AF-AOTF and the technical gap between current multi-stage AF-AOTF and the desired performance required by the next generation of all-optical networks. The tunability is recognized as the next concern of application of AF-AOTF in all-optical dynamic communication. Next, the tunability of the multi-stage AF-AOTF is introduced and a quantitative measure of the tunability is proposed as the phase mismatch error variation with respect to the system operation wavelength. The effectiveness of the definition of the tunability is illustrated by considering a flat-stopband transmission produced by two cascading AF-AOTFs. Finally, the more detailed expressions of those physical parameters used in the thesis are briefed in the appendix where the design of the flat-stopband filter is elaborated.

Chapter 3 presents the strain control scheme for improving the tunability of the transmission produced by multi-stage AF-AOTF. In this chapter, we first analyze the tunability problem for traditional cascading multi-stage AF-AOTF subject to frequency difference control. The strain effect on the tunability of the composite transmission of multi-stage AF-AOTF is studied and analyzed. For the first time, it

shows analytically that in a cascading multi-stage AF-AOTF, the tunability of the composite transmission can be enhanced by increasing the axial strain in the optical fiber where the AO interactions occur. Secondly, we propose a strain difference control scheme to improve the tunability of multi-stage AF-AOTF. This scheme applies differential strains on the AO interactions to deliver a tunable complex transmission. The acoustic frequency is only used to change the position of the complex transmission. It is shown analytically that the composite transmission obtained by the strain difference control scheme can be maintained better than those obtained by the frequency difference control schemes. Simulation and experimental studies are also conducted to verify the theoretical analysis.

Chapter 4 addresses the key implementation issues of the strain difference control scheme. A loop structure AF-AOTF is proposed to implement the strain difference control scheme. The loop structure AF-AOTF overcomes the limitations of traditional AF-AOTF. To see this, The characteristics of different AF-AOTF integration structures are also discussed and their advantages and disadvantages in particular applications are first analyzed. Then, the loop structure AF-AOTF is demonstrated to produce an enhanced notch transmission. This solves the weak AO coupling efficiency problem in traditional single-stage AF-AOTF which is usually used to produce notch transmission. Next, the loop structure AF-AOTF is designed to produce a complex transmission by overcoming the synchronizing problems faced by traditional multi-stage AF-AOTF.

Chapter 5 concentrates on the pilot studies of using AF-AOTF in two typical and important applications in optical communication. Firstly, the application of multi-stage AF-AOTF in dynamic optical Add/Drop multiplexing is discussed. In this application, using multi-stage AF-AOTF to implement a broad band stopband filter with fast roll-off factor is concerned. Secondly, static and dynamic EDFA gain equalization using multi-stage AF-AOTF are reported. For the static gain equal-

ization, an improved genetic algorithm is proposed to use multi-stage AF-AOTF to implement a dynamic EDFA gain equalization. Using the equalizer, the overall gain profile with excellent flatness is archived and the transmission profile distortion due to the gain tile effect of EDFA is suppressed. For the dynamic gain equalization, the application of AF-AOTF in all-optical EDFA gain clamping is studied. A dynamic optical feedback level control scheme using AF-AOTF is proposed to suppress the unwanted EDFA gain transients. By using the proposed EDFA gain clamping scheme, the relaxation oscillation transient is strongly suppressed and transmission profile distortion of EDFA is greatly reduced. This achievement makes EDFA can be widely employed in the future high-speed dynamic all-optical communication networks.

In Chapter 6, the conclusions of the thesis are drawn and some suggestions for future research are made.

Chapter 2

Tunability of Multi-stage AF-AOTF for Optical Communication

2.1 Introduction

In this chapter, we address the tunability of the tunable complex transmission generated by using multi-stage AF-AOTF. We first illustrate the basic operation principle and mathematical model of single-stage AF-AOTF in Section.2.2. This illustration provides the necessary prerequisite for the further discussion in the rest parts of this thesis. Then, we give a brief review on the state of art of current AF-AOTF technologies in Section.2.3. On one hand, it can be seen from the review that various efforts have been devoted to the performance improvement of single-stage AF-AOTF. These achievements have demonstrated the potential of AF-AOTF as tunable optical filters. They have laid down a good basis to explore using AF-AOTF to achieve more powerful optical signal processing functions for optical communication. On

the other hand but more importantly, overview of this technology helps us to find that the use of multi-stage AF-AOTF to tunable complex transmission would be the most promising niche technology which will help to narrow the technical gap and push this technology to the next generation all-optical dynamic optical communication. To obtain improved performance of tunable transmission, it is of great interest and importance to quantitatively assess the tunability of the complex transmission formed by notch transmissions. Section 2.4 formulates the tunability problem of multi-stage AF-AOTF and introduces a quantitative measure of tunability.

2.2 Operation Principle of AF-AOTF

All acousto-optical (AO) devices are based on the acousto-optic effect which is also known in the scientific literature as acousto-optic interaction or diffraction of light by acoustic waves. The acousto-optic effect states that through interacting with an acoustic wave, the refractive index of an optical material can be temporarily varied or modulated, and thus optical beam passing this optical material will be deflected or modulated. Applying this principle on a piece of fiber gives rise to the AF-AOTF.

In AF-AOTF, the most commonly used acoustic mode to generate AO coupling is the flexural acoustic wave because flexural acoustic wave can provide high coupling efficiency than other two acoustic modes [72]. The basic operation principle of AO interaction in the fiber is illustrated as in Fig.2.1 and can be briefly described like this. Flexural acoustic wave is generated by an acoustic transducer and propagates along the fiber. It causes micro-bending along the fiber and results periodical refractive index modulation just like grating. When light passes through this "acousto-optical" grating, optical power exchange happens among different optical modes. At the out port of AF-AOTF, the optical power in one or part of optical modes is filtered out by using some mode selective components. Because

for a single frequency acoustic wave, the mode coupling only happens in a narrow optical bandwidth, the optical power in this optical bandwidth will be filtered out by AF-AOTF while the optical power in other wavelengths are still guided by the fiber. As a result, the transmission of a single-stage AF-AOTF has a notch or peak transmission.

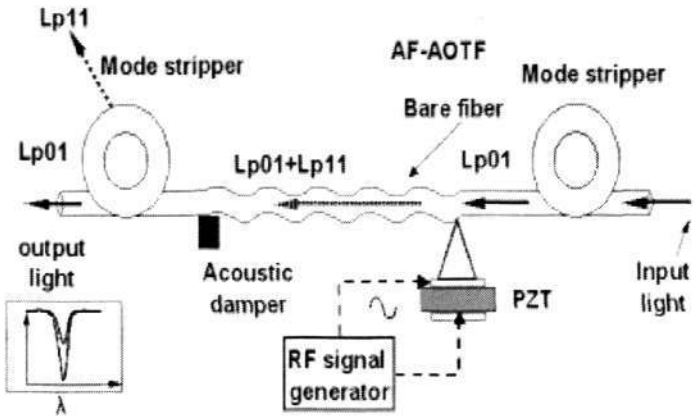

Figure 2.1: Schematic of all-fiber acousto-optic tunable filter operation principle.

To give more details about AF-AOTF operation principle, we illustrate the operation principle of single-stage AF-AOTF by introducing its hardware setup and its transmission model, respectively.

2.2.1 Typical Setup of a Single-stage AF-AOTF

The simple AF-AOTF setup consists of fours parts which are respectively the acoustic wave generation module, the AO interaction medium, the mode selection filter, and the acoustic wave modulation and control module. Fig.2.2 shows a photograph of a typical experimental setup of AF-AOTF.

The first part is the acoustic wave generation module. This part includes a radio frequency signal source, an acoustic transducer and a horn. The acoustic trans-

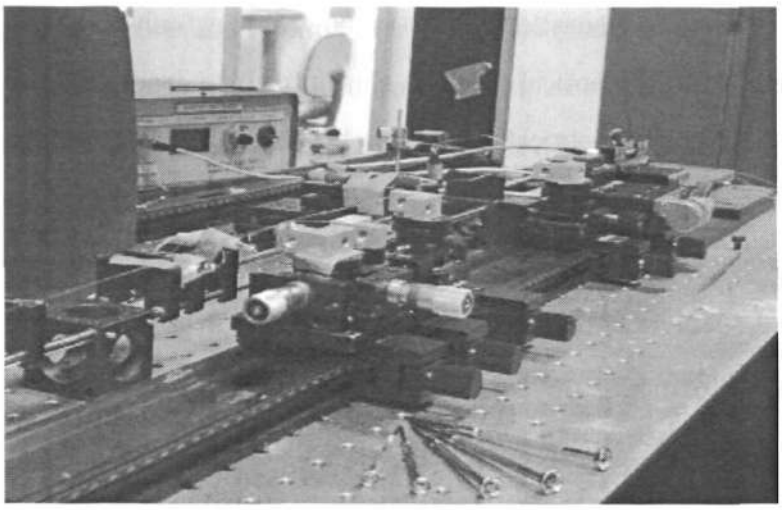

Figure 2.2: Experimental setup of single-stage AF-AOTF.

ducer is fabricated from some piezoelectric material such as lithium niobate. The piezoelectric material is cut into disk or plate shape with a cross-section area about several square millimeters. The plate is made as thin as possible within a fabrication tolerant range to obtain high AO coupling efficiency. The piezoelectric material of the plate is carefully oriented to guarantee only longitudinal mode vibration be generated. For a plate, electrodes are deposited on the top and bottom surfaces of the piezoelectric material. These electrodes are connected with the RF signal generator through copper wires bonded at the edge. Because the PZT generates a lot of heat when it operates, a heat sink is bonded on the bottom electrode to dissipate the overheat problem that will cause damage to the acoustic transducer. The heat sink also provides solid mechanical support to the acoustic transducer. It is a metal block with excellent thermal conductibility and large surface area. The top electrode is bonded with the bottom of the horn by using organic compounds such as epoxy and phenyl compounds. Because the acoustic impedance mismatch between the organic compounds is quite large, the bond thickness must be made as thin as possible in order that mismatch will not substantially reduce the efficiency and bandwidth of the transducer. The horn is made of either aluminium, or copper, or silica. The

horn bottom has a diameter slightly smaller than that of the acoustic transducer. The tip diameter of horn should match that of the AO interaction medium, usually smaller than $130\mu m$. The height of the horn is in the range from $1mm$ to $5mm$ depending on the desired acoustic frequency. The horn surface is specially designed to have a taper shape with linear or exponential slope. This design can focus the acoustic power and amplify the longitudinal acoustic wave amplitude.

There is another type of acoustic transducer. The fabrication of this kind of acoustic transducer is similar to the one illustrated above, except for that the employed piezoelectric material is oriented for shear mode excitation and is placed in parallel with the optical fiber. A hole is made in the center of PZT, horn and heat sink so that a bare fiber threads can go through the hole and is bonded with the transducer using epoxy compounds. This design can generate flexural acoustic wave in fiber with a higher power utility efficiency. Fig.2.3 and Fig.2.4 show the two types of acoustic transducers and horns with different sizes.

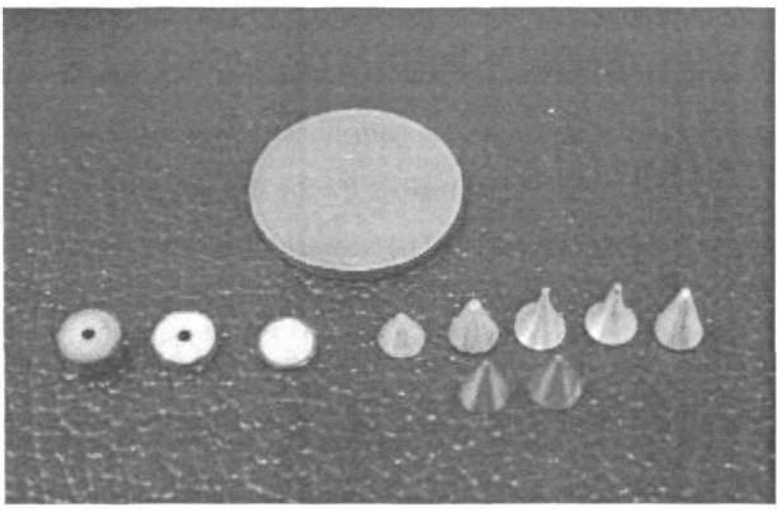

Figure 2.3: Piezoelectric transducers and horns for AF-AOTF.

The second part is the AO interaction medium. In AF-AOTF, the AO interaction medium is a piece of optical fiber or some fiber components like a fiber coupler. The

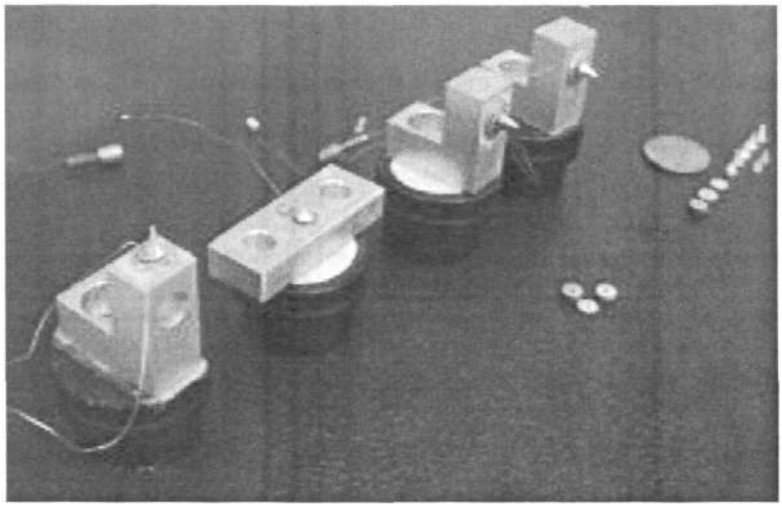

Figure 2.4: Acoustic transducers for AF-AOTF.

fiber can be any kinds such as multi-mode fiber, two-mode fiber, single mode fiber, photonic crystal fiber, polarization maintenance fiber. A fiber coupler can be also used as the AO interaction medium of AF-AOTF. The AO interaction processes in all these mediums are similar except for small difference on the participant optical modes. To avoid serious acoustic power attenuation, the plastic coating of the fiber are removed beforehand. In the bare fibers, both acoustic field and optical field exist. The acoustic field is generated by the flexural wave that coupled from the longitudinal wave in the horn. The acoustic field changes the optical power distribution among all possible guided and cladding modes in a narrow bandwidth. The mode coupling ratios depend on the refraction variation amplitude, the fiber length, the phase mismatch and the field overlap between different optical modes.

The third part of AF-AOTF is the optical mode selection or split filter. It connects with the end of the AO interaction medium. This part is used to implement two functions, isolating the acoustic wave and splitting the optical power in different modes. It consists of an acoustic absorber and an optical mode splitter. Usually, the plastic coating of the fiber can sufficiently isolate the acoustic power and can

function as the absorber. To further reduce the unwanted acoustic reflection, elastic and emplastic materials can be used to clamp the fiber and isolate the acoustic power. The optical mode splitter includes the optical mode stripper and the optical mode selective coupler. The former has only one output port. It only allows one or part of the optical modes pass through. The optical power in the rest modes will be diffracted or attenuated. The optical mode stripper is also used in the applications such as the tunable optical attenuator and optical bandstop filter to filter out the optical power in the stopband wavelength. The most commonly used mode stripper is the cladding mode and LP_{11} mode stripper, which is fabricated by bending a piece of fiber several rounds in a suitable diameter. The optical mode coupler has more than one output ports. In fact, it is an optical coupler with different coupling ratio between the different optical modes [73]. It splits the optical power transmitting in different modes to different out ports. The modes can be strongly guided in the fiber for long distance transmission except for the different optical path. With the help of mode selection coupler, AF-AOTF can deliver the bandpass transmission, thus it can be used to do the optical add/drop multiplexing.

The last part of a AF-AOTF is the modulation and control module. It includes the computer and some electric signal control circuits. They are used to modulate and control the driving RF signal in different applications.

2.2.2 Model of Transmission of a Single-stage AF-AOTF

The optical power transmission of AF-AOTF is given by [56]

$$\begin{aligned} G(\lambda) &= 10\log\frac{P_{out}}{P_{in}} \\ &= 10\log\left(1-\frac{C^2}{C^2+\delta^2(\lambda)}\sin^2\left(L\sqrt{C^2+\delta^2(\lambda)}\right)\right) \end{aligned} \tag{2.1}$$

where L is the AO coupling length of AF-AOTF, C is the AO coupling coefficient, δ is the phase mismatch coefficient, P_{in} and P_{out} are the power of input light and output light in the fundamental mode, respectively. In wavelength spectrum, $G(\lambda)$ is basically a notch.

If the transmission of certain mode is of concern, a mode selective coupler is connected to AF-AOTF output port. The transmission of the AF-AOTF with a mode selection coupler is a spike like bandpass transmission[74] and it is given by

$$G(\lambda) = 10\log\frac{C^2}{C^2+\delta^2(\lambda)}\sin^2\left(L\sqrt{C^2+\delta^2(\lambda)}\right) \tag{2.2}$$

In the transmission, the AO coupling coefficient and the phase mismatch coefficient, C and $\delta(\lambda)$, are given by

$$\begin{aligned}\delta(\lambda) &= \frac{1}{2}(\beta_0-\beta_1-\kappa)\\ &= \pi\left(\frac{1}{L_B}-\frac{1}{\Lambda}\right) \qquad (2.3)\\ C &= \frac{\pi}{\lambda}\int_A \xi_0(x,y)\triangle n(x,y)\xi_1(x,y)dxdy \qquad (2.4)\end{aligned}$$

where β_0 and β_1 are propagation vectors of the fundamental mode and the other participant optical mode; f is the frequency of the acoustic wave; A is the cross section of the optical fiber; $L_B = \frac{2\pi}{\beta_0-\beta_i}$ is the optical mode beatlength; $\Lambda = \frac{2\pi}{\kappa}$ is the acoustic wavelength; ξ_0 and ξ_i are the field distributions of the two participant optical modes, respectively. In above equations, all β and L_B are optical wavelength dependent. We omit the optical wavelength dependent term (λ) for the sake of simplicity.

Above model of AF-AOTF is based on following assumptions.

- All input optical power is guided in the fundamental mode.

- In an optical bandwidth of several tens of nanometers, in one time, single frequency acoustic wave can only excite one strong mode coupling process between the fundamental optical mode and another optical mode. The mode couplings between other modes are well self-resonance[51].
- The power in the one of participate optical modes is completely attenuated or stripped off before go out of AF-AOTF.

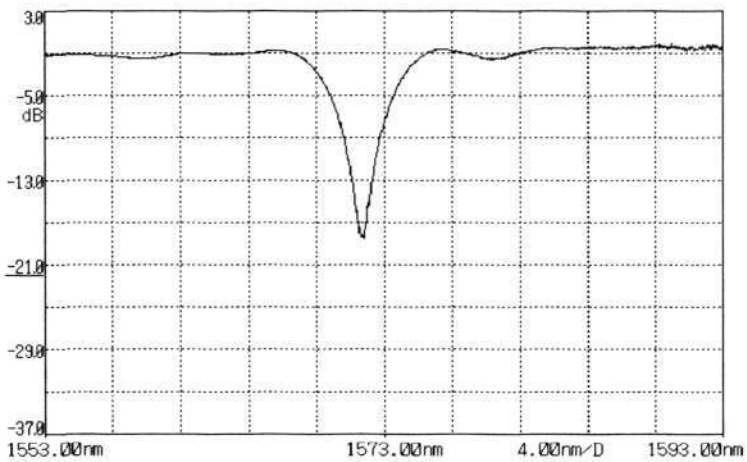

Figure 2.5: Transmission of single-stage AF-AOTF.

Fig.2.5 shows an example of the common transmission profile of AF-AOTF. This notch transmission profile is produced by a single-stage AF-AOTF fabricated from a piece of SMF-28 fiber.

From (2.1) and the common transmission profile shown in Fig.2.5, some basic properties of AF-AOTF can be simply derived. Firstly, maximum mode coupling happens on the optical wavelength where the phase match condition (2.5) is satisfied. The mode coupling processes with large $|\delta|$ value are self-resonance and not the change the static power distribution between different optical modes.

$$\delta = 0 \tag{2.5}$$

Secondly, it can be derived from the typical transmission of AF-AOTF shown in Fig.2.5 that in all kinds of fiber-based optical medium except the strongly etched fiber structure [75], the wavelength dependence of the absolute value of δ is much stronger than that of C. For the AO coupling excited by a stable acoustic wave with fixed frequency, the AO coupling coefficient C is almost same for all optical wavelength. The theoretical cause of this phenomenon will be presented later in this chapter. Thus, $\frac{\delta^2}{C^2}$ has a zero or small value only in a narrow optical bandwidth. Resonance AO coupling happens in this optical bandwidth. Out of this optical bandwidth, $\frac{\delta^2}{C^2}$ quickly increase to a large value and $G \approx 1$. Therefore, AF-AOTF has a narrow notch transmission profile.

In the model of AF-AOTF (2.1), the possible tuning parameters are the phase mismatch coefficient δ, AO coupling coefficient C and AO interaction length L. The tuning process of AF-AOTF is based on the modulation of these three parameters. However, the on-line tuning of AO interaction length L is very difficult in real applications. Thus, the modulation AO interaction length L is possible only during the system design process and fabrication process to obtain some static performance such as broad bandwidth and relative high coupling efficiency. In most cases, once an AF-AOTF is fabricated, the AO interaction length L is fixed. The on-line tuning parameter for AF-AOTF is the phase mismatch coefficient δ and AO coupling coefficient C. Both δ and C are determined by the acoustic field and optical field in the fiber shown in Appendix.A and Appendix.B. The AF-AOTF model (2.1) is for AF-AOTF based on coupler, it also available for the AF-AOTF based on other fiber structures such as single mode fiber and multi-mode fiber [58]. For those AF-AOTF, the only difference is in the calculation of C and δ, the details can be found in Appendix.C.

2.3 State of the Art of AF-AOTF Technology

Although the first AO device was experimentally demonstrated by Lucas in 1932, the first modern all-fiber acousto-optical filter was not proposed until 1986 by Kim. Since then, AF-AOTF technology has been developed for more than twenty years. The momentum pushing the AF-AOTFs is due to the needs of all-optical fiber components that have good compatibility with the fiber link used in optical communication. Overview of this technology not only enables us to know its state of art, but more importantly, enable us to find the most promising niche technology which will narrow the technical gap and push this technology to the next generation all-optical dynamic optical communication.

The earliest fiber based AO devices were developed in the middle of 1980s and used to realize the phase modulation and frequency shifting [52, 53, 54]. Actually, these fiber-based acousto-optical devices are the fiber-optic counterparts of the conventional integrated AOTF. In these earlier fiber-optic AO devices, the electric power is used to generate some surface acoustic wave and bulk acoustic wave. The acoustic power is coupled into the fiber through some sandwich structure as shown in Fig. 2.6. As it is free of the pigtails attenuation and crystal absorption, the device insertion loss is reduced to a negligible value. However, these fiber-optic AO devices are quite inefficient on the utilization of electric power because of the low coupling efficiency and sideband suppression. Furthermore, their performance is strongly sensitive to the polarization.

The first real all-fiber acousto-optical tunable filter (AF-AOTF) was proposed by Kim [55] in 1986. Its schematic is shown in Fig.2.7.1. In this filter, longitudinal wave propagating in the vertical direction is generated by a piezoelectric transducer (PZT) driven by radio frequency alternating signal. The power of this longitudinal wave is focused and coupled into the bare optical fiber through a taper shape horn

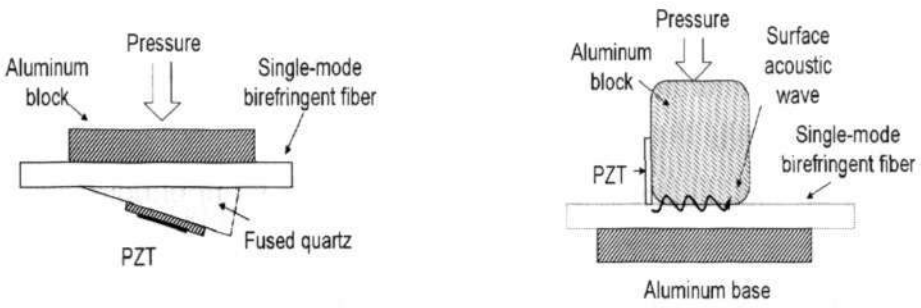

2.6.1: 2.6.2:

Figure 2.6: Schematic of two fiber-optic Acousto-optical devices.

and propagates along the fiber in the form of flexural acoustic wave. This flexural acoustic wave introduces periodic micro bending along the fiber and results in the AO interaction when light passes through this piece of fiber.

Kim's design greatly improves the performance of AF-AOTF in almost all aspects. It soon became the basic and standard structure of AF-AOTF. In the following decades, AO interaction was successively implemented on different kinds of fiber such as birefringent fiber, multi-mode fiber, two-mode fiber, single-mode fiber and photonic crystal fiber [54, 55, 57, 76, 77]. The same principle was also applied on fiber coupler, fiber taper, dispersion-enhanced fiber and etched fiber to further improve the performance or obtain some desired optical signal transmission control [56, 60, 76, 78, 75]. Moreover, innovation design of the accessory elements for AF-AOTF such as acoustic transducer and mode selective components were continuously invented and developed [59, 73, 74, 79]. The schematic of some of these designs are shown in Fig. 2.7.

With these research efforts, most traditional problems of a single-stage AF-AOTF such as weak coupling efficiency, bandwidth limitation and side ripple suppression are partially or fully solved. The static transmission performance of a single-stage

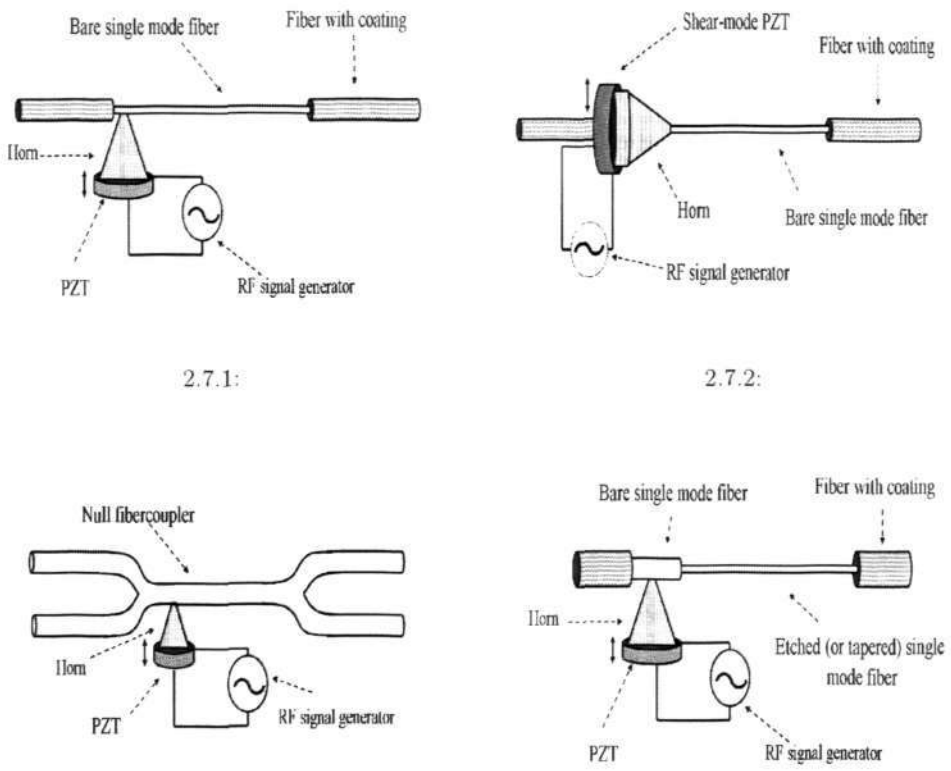

Figure 2.7: Schematics for several basic all-fiber acousto-optical tunable filter.

AOTF is greatly improved. Current AF-AOTF can deliver not only notch transmission but also spike like bandpass transmissions [74]. The transmission bandwidth can be controlled in the range from one nanometer to several hundred nanometers. The driving power is reduced to the level of hundred milliwatts. These advancements have shown that AF-AOTF has a great potential besides their basic merits in the wide tunable range and the good compatibility with fiber links. Considering any transmission can be formed by superposing notch or spike like passband transmissions, AF-AOTF technology is recognized as one suitable candidate to implement optical tunable filter with complex transmission for the next generation all-optical network.

However, there are several factors that limits the AF-AOTF from being applied to achieve the optical signal processing functions required by all-optical networks. The first factor is that the notch transmission of single-stage AF-AOTF is limited with its isolation and bandwidth. The second but more important factor is the synchronization of several AF-AOTFs. This is because a desired complex transmission is a composite of several notch transmissions. When it is required to tune, all participant notch transmissions must be tuned in a synchronous manner so that the complex transmission preserves its profile as designed. For this application, the implementation of a desired complex transmission requires more than one AO interaction stages. So far, two traditional methods are developed for this application. One is to cascade several AF-AOTFs together and the other is to apply multiple RF signals on a single-stage AF-AOTF. As the both cases have the same feature, we refer to the superposition of several AO interactions as multi-stage AF-AOTF in the subsequential parts of the thesis. The notch transmission is a nonlinear function of the control variables of the AF-AOTF. Synchronizing AF-AOTF to maintain the complex transmission profile would need complicated calculation of the control variables at all wavelengths in the tuning range. It is almost impossible. The situation is even worse when more stages of AO interactions are required. Therefore, efficient synchronization control of all AF-AOTFs is the major challenge for AF-AOTF to be used for all-optical network. The solutions of this second problem also provide remedy to overcome the first limitation factor in isolation and bandwidth of AF-AOTF.

2.4 Tunability Measure of Multi-stage AF-AOTF

In order to achieve an automatic synchronous control, a measure is needed to evaluate the synchronization or the asynchronization. In this section, the synchronization control issue is addressed by the concept of the tunability of the complex trans-

mission. For a clear illustration, we first study the implementation of a complex transmission by using multi-stage AF-AOTF. Through a typical application of designing maximally flat bottom stopband transmission, we identify the key parameter controlling the transmission profile. Then, we analyze the factors contributing distortions to the designed transmission when it is tuning. Finally, a tunability measure is introduced.

2.4.1 Implementation of Complex Transmission by Multi-stage AF-AOTF

To achieve complex transmission profile, several AO interactions are superposed to form a multi-stage AF-AOTF. This can be done by either cascading several AF-AOTFs or applying several RF signals on a single AO interaction medium. Each AO interaction is controlled by one RF signal generator and used to generate a notch transmission at certain wavelength. The throughout transmission of the multi-stage AF-AOTF is the superposition of all notch transmissions. The transmission can be controlled to attain any shape through carefully adjusting the relative position of each notch transmission. According to model (2.1), the composite transmission of assembled AF-AOTFs is given by:

$$G_c(\lambda) = \sum_{i=1}^{n} 10 \log \left(1 - \frac{C_i^2}{C_i^2 + \delta_i^2} \sin^2 \left(L_i \sqrt{C_i^2 + \delta_i^2} \right) \right) \tag{2.6}$$

where C_i, L_i and δ_i denotes the AO coupling coefficient, AO interaction length and phase mismatch coefficient of ith AF-AOTF, respectively. The design of cascading AF-AOTFs to achieve a desired transmission can be described as one of choosing the δ_i, C_i and L_i such that the composite transmission $G(\lambda)$ satisfies a desired complex transmission.

Now we use the design of the maximally flat stopband transmission as an example

to show the design process of complex transmission. The reason of selecting such a transmission is due to the following considerations. On one hand, the maximally flat stopband filter is a fundamental filter in the optical communication system and optical signal processing. It is widely used in the many processes such as the Add/Drop modulation, equalization and filtering. On the other hand, the tunable flat stopband transmission can be used as an element spline function to approximate more complex transmissions. Thus, the obtained result can be extended to the design of the filter with other complex transmissions. In addition, the maximally flat stopband transmission is a standard transmission. The deformation of the transmission is easy to be quantitatively analyzed. The measure found to evaluate the deformation is also suitable for complex transmission.

The desired symmetric stopband transmission can be looked as the composition of two identical but shifted notch transmission. To keep the identity of these two notch spectra, the AO coupling coefficients and AO interaction length are set the same values. It can be expressed as $C_1 = C_2 = C$ and $L_1 = L_2 = L$, respectively. For convenience of illustration, the following denotations are introduced:

$$\alpha_i \triangleq \frac{\pi}{\Lambda_i}, \tag{2.7}$$

$$\eta(\lambda) \triangleq \frac{\pi}{L_b(\lambda)} \tag{2.8}$$

$$\delta_i(\lambda) \triangleq \eta(\lambda) - \alpha_i, \tag{2.9}$$

where Λ_i denotes the acoustic wavelength along the bare fiber of i-th AF-AOTF. From (2.5), these two acoustic signals with wavelength Λ_i satisfy following condition and generate two notch transmissions at the wavelengths λ_i.

$$\delta_i(\lambda_i) = 0, \quad (i = 1, 2) \tag{2.10}$$

Using the result in [56], the function $\eta(\lambda)$ in equation (2.8) can be approximated as

a linear function in the region of several nm.

$$\eta(\lambda_c) = (\alpha_1 + \alpha_2)/2 \tag{2.11}$$

where λ_c denotes the central wavelength of the composite stopband transmission. The first considered specification of the designed filter is the flatness. To determine α_i for $i = 1, 2$, define that

$$\sigma(\lambda_c) \triangleq \delta_1(\lambda_c) - \delta_2(\lambda_c) \tag{2.12}$$

where $\sigma(\lambda)$ denotes the difference between the phase mismatch coefficients of these two AF-AOTFs while the center wavelength of composite transmission is λ. In the later discussion, it is referred to the phase mismatching difference as a short denotation. It follows from the definitions of $\delta_i(\lambda)$ that $\sigma(\lambda_c) = \alpha_2 - \alpha_1$. For the sake of simplicity, $\sigma(\lambda_c)$ is denoted as σ. Clearly, the design is independent of whether $\alpha_2 > \alpha_1$ or $\alpha_2 < \alpha_1$. Thus, σ is assumed to be positive without loss of generality. Substituting (2.12) into (2.6), the transmission of the filter is represented as

$$\begin{aligned} G_c(\lambda) \triangleq\ & 10\log\left(1 - \frac{C^2\sin^2\left(L\sqrt{C^2 + (\eta(\lambda) - \alpha_1)^2}\right)}{C^2 + (\eta(\lambda) - \alpha_1)^2}\right) \\ +\ & 10\log\left(1 - \frac{C^2\sin^2\left(L\sqrt{C^2 + (\eta(\lambda) - \alpha_1 - \sigma)^2}\right)}{C^2 + (\eta(\lambda) - \alpha_1 - \sigma)^2}\right) \end{aligned} \tag{2.13}$$

For convenience of discussion, define that $G_c(\lambda) \triangleq 10log(F(\lambda))$. Then

$$\begin{aligned} F(\lambda) =\ & \left(1 - \frac{C^2\sin^2\left(L\sqrt{C^2 + (\eta(\lambda) - \alpha_1)^2}\right)}{C^2 + (\eta(\lambda) - \alpha_1)^2}\right) \\ \times\ & \left(1 - \frac{C^2\sin^2\left(L\sqrt{C^2 + (\eta(\lambda) - \alpha_1 - \sigma)^2}\right)}{C^2 + (\eta(\lambda) - \alpha_1 - \sigma)^2}\right) \end{aligned} \tag{2.14}$$

In order to obtain the maximally flat stop-band optical filter, the j-th order derivatives of the $F(\lambda)$ with respect to λ should be zero at the center wavelength of the stop band for $j = 1, 2, ..n$ with n as large as possible. Assuming $\eta(\lambda)$ is a linear function and has constant first order derivative in a small optical wavelength range.

$$\begin{aligned} \frac{d\eta(\lambda)}{d\lambda} &= K \\ \frac{d\eta^n(\lambda)}{d\lambda^n} &= 0 \qquad n >= 2. \end{aligned} \tag{2.15}$$

where K is a constant not equal to zero. This assumption is reasonable when the fiber diameter is far away from the critical point mentioned in [78].

$$\begin{aligned} \frac{d^n F(\lambda)}{d\lambda^n} &= \frac{d^n F(\eta)}{d\eta^n}\left(\frac{d\eta(\lambda)}{d\lambda}\right)^n \\ &= \frac{d^n F(\eta)}{d\eta^n} K^n \qquad n = 1, 2. \end{aligned} \tag{2.16}$$

Thus, the flatness of the stopband filter transmission can be more easily evaluated by the j-th order derivatives of $F(\eta)$ to η instead the derivatives of the $F(\lambda)$ with respect to λ. It is apparent that the transmission $F(\eta)$ exhibits a symmetrical to its value $\eta_c = \eta(\lambda_c) = (\alpha_1 + \alpha_2)/2$. η_c denotes the reciprocal of the optical beatlength at the centerwavelength λ_c.

$$\begin{aligned} F(\eta_c - x) &= 1 - \frac{C^2}{C^2 + (-x)^2}\sin^2\left(L\sqrt{C^2 + (-x)^2}\right) \\ &= 1 - \frac{C^2}{C^2 + x^2}\sin^2\left(L\sqrt{C^2 + x^2}\right) \\ &= F(\eta_c + x) \end{aligned} \tag{2.17}$$

Thus, all odd order derivatives of $F(\lambda)$ are zeros. Then, it is sufficient to start with the second order derivative of $F(\lambda)$. After simple calculations, the second order

derivative of $F(\lambda)$ at the center wavelength is obtained as

$$\begin{aligned}\left.\frac{d^2F(\lambda)}{d\eta^2(\lambda)}\right|_{\eta(\lambda_c)} =& \frac{-128C^4\sigma^2}{(4C^2+\sigma^2)^5}\sin^2\left(L\sqrt{C^2+\frac{\sigma^2}{4}}\right)\\ &\times\left(L(4C^2+\sigma^2)\cos\left(L\sqrt{C^2+\frac{\sigma^2}{4}}\right)-2\sqrt{4C^2+\sigma^2}\sin\left(L\sqrt{C^2+\frac{\sigma^2}{4}}\right)\right)^2\\ &-\frac{16C^2}{(4C^2+\sigma^2)^4}\left(2C^2+\sigma^2+2C^2\cos\left(L\sqrt{4C^2+\sigma^2}\right)\right)\\ &\times\left(-8C^2+6\sigma^2+(-6\sigma^2+L^2\sigma^4+8C^2+4C^2L^2\sigma^2)\cos(L\sqrt{4C^2+\sigma^2})\right)\\ &-\frac{64LC^2}{(4C^2+\sigma^2)^{\frac{7}{2}}}(2C^2+\sigma^2+2C^2\cos(L\sqrt{4C^2+\sigma^2}))(C^2-\sigma^2)\\ &\times\sin(L\sqrt{4C^2+\sigma^2}) \end{aligned} \tag{2.18}$$

To obtain the maximally flat stopband filter, σ is chosen to satisfy the following condition.

$$\left.\frac{d^2F}{d\eta^2}\right|_{\eta=\eta_c}=0 \tag{2.19}$$

Equation (2.19) involves transcendental functions. For any given values of C and L, its roots can be obtained numerically. However, only the smallest positive root of (2.19), denoted as σ_0, can be used to form a flat stopband. It is clearly that for any pairs of C and L, there is always an optimized σ_0 to guarantee maximally flatness of the system transmission. The second order derivatives of the transmission for different C and L are plotted in Fig.2.8. Further examination shows that the stopband filter is actually third order maximally flat. Only for some special isolated value of C and L, it is possible that $\left.\frac{d^2F(\lambda)}{d\eta^2(\lambda)}\right|_{\eta=\eta_c}=0$ and $\left.\frac{d^4F(\lambda)}{d\eta^4(\lambda)}\right|_{\eta=\eta_c}=0$ to hold simultaneously.

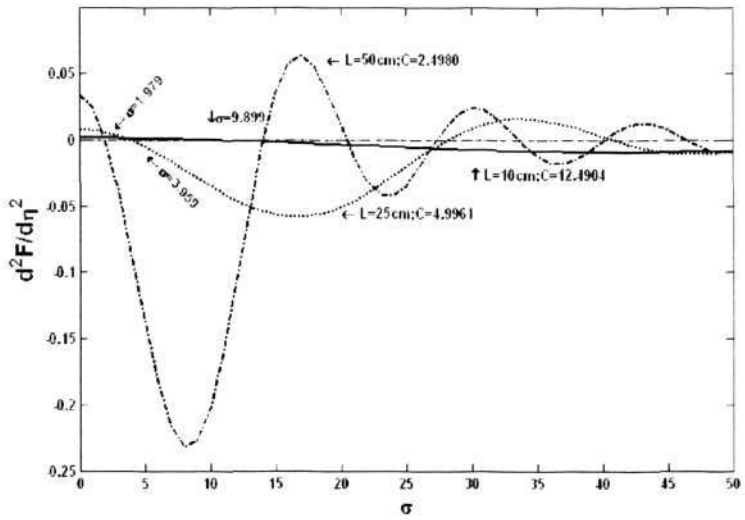

Figure 2.8: Second order derivatives of the transmission F with respect to σ.

Substituting $m = CL$ and $\beta = \sigma L$ into (2.18), gives

$$\begin{aligned}\left.\frac{d^2F(\lambda)}{d\eta^2(\lambda)}\right|_{\eta(\lambda_c)} = &-\frac{128m^4\beta^2}{L^2(4m^2+\beta^2)^5}\sin^2\left(L\sqrt{m^2+\frac{\beta^2}{4}}\right)\\ &\times\left((4m^2+\beta^2)\cos\left(\sqrt{m^2+\frac{\beta^2}{4}}\right)-2\sqrt{4m^2+\beta^2}\sin\left(\sqrt{m^2+\frac{\beta^2}{4}}\right)\right)^2\\ &-\frac{16m^2}{L^2(4m^2+\beta^2)^4}\left(2m^2+\beta^2+2m^2\cos\left(\sqrt{4m^2+\beta^2}\right)\right)\\ &\times\left(-8m^2+6\beta^2+(-6\beta^2+\beta^4+8m^2+4m^2\beta^2)\cos(\sqrt{4m^2+\beta^2})\right)\\ &-\frac{64m^2}{L^2(4m^2+\beta^2)^{\frac{7}{2}}}(2m^2+\beta^2+2m^2\cos(\sqrt{4m^2+\beta^2}))(m^2-\beta^2)\\ &\times\sin(\sqrt{4m^2+\beta^2})\end{aligned} \tag{2.20}$$

m indicates the maximum optical isolation of the notch transmission produced by each AF-AOTF. For any given value of m, $\sigma_0 L$ is constant. The relationship between $\sigma_0 L$ and CL is shown in Fig.2.9.

The design rule of σ mentioned above is based on the consideration of the flatness of

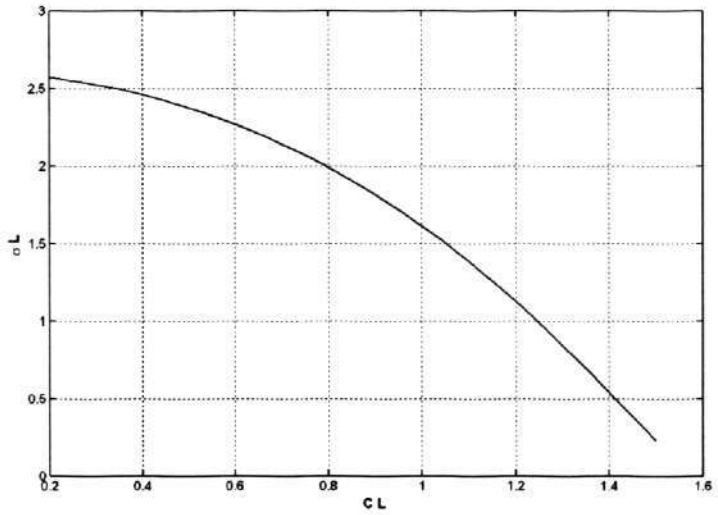

Figure 2.9: Relationship between $\sigma_0 L$ and CL for the maximally flat stopband filter.

the overall transmission. However, there are some other performance requirements such as isolation, roll off factor and bandwidth on the overall transmission. These requirements must be considered in the design process of the filter. Thus, it is necessary to discuss the optimization of C and L under the maximum flatness constraint (2.19). Substituting $\eta = \alpha_1 + \sigma/2 = \alpha_2 - \sigma/2$ into (2.13), the isolation of the stopband transmission, defined as the isolation of the filter at the centerwavelength λ_c, can be expressed as

$$\begin{aligned} G(\lambda_c) &= -10\log\left(F(\lambda_c)\right) \\ &= -20\log\left(1 - C^2\frac{\sin^2\left(L\sqrt{C^2+\sigma^2/4}\right)}{C^2+\sigma^2/4}\right) \end{aligned} \tag{2.21}$$

Let $G(\lambda_c) = -10\log(I_d)$, where I_d is the desired stopband isolation and $I_j = 10^{(-j/10)}$ is the attenuation corresponding to jdB isolation. For any given value of CL, the required value of σL to achieve the desired isolation I_d is a constant. It denoted as

$\sigma_p L$ to distinguish with the $\sigma_0 L$ mentioned above. Denote

$$x = \sqrt{L^2C^2 + \sigma_p^2 L^2/4}; \tag{2.22}$$

Through (2.21), it can be obtained that

$$\frac{\sin^2(x)}{x^2} = \frac{1 - \sqrt{I_d}}{C^2 L^2} \tag{2.23}$$

(2.23) can be numerically solved. The optimized σ_p is

$$\sigma_p L = 2\sqrt{x_0^2 - L^2C^2} \tag{2.24}$$

where x_0 is he root of equation (2.23) for given CL. The required $\sigma_p L$ can be calculated for different CL. To simultaneously achieve maximally flat stopband and desired optical isolation, it is required that $\sigma_0 = \sigma_p$. Thus, the optimal value of CL occurs at the cross point of $\sigma_0 L$ and $\sigma_p L$ as shown in Fig.2.10.

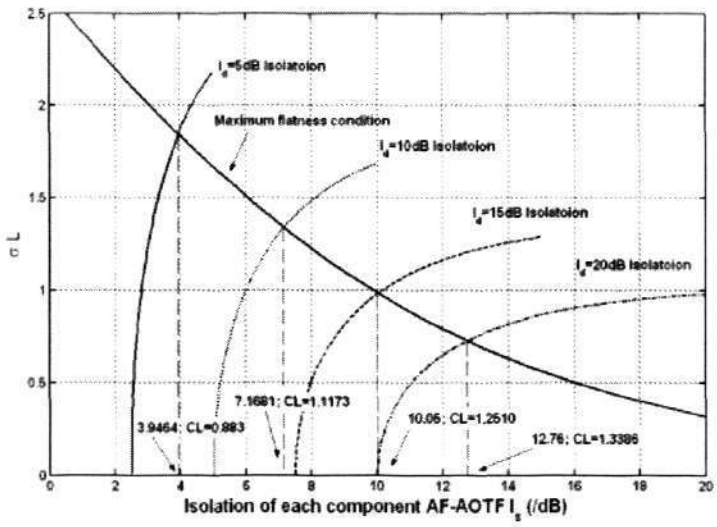

Figure 2.10: The optimized value of σL for the AF-AOTFs with different isolation.

Next the bandwidth of the designed optical tunable stopband filter is examined. It is usually evaluated by the width of the system spectral line (in frequency or wavelength) between the points where the filter transmission reaches the desired xdB isolation. The $-xdB$ bandwidth of the designed optical filter is obtained as follows: By expanding $F(\lambda)$ to Taylor series at the centerwavelength of the filter and retaining the term lower than fourth order, it is obtained that:

$$\begin{aligned} F(\eta) &= F(\eta_c) + \left.\frac{dF(\eta)}{d\eta}\right|_{\eta=\eta_c}(\eta-\eta_c) + \frac{1}{2!}\left.\frac{d^2F(\eta)}{d\eta^2}\right|_{\eta=\eta_c}(\eta-\eta_c)^2 \\ &+ \frac{1}{3!}\left.\frac{d^3F(\eta)}{d\eta^3}\right|_{\eta=\eta_c}(\eta-\eta_c)^3 + \frac{1}{4!}\left.\frac{d^4F(\eta)}{d\eta^4}\right|_{\eta=\eta_c}(\eta-\eta_c)^4 \end{aligned} \tag{2.25}$$

For the maximally flat stopband filter, the following equations are satisfied.

$$\begin{aligned} \left.\frac{dF(\eta)}{d\eta}\right|_{\eta=\eta_c} &= 0 \\ \left.\frac{d^2F(\eta)}{d\eta^2}\right|_{\eta=\eta_c} &= 0 \\ \left.\frac{d^3F(\eta)}{d\eta^3}\right|_{\eta=\eta_c} &= 0 \end{aligned} \tag{2.26}$$

(2.25) is reduced to

$$F(\eta) = F(\eta_c) + \frac{1}{4!}\left.\frac{d^4F(\eta)}{d\eta^4}\right|_{\eta=\eta_c}(\eta-\eta_c)^4 \tag{2.27}$$

Denote

$$F(\eta_x) = I_x \tag{2.28}$$

$$F(\eta_c) = I_d \tag{2.29}$$

where η_x denotes the value of η at the wavelength where the filter have xdB isolation.

$$\eta_x = \left(\frac{4!(I_x - I_d)}{\left.\frac{d^4F(\eta)}{d\eta^4}\right|_{\eta=\eta_c}} \right)^{(1/4)} + \eta_c \tag{2.30}$$

The $-xdB$ bandwidth $\triangle\lambda$ can be expressed as

$$\begin{aligned} \triangle\lambda &= \frac{2\eta_x}{\frac{\partial\eta}{\partial\lambda}} \\ &= \frac{2\left(\left(\frac{4!(I_x - I_d)}{\left.\frac{d^4F(\eta)}{d\eta^4}\right|_{\eta=\eta_c}} \right)^{(1/4)} + \eta_c \right)}{\frac{\partial\eta}{\partial\lambda}} \end{aligned} \tag{2.31}$$

For stopband filter, another important index often used to evaluate the performance is the shape factor. Usually, the shape factor is defined as the desired $-xdB$ bandwidth over $-3dB$ bandwidth

$$Q = \frac{\Delta\lambda_x}{\Delta\lambda_3} \tag{2.32}$$

Substituting (2.31) into (2.32), the shape factor of the designed filter can be simply obtained as

$$Q = \frac{\left(\frac{4!(I_x - I_d)}{\left.\frac{d^4F(\eta)}{d\eta^4}\right|_{\eta=\eta_c}} \right)^{(1/4)} + \eta_c}{\left(\frac{4!(I_3 - I_d)}{\left.\frac{d^4F(\eta)}{d\eta^4}\right|_{\eta=\eta_c}} \right)^{(1/4)} + \eta_c} \tag{2.33}$$

For any required shape factor Q_d, the fourth order derivative can be calculated as

$$\left.\frac{d^4F(\eta)}{d\eta^4}\right|_{\eta=\eta_c} = \left(\frac{Q(4!(I_3 - I_d))^{1/4} - (4!(I_x - I_d))^{1/4}}{\eta_c(1-Q)} \right)^4 \tag{2.34}$$

The value of $\frac{d^4F(\eta)}{d\eta^4}$ can be calculated as

$$\begin{aligned}\left.\frac{d^4F(\lambda)}{d\eta^4(\lambda)}\right|_{\eta(\lambda_c)} = &-\frac{64C^2}{(4C^2+\sigma^2)^6}((384C^8L^2-\sigma^6(120-36L^2\sigma^2+L^4\sigma^4)\\ &-32C^6(-24+51L^2\sigma^2+L^4\sigma^4)-16C^4\sigma^2(-96+51L^2\sigma^2+2L^4\sigma^4)\\ &+C^2(624\sigma^4+48L^2\sigma^6-10L^4\sigma^8))\cos(L\sqrt{4C^2+\sigma^2})+4(-48C^6\\ &-504C^4\sigma^2-147C^2\sigma^4-24C^4L^2\sigma^4-32C^6L^4\sigma^4+30\sigma^6+12C^2L^2\sigma^6\\ &-16C^4L^4\sigma^6-2C^2L^4\sigma^8+3C^2(32C^6L^2+40C^2\sigma^2-3\sigma^4\\ &+8C^4(-6+L^2\sigma^2))\cos(2L\sqrt{4C^2+\sigma^2})-2L\sqrt{4C^2+\sigma^2}(12\sigma^6-L^2\sigma^8\\ &+2C^4\sigma^2(-135+L^2\sigma^2)+12C^6(1+2L^2\sigma^2)-C^2\sigma^4(36+5L^2\sigma^2))\\ &\sin(L\sqrt{4C^2+\sigma^2})-108C^6L\sqrt{4C^2+\sigma^2}\sin(2L\sqrt{4C^2+\sigma^2})\\ &+36C^4L\sigma^2\sqrt{4C^2+\sigma^2}\sin(2L\sqrt{4C^2+\sigma^2})))\end{aligned} \tag{2.35}$$

From (2.24), (2.12) and (2.34), the optimized values of σ_0, C and L can be calculated. The values of α_1 and α_2 corresponding to σ can be obtained as

$$\alpha_1 = \eta(\lambda_c) - \frac{\sigma_o}{2} \quad \text{and} \quad \alpha_2 = \eta(\lambda_c) + \frac{\sigma_o}{2} \tag{2.36}$$

The design of AF-AOTF with maximally flat stopband transmission is summarized as follows.

Design scheme for AF-AOTF based maximally flat stopband transmission

Step.1 Calculate η_c, shape factor Q and optical isolation I_d of the desired optical filter.

Step.2 Calculate the optimal phase mismatch difference $\sigma_0 L$ for different value of CL under the flatness condition.

Step.3 Calculate the required optimal phase mismatch difference $\sigma_p L$ for different value of CL to achieve desired stopband isolation.

Step.4 Obtain the optimal value of isolation of each AF-AOTF m_o by solve the equation $\sigma_0 = \sigma_p$ or find the cross point in the Fig.2.10.

Step.5 From (2.32) and (2.34) calculate the value of fourth order derivative $\left.\frac{d^4F(\eta)}{d\eta^4}\right|_{\eta=\eta_c}$ at the centerwavelength λ_c.

Step.6 Obtain the optimal AO interaction length L and AO coupling coefficient C to achieve the desired bandwidth under the condition $CL = m_o$. Next, calculate the corresponding phase mismatching difference σ_0 by solving equation (2.19).

For the general case of using multi-stage AF-AOTF to implement the flat stopband filter, the design can be separated to several two-stage stopband filter design. Thus, for simplicity, we only consider the design of flat stopband transmission by using two AF-AOTF stages without loss of generality. To see the key parameters in the transmission design, we consider a numerical example of designing a maximally flat stopband filter with $-5dB$ isolation. From (2.20), the optimal value of CL is 0.883. The AO interaction length L is set from 10cm to 60cm with an increment of 10cm. The corresponding AO interaction length and required phase mismatch is calculated according to the design scheme mentioned above. The corresponding transmission is shown in Fig.2.11. It shows that the variation of the AO interaction

length L only changes the stopband bandwidth, when the isolation of the maximal flat stopband filter is fixed at $-5dB$. Fig.2.12 shows the maximal flat stopband filter

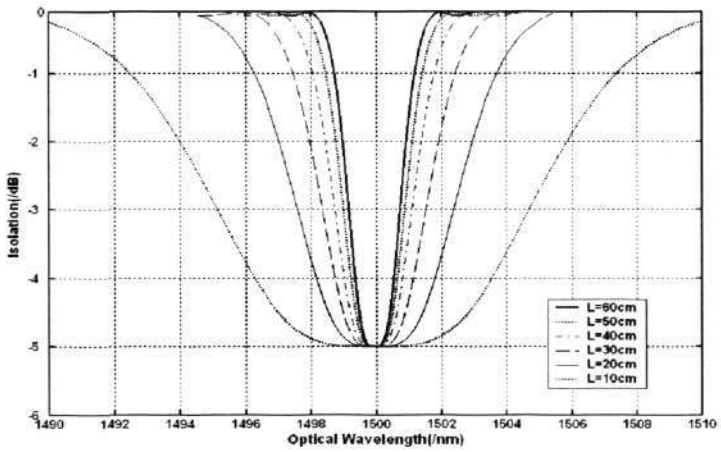

Figure 2.11: Transmission of maximal flat stopband filters with different bandwidths but same transmission isolation of $-5dB$.

design for different transmission isolation of $-5dB$, $-10dB$ and $-15dB$ using the proposed design scheme. The corresponding optimal values of CL are 0.883, 1.1173 and 1.250. In all of these three filter design, the AO interaction length L are set as $60cm$. The corresponding σ_0 are numerically obtained as 3.0785, 2.2342 and 1.6453, respectively.

From the design of maximally flat stopband filter, it is identified that the values of phase mismatch difference σ, AO coupling coefficient C and AO interaction length L are solely determined by the parameters of the desired transmission such as flatness, isolation and bandwidth. In the same time, if the value of σ, C and L are given, the composite transmission is also solely determined.

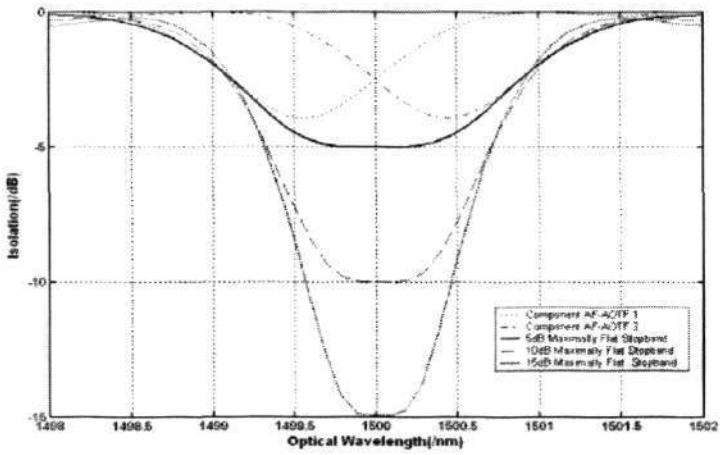

Figure 2.12: Transmission of maximal flat stopband filters with different transmission isolations.

2.4.2 Tunability of Multiple-Stage AF-AOTF.

So the parameters that determine the transmission profile have been discussed. Next, we analyze how they change when the obtained complex transmission is tuned from one position to another position along the optical axis. It is well known that the notch profile of single-stage AF-AOTF can be controlled electronically by the frequency and the amplitude of its driving RF signal. The details of the relationship between the notch profile and the control variables can be found in Appendix.C. Then, the realization of tunable complex transmission looks quite simple: simultaneously tuning all single-stage AF-AOTFs in the same manners.

In the tuning process of multi-stage AF-AOTF, however, the unwanted transmission distortion will occur if no special treatment is taken. The cause of this distortion primarily comes from the following aspects:

✓ First of all, as shown in equation (2.5), the notch transmission profile of AF-AOTF depends on the mismatch of two major characteristic parameters: the optical mode beatlength and the acoustic wavelength. These two parameters

are determined by a number of complicated factors such as applied RF signal frequency, fiber composition, fiber dimensions, fiber optical characteristic and PZT acoustic property (e.g. mechanical impedance). The dependence of a notch transmission on the control variables of an AF-AOTF is a multi-variable nonlinear function. Since the complex transmission of a multi-stage of AF-AOTF is actually the composition of all notch transmissions, the synchronization of all AF-AOTFs to maintain the desired composite transmission during the tuning process requires solving nonlinear equations for any wavelength in the tuning range. This is quite difficult to be implemented in practice.

- ✓ The second cause of the overall transmission deformation is the nonlinearity in the PZT acoustic response. The PZT has unequal response with respect to the driving RF signal frequency. When the transmission is tuned from one wavelength to another, the frequencies of each driving RF signals are changed. However, the acoustic amplitudes of different acoustic frequency elements vary not in the same manners. Some notch transmissions are enhanced while the others are weakened. As a result, the overall transmission will be distorted.

- ✓ Finally, due to the fabrication and manufacturing accuracy, the acoustic and optical properties of different AF-AOTFs are not identical. As a result, the variations of the notch transmission of different AF-AOTFs with respect to the optical wavelength are not identical as well.

Clearly, given a desired transmission, the design parameters depend on the position of the desired transmission. When the designed transmission is tuned to a new position, all the parameters need to be recalculated in order to maintain the desired transmission. However, due to the reasons mentioned above, the nonlinear manners in which the control variables of the AF-AOTFs affect the composite transmission make the recalculation time consuming. As a result, the time response performance of the optical filter is deteriorated. Furthermore, separately control each AF-AOTF

requires a lot of accessory control and measurement components such as electronic calculation modules and optical detectors, which are used to implement the synchronization between different AF-AOTF in the system calibration and tuning process. These accessory components will make the whole system quite expensive.

Therefore, in practice, one hopes that the desired transmission can be tuned in a simple and cost effective manner like this: The overall complex transmission is tuned by adding a simple increment to each adjustable parameter, just like operating a single-stage AF-AOTF. But the system transmission must maintain the same profile during the tuning process mentioned above. This gives rise to the tunability of the composite transmission, which defines the transmission distortions when the transmission is tuned to a new wavelength through the simple tuning method mentioned above.

2.4.3 Measure of the Tunability of Multi-stage AF-AOTF

To achieve an automatic synchronization control, a measure is needed to evaluate the transmission distortion during the tuning process. For certain complex transmission, there are many choices of the tunability measure used to evaluate the transmission distortion, for example, the transmission distortion of the bandstop or bandpass filter can be evaluated by the ripple or the bandwidth. However, if multi-stage AF-AOTF is used to deliver some other transmissions such as the enhanced notch profile, ripple and bandwidth are obviously inefficient. Therefore, the measure of the tunability must be chosen from the general parameters in the model of multi-stage AF-AOTF.

As shown in Section 2.4.1, the composite transmission is solely determined by the phase mismatching difference σ, AO coupling coefficient C and AO interaction length L. Since L is usually fixed for AF-AOTF and C is mainly used to control the isolation

of the notch, the tunability of the composite transmission can be reasonably assessed by the sensitivity of the phase-mismatch difference σ with respect to the control variables of AF-AOTF.

Without loss of generality, we assume that the phase-mismatch difference at the central wavelength λ_c is chosen exactly as the optimal phase-mismatch difference as in the design of the maximally flat stopband transmission shown in Section 2.4.1, that is, $\sigma(\lambda_c') = \sigma_0$. Denote the phase-mismatch difference obtained at the new wavelength λ_c' as $\sigma(\lambda_c')$. Then, we evaluate a phase-mismatch error $\Delta\sigma$ defined by

$$\begin{aligned} \Delta\sigma &\triangleq \sigma(\lambda_c') - \sigma(\lambda_c) \\ &= \sigma(\lambda_c') - \sigma_0 \end{aligned} \tag{2.37}$$

The value of σ_0 is determined by the requirement on the complex transmission. For a given transmission, the optimized value σ_0 is independent of wavelength where the filter is operating. During the whole tuning process, σ_0 should be a constant in order to obtain the desired transmission. For example, during the design process of the tunable maximally flat bandstop transmission shown in Section 2.4.1, the value of σ_0 in (2.19) and σ_p in (2.24) are only determined by AO coupling efficiency and AO interaction length. As long as the phase mismatch difference takes this value, a flat stopband transmission is obtained regardless of where the central wavelength of the stopband is.

The reasons for using $\Delta\sigma$ as the tunability measure of AF-AOTF transmission deformation are summarized as follows

- Phase mismatch error is suitable to quantitatively evaluate the tunability of multi-stage AF-AOTF with any transmission profile, either the bandstop filter or bandpass filter, either the notch filter or the EDFA gain equalization filter.

- The definition of phase mismatch error is independent of the control variables and the tuning mechanisms of the multi-stage AF-AOTF. No matter the tuning process of the filter is implemented through the control of the driving RF signal or the control of the strain in the fiber, phase mismatch error can always quantitively evaluate the tunability of the system.
- The relationship between the overall transmission deformation and the phase mismatch error is solely determined.
- Phase mismatch error has high sensitivity to the system overall transmission deformation.
- Phase mismatch error is independent of the AO interaction medium and the structure of AF-AOTF. No matter the AF-AOTFs are fabricated from single mode fiber, multi-mode fiber or fiber coupler structure, the definition of phase mismatch is same.
- The calculation of the phase mismatch error is simple.

2.5 Conclusion

Multi-stage AF-AOTF is used to provide tunable complex transmission required by all-optical networks. But the obtained complex transmission is a composition of all notch transmissions, each of whom is introduced by one AO interaction stage. The tuning of this composite transmission is implemented by simultaneously controlling all AO interaction stages. However, due to the nonlinearity in the system operation process and manufacturing limitation, the complex transmission is distorted when it is being tuned. It results in unwanted system performance degradation. This chapter addresses the tunability of the composite transmission, which represents

the distortion of the composite transmission being tuned. A quantitative measure of the tunability is well defined for the first time.

Chapter 3

Tunability Improvement of Multi-stage AF-AOTF by Strain Control

3.1 Introduction

Multi-stage AF-AOTF has become a promising means to provide tunable complex transmissions. By integrating several AO interaction stages together, the obtained complex transmission is a composition of several notch transmissions. However, as shown in last chapter, the nonlinear dependence of the notch transmission on the control variables of AF-AOTF creates a difficulty in synchronizing all AO interactions to maintain the desired composite transmission while it is being tuned over a wide wavelength range. The distortions resulting from the nonlinearity become more serious when the tapered fiber is used to enhance the acousto-optical coupling efficiency [80, 81, 82].

In this chapter, we systematically develop a strain control scheme to improve the

tunability of the complex transmission produced by multi-stage AF-AOTF. Firstly in Section 3.2, we studied the strain effect on the tunability of the composite transmission by using traditional cascading AF-AOTFs subject to frequency difference control. It is shown in theory for the first time that by applying high axial strain on each AO fiber in the cascading AF-AOTFs, the tunability of the resultant composite transmission can be enhanced. For the sake of clarity, the proof is first derived by considering the use of two AF-AOTFs to design an optical filter with a composite flat-stopband transmission. In this case, the flatness of the composite transmission can be used to visually describe the transmission profile distortions due to the asynchronous tuning of AF-AOTFs. Through detailed mathematical derivations, the transmission profile distortion is proven to be a decreasing function of the strain, which in turn draws the derived conclusion. When more AF-AOTFs are cascaded, the tunability can be defined as an absolute sum of all differences between the phase mismatching coefficients of two adjacent component AF-AOTFs. Thus, the conclusion is still valid for the general case where more AF-AOTFs are cascaded to form a complex transmission. At the last of this section, simulation results of the maximally flat bandstop transmissions by a two-stage and a four-stage AF-AOTF are reported to verify the theoretical conclusion.

Secondly in Section 3.3, the strain difference control scheme is developed to improve the tunability. In this scheme, the desired overall transmission is realized by applying different but constant strain on the fiber in each AO interactions in multi-stage AF-AOTF. Unlike the frequency difference control scheme, the acoustic frequency is only used to change the position of the whole composite transmission profile. The tunability of the multi-stage AF-AOTF subject to the proposed scheme is evaluated and compared with those subject to the frequency difference control scheme for the same application case. It is shown analytically that the composite transmission obtained by the strain difference control scheme can be maintained better than those obtained by the frequency difference control schemes. To verify the theoretical

analysis, simulation and experimental studies are done based on a two stage AF-AOTF to deliver the maximally flat stopband transmission.

3.2 Tunability Improvement by Incorporating Strain Control with Frequency Difference Control Scheme

In the traditional multi-stage AF-AOTF design, all AO interactions are driven by the RF signals with different frequencies to superpose the desired complex transmission profile. During the tuning process of the composite complex transmission, the frequencies of the driving RF signals of all AF-AOTFs are equally increased or decreased to shift the composite transmission profile along the optical wavelength. This operation has taken into account of the conveniences of tuning multi-stage AF-AOTF in practice.

To see the strain control principle, the dependence of the composite transmission on an axial strain is derived first. Without loss of generality, we consider the use of two stages of AF-AOTFs to implement a tunable flat-stopband transmission. The reason of using such a transmission is the same as that shown in Section 2.4.1 because any composite transmission can always be expressed as weighted summation of several flat stopband transmissions. When more AF-AOTFs are integrated together, the tunability can be defined as an absolute sum of all differences between the phase mismatching coefficients of two adjacent component AF-AOTFs. Thus, the conclusion is still valid for the general case where more AF-AOTFs are cascaded to form any complex transmission.

3.2.1 Transmission of Two-stage AF-AOTFs Subject to Frequency Difference Control With Strain Control

In this case, the transmission of the multi-stage AF-AOTF is expressed by the model obtained in (2.6) and (A.12). The design problem of using AF-AOTF to implement a composite transmission profile can be described as choosing appropriate parameters, including f_i and s_i, so that the resultant composite transmission profile has the required shape. The tunability of the composite transmission profile can thus be assessed by analyzing the sensitivity of the transmission profile with respect to the design parameters.

Here, the value of C is obtained by assuming that employed PZTs can provide enough high and stable AO coupling efficiency. This assumption is reasonable when the required isolation of the filter is in a range of relative small values. All AF-AOTFs are assumed to be made from same type of fiber. To build the desired stopband transmission profile, the two AF-AOTFs are fabricated with the same AO lengths and the same AO coefficients, i.e. $L_1 = L_2 = L$ and $C_1 = C_2 = C$ without loss of generality. For the sake of simplicity, the axial strain on these AF-AOTFs are assumed to be the same, i.e. $s_1 = s_2 = s$. Substituting (A.12) and (2.7) into (2.12) gives

$$\begin{aligned} \sigma &= \alpha_2 - \alpha_1 \\ &= \frac{\pi\sqrt{2}f_2}{\sqrt{\sqrt{s^2 + \frac{4\pi^2 r^2 f_2^2}{C_{ext}^2}} + sC_{ext}}} - \frac{\pi\sqrt{2}f_1}{\sqrt{\sqrt{s^2 + \frac{4\pi^2 r^2 f_1^2}{C_{ext}^2}} + sC_{ext}}} \end{aligned} \tag{3.1}$$

Substituting (A.12) into (2.36), the corresponding acoustic frequencies f_1 and f_2 are

$$\begin{aligned} f_1(\sigma_0, \lambda_c) &= C_{ext}\left(\eta(\lambda_c) - \tfrac{\sigma_0}{2}\right)\sqrt{s + \pi^2 r^2\left(\eta(\lambda_c) - \tfrac{\sigma_0}{2}\right)^2} \\ f_2(\sigma_0, \lambda_c) &= C_{ext}\left(\eta(\lambda_c) + \tfrac{\sigma_0}{2}\right)\sqrt{s + \pi^2 r^2\left(\eta(\lambda_c) + \tfrac{\sigma_0}{2}\right)^2} \end{aligned} \tag{3.2}$$

With these RF frequencies, the cascading AF-AOTFs forms an optical filter that has the desired stopband transmission profile with the center wavelength of λ_c. The tuning process of the traditional frequency difference control scheme is implemented simply as shifting the central wavelength of the transmission from wavelength λ_c to other wavelength position λ_c' by adding an identical increment Δf to both f_1 and f_2, while the strain s maintained unchanged.

3.2.2 Tunability of Multi-stage AF-AOTF Subject to Frequency Difference Control and Strain Control

At the position where the maximum stopband transmission profile is initially designed, the phase mismatching difference is chosen exactly as the optimal phase mismatch difference, that is, $\sigma(\lambda_c) = \sigma_0$. In order to maintain the desired transmission at other wavelength, the required value of the phase mismatch difference should be σ_0 as well.

However, the value of σ shifts away from its optimal value σ_0 when the composite transmission shifts from λ_c to λ_c'. The transmission profile at the λ_c' results from tuning the system transmission designed at λ_c by maintaining a constant RF frequency difference $\Delta f(\sigma_0, \lambda_c)$.

Denote the phase mismatch difference obtained at the new wavelength λ_c' as $\sigma(\lambda_c')$. Then, the frequency difference control scheme specifies

$$f_1(\sigma(\lambda_c'), \lambda_c') - f_2(\sigma(\lambda_c'), \lambda_c') = \Delta f(\sigma_0, \lambda_c) = f_1(\sigma_0, \lambda_c) - f_2(\sigma_0, \lambda_c). \tag{3.3}$$

Equation (3.2) shows that in order to obtain a phase mismatching difference $\sigma(\lambda_c')$ at wavelength λ_c', two RF frequencies $f_1(\sigma(\lambda_c'), \lambda_c')$ and $f_2(\sigma(\lambda_c'), \lambda_c')$ shall take values

given by

$$\begin{aligned} f_1(\sigma(\lambda_c'),\lambda_c') &= C_{ext}\left(\eta(\lambda_c')-\tfrac{\sigma(\lambda_c')}{2}\right)\sqrt{s+\pi^2r^2\left(\eta(\lambda_c')-\tfrac{\sigma(\lambda_c')}{2}\right)^2} \\ f_2(\sigma(\lambda_c'),\lambda_c') &= C_{ext}\left(\eta(\lambda_c')+\tfrac{\sigma(\lambda_c')}{2}\right)\sqrt{s+\pi^2r^2\left(\eta(\lambda_c')+\tfrac{\sigma(\lambda_c')}{2}\right)^2} \end{aligned} \tag{3.4}$$

Substituting (3.2) and (3.4) into (3.3) and re-arranging terms, the phase mismatch error $\Delta\sigma$ defined in (2.37) can be expressed as

$$\Delta\sigma = \frac{\sqrt{-s+\sqrt{s^2+4\pi^2r^2\left(v\sqrt{s+\pi^2r^2v^2}+u\sqrt{s+\pi^2r^2u^2}-\psi\sqrt{s+\pi^2r^2\psi^2}\right)^2}}}{\sqrt{2}\pi r} - \tau \tag{3.5}$$

where

$$\begin{aligned} \psi &= \eta(\lambda_c)-\frac{\sigma_0}{2} \\ u &= \eta(\lambda_c)+\frac{\sigma_0}{2} \\ v &= \eta(\lambda_c')-\frac{\sigma_0}{2} \\ \tau &= \eta(\lambda_c')+\frac{\sigma_0}{2} \end{aligned}$$

Clearly, the phase mismatch error $\Delta\sigma$, representing the transmission profile distortions, is determined by the axial strain s. As shown in following parts of this section, $\Delta\sigma$ has the following properties.

Property.1

if η is increasing function with respect to optical wavelength λ,

$$\begin{cases} \Delta\sigma > 0 & \text{if } \lambda_c > \lambda_c' \\ \Delta\sigma < 0 & \text{if } \lambda_c < \lambda_c' \end{cases} \tag{3.6}$$

if η is decreasing function with respect to optical wavelength λ,

$$\begin{cases} \Delta\sigma < 0 & \text{if } \lambda_c > \lambda_c' \\ \Delta\sigma > 0 & \text{if } \lambda_c < \lambda_c' \end{cases} \tag{3.7}$$

Property.2

$$|\Delta\sigma| \text{ is a decreasing function of } s. \tag{3.8}$$

Therefore, it can be concluded that the tunability of a composite transmission profile resulted from cascading AF-AOTFs can be improved by applying axial strain s on the AO fibers. This conclusion can be extended to a general case where more AF-AOTF stages are cascaded to form a composite transmission profile. In this case, it suffices to define a phase-mismatch error as follows:

$$\Delta\sigma = \sum_{i=1}^{n-1} |\sigma_i(\lambda_c') - \sigma_i(\lambda_c)| \tag{3.9}$$

where n denotes the number of cascaded AF-AOTFs and $\sigma_i(\lambda)$ denotes the difference between the phase mismatch coefficients of the ith and $i+1$th AF-AOTF. The central wavelength of the composite transmission is located at λ.

3.2.3 Proof of Property.1 in (3.6) and (3.7)

Before proving the main result, several useful inequalities that can be easily verified are presented first. For any real numbers x, y and s such that $s >= 0$ and $x > y$,

the following inequalities are satisfied:

$$\frac{x^2}{s+\sqrt{s^2+x^2}} > \frac{y^2}{s+\sqrt{s^2+y^2}} \tag{3.10}$$

$$x\sqrt{s^2+x^2} > y\sqrt{s^2+y^2} \tag{3.11}$$

$$\frac{x^2}{\sqrt{s^2+x^2}} > \frac{y^2}{\sqrt{s^2+y^2}} \tag{3.12}$$

$$x\sqrt{s+\pi^2r^2x^2}-(x-\Delta)\sqrt{s+\pi^2r^2(x-\Delta)^2} > y\sqrt{s+\pi^2r^2y^2}-(y-\Delta)\sqrt{s+\pi^2r^2(y-\Delta)^2} \quad \text{for } 2x>\Delta>0 \tag{3.13}$$

$$x\sqrt{s+\pi^2r^2x^2}-(x-\Delta)\sqrt{s+\pi^2r^2(x-\Delta)^2} < y\sqrt{s+\pi^2r^2y^2}-(y-\Delta)\sqrt{s+\pi^2r^2(y-\Delta)^2} \quad \text{for } \Delta<0 \tag{3.14}$$

The sign of $\Delta\sigma$ is examined. For easy reference, the expression of $\Delta\sigma$ is rewrote as follows:

$$\Delta\sigma = \frac{\sqrt{-s+\sqrt{s^2+4\pi^2r^2\left(v\sqrt{s+\pi^2r^2v^2}+u\sqrt{s+\pi^2r^2u^2}-\psi\sqrt{s+\pi^2r^2\psi^2}\right)^2}}}{\sqrt{2}\pi r} - \tau \tag{3.15}$$

where

$$\psi = \eta(\lambda_c) - \frac{\sigma_0}{2} \tag{3.16}$$

$$u = \eta(\lambda_c) + \frac{\sigma_0}{2} \tag{3.17}$$

$$v = \eta(\lambda_c') - \frac{\sigma_0}{2} \tag{3.18}$$

$$\tau = \eta(\lambda_c') + \frac{\sigma_0}{2} \tag{3.19}$$

The sign of $\Delta\sigma$ can be evaluated through examining the sign of $\sqrt{2}\pi r\Delta\sigma$. It can clearly be expressed as $\sqrt{2}\pi r\Delta\sigma = A - B$, where A and B are defined as

$$A = \sqrt{-s + \sqrt{s^2 + 4\pi^2 r^2 \left(v\sqrt{s + \pi^2 r^2 v^2} + u\sqrt{s + \pi^2 r^2 u^2} - \psi\sqrt{s + \pi^2 r^2 \psi^2}\right)^2}} \tag{3.20}$$

$$B = \sqrt{2}\pi r\tau \tag{3.21}$$

Thus, the sign of $\Delta\sigma$ can be judged by comparing A^2 and B^2. Using the definitions of A and B, it is readily to see that

$$\begin{aligned} A^2 &= \frac{4\pi^2 r^2 \left(v\sqrt{s + \pi^2 r^2 v^2} + u\sqrt{s + \pi^2 r^2 u^2} - \psi\sqrt{s + \pi^2 r^2 \psi^2}\right)^2}{s + \sqrt{s^2 + 4\pi^2 r^2 \left(v\sqrt{s + \pi^2 r^2 v^2} + u\sqrt{s + \pi^2 r^2 u^2} - \psi\sqrt{s + \pi^2 r^2 \psi^2}\right)^2}} \\ &= \frac{\left(2\pi r(v\sqrt{s + \pi^2 r^2 v^2} + u\sqrt{s + \pi^2 r^2 u^2} - \psi\sqrt{s + \pi^2 r^2 \psi^2})\right)^2}{s + \sqrt{s^2 + \left(2\pi r(v\sqrt{s + \pi^2 r^2 v^2} + u\sqrt{s + \pi^2 r^2 u^2} - \psi\sqrt{s + \pi^2 r^2 \psi^2})\right)^2}} \end{aligned} \tag{3.22}$$

$$\begin{aligned} B^2 &= (\sqrt{2}\pi r\tau)^2 \\ &= \frac{2\pi^2 r^2\tau^2(s+\sqrt{s^2+4\pi^2r^2\tau^2(s+\pi^2r^2\tau^2)})}{s+\sqrt{s^2+4\pi^2r^2\tau^2(s+\pi^2r^2\tau^2)}} \\ &= \frac{2\pi^2 r^2\tau^2(s+\sqrt{(s+2\pi^2r^2\tau^2)^2})}{s+\sqrt{s^2+4\pi^2r^2\tau^2(s+\pi^2r^2\tau^2)}} \\ &= \frac{4\pi^2 r^2\tau^2(s+\pi^2r^2\tau^2)}{s+\sqrt{s^2+4\pi^2r^2\tau^2(s+\pi^2r^2\tau^2)}} \\ &= \frac{(2\pi r\tau\sqrt{s+\pi^2r^2\tau^2})^2}{s+\sqrt{s^2+(2\pi r\tau\sqrt{s+\pi^2r^2\tau^2})^2}} \end{aligned} \tag{3.23}$$

To proceed, $\Delta\eta$ is defined as $\Delta\eta = \eta(\lambda_c') - \eta(\lambda_c)$. From (3.16)-(3.19), it is immediately obtained that

$$\Delta\eta = v - \psi = \tau - u \tag{3.24}$$

Then

$$\begin{aligned} &2\pi r\left(v\sqrt{s+\pi^2r^2v^2}+u\sqrt{s+\pi^2r^2u^2}-\psi\sqrt{s+\pi^2r^2\psi^2}-\tau\sqrt{s+\pi^2r^2\tau^2}\right) \\ &= 2\pi r\left((v\sqrt{s+\pi^2r^2v^2}-\psi\sqrt{s+\pi^2r^2\psi^2})-(\tau\sqrt{s+\pi^2r^2\tau^2}-u\sqrt{s+\pi^2r^2u^2})\right) \\ &= 2\pi r(v\sqrt{s+\pi^2r^2v^2}-(v-\Delta\eta)\sqrt{s+\pi^2r^2(v-\Delta\eta)^2}) \\ &-2\pi r(\tau\sqrt{s+\pi^2r^2\tau^2}-(\tau-\Delta\eta)\sqrt{s+\pi^2r^2(\tau-\Delta\eta)^2}) \end{aligned} \tag{3.25}$$

Noted that $\eta(\lambda)$ is an increasing function of λ, for example, [55] for strong etched fiber based AF-AOTF. Thus, it is can be derived that when $\lambda_c > \lambda_c'$, $\Delta\eta < 0$. As σ_0 is always positive, $\tau > v$. Applying (3.14) on (3.25) gives

$$2\pi r\left(v\sqrt{s+\pi^2r^2v^2}+u\sqrt{s+\pi^2r^2u^2}-\psi\sqrt{s+\pi^2r^2\psi^2}\right) > 2\pi r\tau\sqrt{s+\pi^2r^2\tau^2} \tag{3.26}$$

Therefore, $A^2 > B^2$ can be concluded using the inequality in (3.10), which in turn

concludes that

$$\Delta\sigma > 0, \quad \text{if } \lambda_c > \lambda_c' \tag{3.27}$$

When $\lambda_c < \lambda_c'$, $\Delta\eta$ is positive. On the other hand, $\tau + u > 0$ gives $\tau - u < 2\tau$, and in turn, $\Delta\eta < 2\tau$. Using the fact $v < \tau$ and applying inequality (3.13) on (3.25), the following equation is deduced.

$$2\pi r\left(v\sqrt{s+\pi^2r^2v^2}+u\sqrt{s+\pi^2r^2u^2}-\psi\sqrt{s+\pi^2r^2\psi^2}\right) < 2\pi r\tau\sqrt{s+\pi^2r^2\tau^2} \tag{3.28}$$

Again, it follows from (3.10) that

$$\begin{aligned} & \frac{4\pi^2r^2\left(v\sqrt{s+\pi^2r^2v^2}+u\sqrt{s+\pi^2r^2u^2}-\psi\sqrt{s+\pi^2r^2\psi^2}\right)^2}{s+\sqrt{s^2+4\pi^2r^2\left(v\sqrt{s+\pi^2r^2v^2}+u\sqrt{s+\pi^2r^2u^2}-\psi\sqrt{s+\pi^2r^2\psi^2}\right)^2}} \\ < & \frac{(2\pi r\tau\sqrt{s+\pi^2r^2\tau^2})^2}{s+\sqrt{s^2+(2\pi r\tau\sqrt{s+\pi^2r^2\tau^2})^2}} \end{aligned} \tag{3.29}$$

Thus, the following conclusion can be drawn that when $\lambda_c < \lambda_c'$,

$$\Delta\sigma < 0. \tag{3.30}$$

Through similar derivation, the conclusion of (3.7) for the case $\eta(\lambda)$ is an decreasing function of λ can be simply proved.

3.2.4 Proof of Property 2 in (3.8)

To prove the conclusion, the following denotations are introduced:

$$f(s) = \sqrt{s^2 + 4\pi^2 r^2 \left(\upsilon\sqrt{s + \pi^2 r^2 \upsilon^2} + \nu\sqrt{s + \pi^2 r^2 \nu^2} - \psi\sqrt{s + \pi^2 r^2 \psi^2}\right)^2} - s \tag{3.31}$$

$$h(s) = \upsilon\sqrt{s + \pi^2 r^2 \upsilon^2} + \nu\sqrt{s + \pi^2 r^2 \nu^2} - \psi\sqrt{s + \pi^2 r^2 \psi^2} \tag{3.32}$$

It is clear that $\Delta\sigma$ and $f(s)$ have the same monotonicity respect to s. Thus, it suffices to prove that f(s) is a decreasing function of s. To this end, the first derivative of $f(s)$ is evaluated. After some simple calculations, the derivative is obtained by

$$\frac{df(s)}{ds} = \frac{s + 4\pi^2 r^2 h(s)h(s)' - \sqrt{s^2 + 4\pi^2 r^2 h(s)^2}}{\sqrt{s^2 + 4\pi^2 r^2 h(s)^2}} \tag{3.33}$$

where $h(s)'$ denotes the first derivative with respect to s. On the other hand, a new function $g(v)$ is defined as follows:

$$g(v) = 4\pi^2 r^2 h(s)h(s)'^2 + 2h(s)'s - h(s) \tag{3.34}$$

where $h(s)$ is given in (3.32). Next, proof of $g(v) < 0$ for all $s >= 0$ is presented. The proof is divided into two cases where $\lambda_c > \lambda_c'$ and $\lambda_c < \lambda_c'$ are assumed respectively.

The case where $\lambda_c > \lambda_c'$ is considered first. The first derivative of $g(v)$ is calculated

as

$$\begin{aligned}\frac{dg(v)}{dv} &= \pi r\left(\sqrt{s'+v^2}+\frac{v^2}{\sqrt{s'+v^2}}\right)\left(\frac{v}{\sqrt{s'+v^2}}+\frac{u}{\sqrt{s'+u^2}}-\frac{\psi}{\sqrt{s'+\psi^2}}\right)^2 \\ &+2\pi r\left(v\sqrt{s'+v^2}+u\sqrt{s'+u^2}-\psi\sqrt{s'+\psi^2}\right) \\ &\left(\frac{v}{\sqrt{s'+v^2}}+\frac{u^2}{\sqrt{s'+u^2}}-\frac{\psi^2}{\sqrt{s'+\psi^2}}\right)\left(\frac{1}{\sqrt{s'+v^2}}-\frac{v^2}{(s'+v^2)^{3/2}}\right) \\ &+\pi r s'\left(\frac{1}{\sqrt{s'+v^2}}-\frac{v^2}{(s'+v^2)(3/2)}\right)-\pi r\sqrt{s'+v^2}-\frac{v^2}{\sqrt{s'+v^2}} \quad (3.35)\end{aligned}$$

where s' is used to denote $\frac{s}{\pi r}$ for convenience of presentation.

Since $\sigma_0 \geq 0$, it is immediately obtained from (3.16) and (3.17) that $u > \psi$, based on which the following relations are obtained:

$$u\sqrt{s'+u^2} > \psi\sqrt{s'+\psi^2} \quad (3.36)$$

$$\frac{u^2}{\sqrt{s'+u^2}} > \frac{\psi^2}{\sqrt{s'+\psi^2}} \quad (3.37)$$

Thus, the expression $\frac{dg}{dv}$ in (3.35) can be reduced by eliminating those items about u and ψ. This results in

$$\begin{aligned}\frac{dg(v)}{dv} &> \pi r\frac{\left(\sqrt{s'+v^2}+\frac{v^2}{\sqrt{s'+v^2}}\right)v^2}{s'+v^2}+2\pi r v^2\left(\frac{1}{\sqrt{s'+v^2}}-\frac{v^2}{(s'+v^2)(3/2)}\right) \\ &+\pi r s'\left(\frac{1}{\sqrt{s'+v^2}}-\frac{v^2}{(s'+v^2)(3/2)}\right)-\pi r\sqrt{s'+v^2} \\ &-\pi r\frac{v^2}{\sqrt{s'+v^2}} \quad (3.38)\end{aligned}$$

By expressing the last second item $\pi r\sqrt{s'+v^2}$ as $\pi r\sqrt{s'+v^2} = \pi r\frac{s'+v^2}{\sqrt{s'+v^2}}$, it can be easily verified that the right hand side of the inequality in (3.38) is zero. Thus, $g(v)$ is monotonously increase function of v. If $\lambda_c > \lambda_c'$, then $v < \psi$ by (3.16) and (3.18), and as a result, $g(v) < g(\psi) = 0$ for all $s \geq 0$. Using this result, it can be readily

verified that

$$\begin{aligned} & s + 4\pi^2 r^2 h(s) h(s)' < \sqrt{s^2 + 4\pi^2 r^2 h(s)^2} \\ \Leftrightarrow \quad & s + 4\pi^2 r^2 h(s) h(s)' - \sqrt{s^2 + 4\pi^2 r^2 h(s)^2} < 0 \end{aligned}$$

Compared to (3.33), it is immediately concluded that

$$\frac{df(s)}{ds} < 0 \tag{3.39}$$

Therefore, $f(s)$ is a decreasing function of s, so is Δ.

Now, the second case where $\lambda_c < \lambda_c'$ is considered. In this case, $v > \psi$. Thus, $g(v) > g(\psi) = 0$. As a result, $\frac{df}{ds} > 0$ and $f(s)$ is an increasing function of s. However, when $\lambda_c > \lambda_c'$, the phase mismatching error $\Delta\sigma$ is negative. Therefore, $|\Delta\sigma|$ is still a decreasing function of s.

3.2.5 Simulation Studies

In this section, simulation studies are conducted to verify the theoretical analysis in the previous section. We consider an optical tunable filter constructed by cascading two single notch AF-AOTFs as shown in Fig.2.1. The two cascading AF-AOTFs are assumed to have the same parameters including the AO coupling coefficients, the AO lengths and the cladding diameters of the fibers. These parameters are chosen as $C_1 = C_2 = 20$, $L_1 = L_2 = 50mm$ and $r_1 = r_2 = 5\mu m$. The choices of these parameters are used as those obtained from the experimental results in [56, 82]. In the simulation, two scenarios are considered. In the first scenario, the performance of the designed filter is investigated when the transmission profile is designed at $\lambda_c = 1705nm$ and tuned to $\lambda_c' = 1005nm$, while the second scenario considers the transmission profile designed at $\lambda_c = 1005nm$ and tuned to $\lambda_c' = 1705nm$. In each

scenario, the performance of the designed filter in the presence and in the absence of the axial strains, *i.e.*, $s = 0.01$ and $s = 0$, are compared respectively.

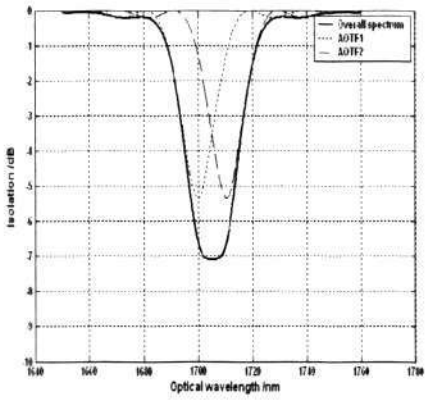

3.1.1: Designed at $\lambda_c = 1705nm$ with $s = 0$

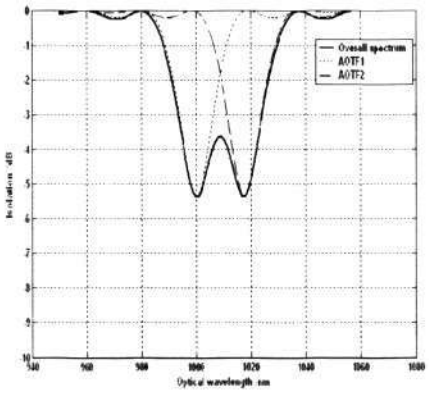

3.1.2: Transmission profile in Fig.3.1.1 tuned to $\lambda_c' = 1005nm$

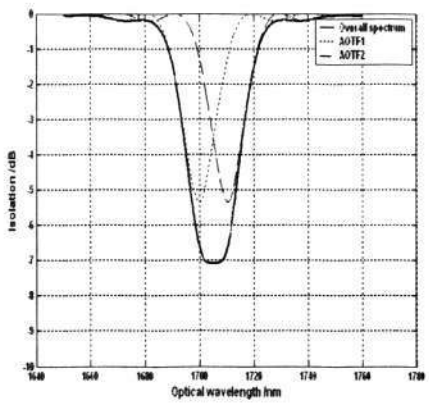

3.1.3: Designed at $\lambda_c = 1705nm$ with $s = 0.01$

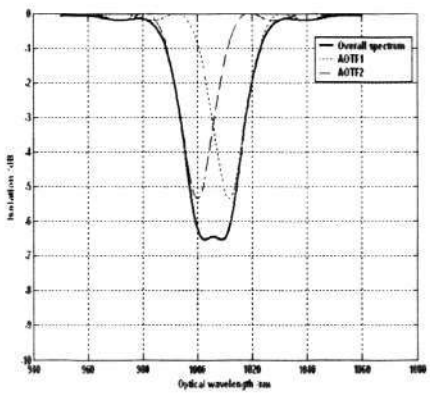

3.1.4: Transmission profile in Fig.3.1.3 tuned to $\lambda_c' = 1005nm$

Figure 3.1: Composite transmission profile of a two-stage cascading structure AF-AOTF (designed at $1705nm$).

Maximum flat stopband transmission with FWHM $23nm$ is achieved with the optimal phase-mismatch difference obtained at $\sigma_0 = 32.26m$. Fig.3.1 shows the simulation results of the first scenario. Fig.3.1.1 and Fig.3.1.3 show the composite

flat-stopband transmission profile designed at $\lambda_c = 1705nm$ in the presence and absence of axial strain, respectively. The corresponding transmission spectra after being tuned to $\lambda_c' = 1005nm$ are shown respectively in Fig.3.1.2 and Fig.3.1.3.

Clearly, the composite flat-stopband transmissions in both cases are distorted when they are tuned away from the designed position. Since η in this simulation case

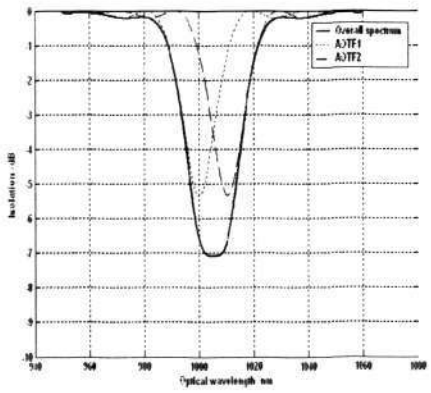

3.2.1: designed at $\lambda_c = 1005nm$ with $s = 0$

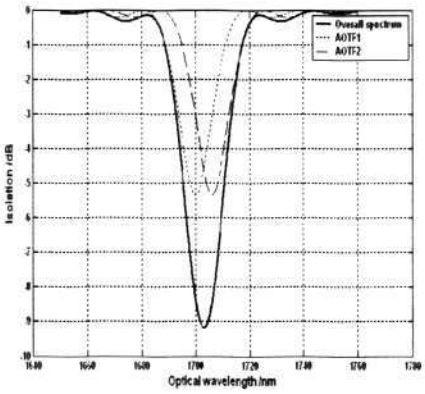

3.2.2: Transmission profile in Fig.3.2.1 tuned to $\lambda_c' = 1705nm$

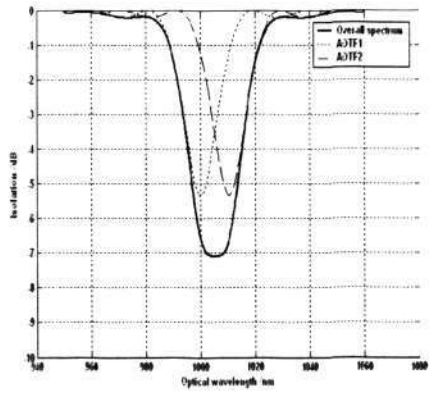

3.2.3: Designed at $\lambda_c = 1005nm$ with $s = 0.01$

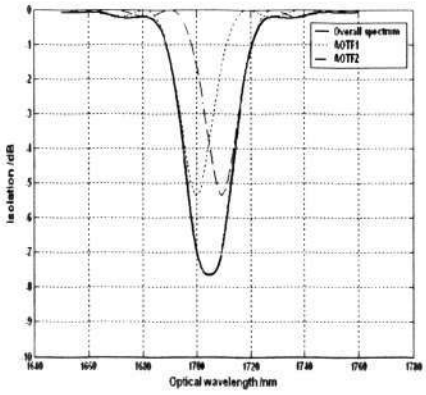

3.2.4: Transmission profile in Fig.3.2.3 tuned to $\lambda_c' = 1705nm$

Figure 3.2: Composite transmission profile of a two-stage cascading structure AF-AOTF (designed at $1005nm$).

is considered as an increasing function with respect to λ [55], $\Delta\sigma > 0$ when the central wavelength decreases. The bottoms of the transmission profile form a hump in the middle of the stopband. This results from the two notches moving away from each other when the transmission is being tuned away from the designed position. Clearly, the distortion in the tuned transmission is less for the case with high axial strain. This agrees with the theoretical analysis above.

The simulation results of the second scenario are summarized in Fig.3.2. In this case, the flat transmission is designed at $\lambda_c = 1005nm$ and the performance is examined by tuning the transmission to the wavelength $\lambda_c' = 1705nm$. Similarly, the transmission initially designed at $1005nm$ with and without an axial strain are respectively shown in Fig.3.2.1 and Fig.3.2.3. The transmission profile after being tuned to $\lambda_c' = 1705nm$ are shown in Fig.3.2.2 and Fig.3.2.4, respectively.

Based on these figures, the same conclusion as in the first scenario can be drawn. In the present case, both tuned transmissions become much sharper towards the bottom than the composite flat-stopband transmission profile as designed. This is because η is an increasing function [56] with respect to λ, $\Delta\sigma < 0$ when the central wavelength increases. Thus, the two notches approach closer to each other when the composite transmission is being tuned. All these curves again confirm that applying high axial strain in the fiber is capable of achieving better tunability of the composite transmission.

Next, we consider cascading more AF-AOTFs to deliver a wider flat stopband transmission with FWHM 36nm. In the simulation, four AF-AOTFs are cascaded. All AF-AOTFs are assumed to have the same parameters as the one used in the simulations mentioned above. The flat transmission is designed with the central wavelength $\lambda_c = 1705nm$. To design this transmission, any adjacent two AF-AOTFs are designed to deliver a composite flat-stopband transmission with FWHM 18nm. The tunability of the complex transmission is examined by tuning the transmis-

sion to a new central wavelength at $\lambda_c' = 1005nm$. Fig.3.3.1 and Fig.3.3.3 show the transmission profile designed with and without an axial strain, respectively. The transmission profile after tuned to $\lambda_c' = 1005nm$ are shown in Fig.3.3.2 and

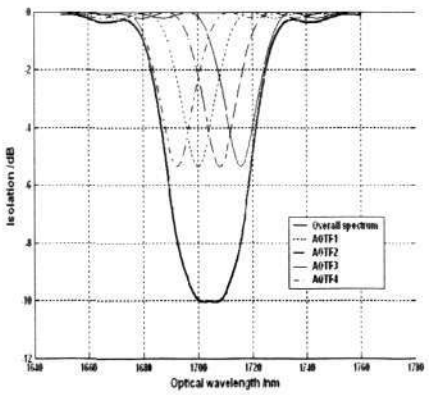

3.3.1: Designed at $\lambda_c = 1705nm$ with $s = 0$

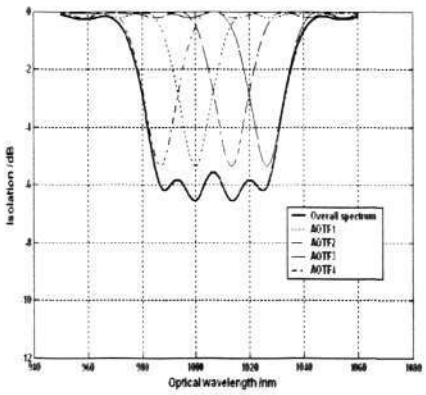

3.3.2: Transmission profile in Fig.3.3.1 tuned to $\lambda_c' = 1005nm$

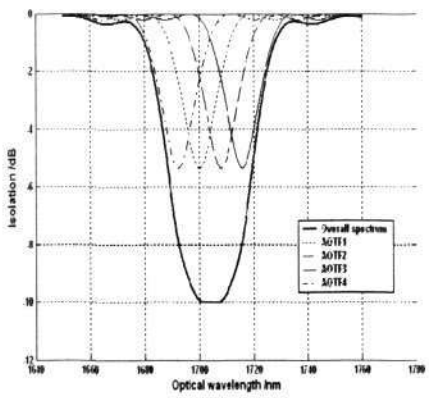

3.3.3: Designed at $\lambda_c = 1705nm$ with $s = 0.01$

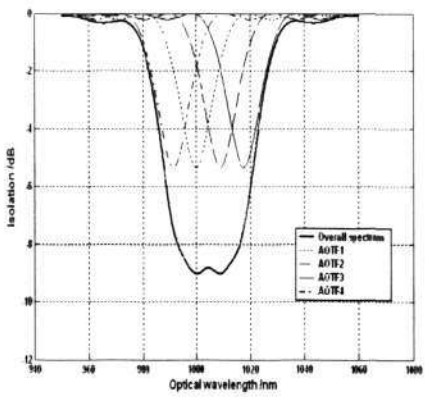

3.3.4: Transmission profile in Fig.3.3.3 tuned to $\lambda_c' = 1005nm$

Figure 3.3: Composite transmission profile of a four-stage cascading structure AF-AOTF (designed at $1705nm$).

Fig.3.3.4, respectively. Comparing the distorted transmissions in these figures, it is obvious that the complex transmissions resulting from axial strain suffer less distortion than those obtained without applying axial strain. This result justifies the

main conclusion of this chapter in the case where multiple AF-AOTFs are cascaded together to deliver a complex transmission.

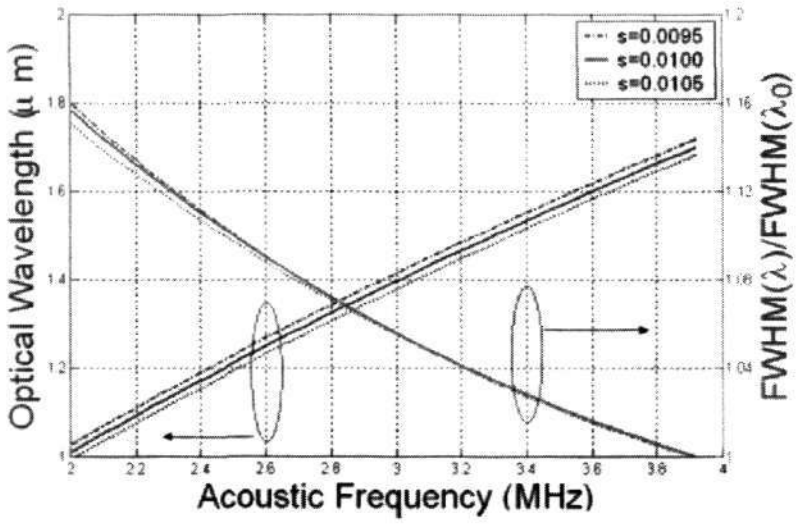

Figure 3.4: Effect of strain on the performance of flat-stopband transmission.

Lastly, the filter performance with respect to the axial strain variation is investigated. To this end, a composite flat-stopband is designed at $\lambda_0 = 1705nm$ by choosing $s = 0.01$, $f_1 = 3.919MHz$ and $\Delta f = 33913.3Hz$. The tunability of the filter is examined for three cases where the axial strain takes values of 0.01, 0.0105 and 0.0095, respectively. This is equivalent to considering $\pm 5\%$ variations on the nominal strain. For each case, the composite flat-stopband is tuned by varying f_1 every $0.039MHz$ from $3.919MHz$ down to $1.977MHz$. At each step during the tuning process, the tunability of the stopband is assessed by measuring the FWHM bandwidth and the central wavelength of the composite flat-stopband. The corresponding results are plotted as curves as shown in Fig.3.4. It is clear that the strain variations not only affect the FWHM bandwidth, but also cause a shift to the central wavelength of the composite flat-stopband. The bigger the strain, the smaller the changes in the FWHM bandwidth, and in turn the better the tunability. However, a bigger strain gives rise to a bigger shift to the central wavelength from

the desired position. This shift can be compensated by using a small value of f_1 when the composite flat-stopband is designed at $1705nm$.

3.3 Tunability Improvement of Multi-stage AF-AOTF by Using Strain Difference Control

In early research of AF-AOTF, the notch transmission of a single-stage AF-AOTF is tuned by controlling the acoustic frequency. Thus, frequency difference control scheme is the only available method to implement the complex transmission by using multi-stage AF-AOTF. Recently, it was found that the axial strain applied on the AO interaction can also substantially used to change the center wavelength of the notch transmission of a single-stage AF-AOTF [83]. However, the strain control scheme is not widely employed in AF-AOTF technology in the following years. This is mainly because dynamically strain control is quite complicated and highly expensive in real applications compared with the conventional acoustic frequency control, which can be easily achieved through electronic means. But exploring the use fixed strain is still valuable in the AF-AOTF transmission profile design in some applications.

In last section, the frequency difference control scheme of using multi-stage AF-AOTF to deliver a complex transmission is presented and discussed. In that case, both the transmission formation and the transmission tuning are controlled through the RF signal frequency modulation. These two kinds of controls are coupled with each other. As a result, the transmission yielded by the frequency difference control suffers transmission distortions.

In this section, a strain difference control scheme for the design of optical tunable filter with complex transmission profile is proposed. In this scheme, an optimized

and fixed strain difference, unlike the frequency difference used in the traditional design, is introduced to obtain the required phase mismatch and in turn form the complex transmission by using shifted notches. All AO interactions stages are driven by the same RF signal, which is used to tune the center wavelength of the transmission. Through theoretical analysis, it is shown that the composite transmission profile obtained by the strain difference control scheme can be maintained better than those obtained by the frequency difference control scheme.

3.3.1 Transmission of Multi-stage AF-AOTF Subject to Strain Difference Control

To illustrate the strain difference control scheme, a two-stage maximally flat stop-band filter design is used as an illustrative design example again for the same reasons as mentioned in the last section. As in the last section, we consider $C_1 = C_2 = C$ and $L_1 = L_2 = L$. The overall transmission profile of the system is determined by phase mismatch difference σ, which indicates the relation between the different phase mismatching coefficients δ_i of all AO interactions. For any δ_i, the tunable parameters are the acoustic frequency f_i and the strain s_i. In conventional frequency difference control scheme, the desired phase mismatch difference σ is obtained through introducing optimized frequency difference $\triangle f$ between f_i. In the strain difference control scheme, the acoustic frequencies applied on all AO interaction stages are chosen the same. The required phase mismatch difference σ is achieved by applying the different axial strains in each piece of bare fiber responsible for the AO interactions.

For a two-stage AF-AOTF, we take $f_1 = f_2 = f$ and $s_1 \neq s_2$. The center wavelength of the transmission is at λ_c. s_1 and s_2 are obtained by solving the equation $\sigma = \sigma_0$ where σ_0 is the desired phase mismatch difference. To implement a flat stop band

transmission, the required axial strains can be derived as

$$\begin{aligned} s_1(\sigma_0, \lambda_c) &= \frac{f^2 - C_{ext}^2 \pi^2 r^2 \left(\eta(\lambda_c) - \frac{\sigma_0}{2}\right)^4}{4C_{ext}^2 \left(\eta(\lambda_c) - \frac{\sigma_0}{2}\right)^4} \\ s_2(\sigma_0, \lambda_c) &= \frac{f^2 - C_{ext}^2 \pi^2 r^2 \left(\eta(\lambda_c) + \frac{\sigma_0}{2}\right)^4}{4C_{ext}^2 \left(\eta(\lambda_c) + \frac{\sigma_0}{2}\right)^4} \end{aligned} \tag{3.40}$$

The strains s_1 and s_2 with values given in (3.40) are applied on two AO fibers respectively and they are fixed during the tuning process. As a result, the flat stopband transmission is obtained at wavelength λ_c. In the strain difference control scheme tuning the transmission to a new wavelength position λ_c' is done very simply by adjusting the driving RF signal frequency f.

3.3.2 Tunability of Multi-stage AF-AOTF Subject to Strain Difference Control

The tunability of the transmission obtained by the strain difference control scheme is analyzed by examining the change of the phase mismatching difference error $\Delta\sigma$. Since only the strain difference is of concern, the axial strain on the first AO interaction stage s_1 is chosen as the base strain and denoted as s in the rest part of this chapter. From (3.40), the strain difference between the two AO interaction stages shall be

$$\begin{aligned} \Delta s(\sigma_o, \lambda_c) &= s_2(\sigma_o, \lambda_c) - s_1(\sigma_o, \lambda_c) \\ &= -\frac{-2\eta(\lambda_c)\sigma_o(16f^2 + C_{ext}^2 \pi^2 r^2 (\sigma_o^2 - 4\eta^2(\lambda_c))^2)}{C_{ext}^2 (\sigma_o^2 - 4\eta^2(\lambda_c))^2} \end{aligned} \tag{3.41}$$

According to the strain difference control scheme proposed in the last subsection, the strain difference Δs and base strain s are maintained as a constant during the

tuning process of the central wavelength from λ_c to λ_c', that is,

$$\begin{aligned} \Delta s(\lambda_c) &= \Delta s(\lambda_c') \\ s(\lambda_c) &= s(\lambda_c') \end{aligned} \tag{3.42}$$

Thus, the phase mismatching error $\Delta\sigma$ defined in (2.37) is obtained as

$$\Delta\sigma\,|_{\Delta s(\sigma_o',\lambda_c')=\Delta s(\sigma_o,\lambda_c)} = \frac{\tau_2\sqrt{2\varphi}}{2\pi r\sqrt{s\tau_1^2-\rho+\sqrt{\varphi\tau_2^4+(s\tau_1^2-\rho)^2}}} - \tau_2' \tag{3.43}$$

where

$$\tau_1 = \eta(\lambda_c) - \frac{\sigma_0}{2} \tag{3.44}$$

$$\tau_2 = \eta(\lambda_c) + \frac{\sigma_0}{2} \tag{3.45}$$

$$\tau_1' = \eta(\lambda_c') - \frac{\sigma_0}{2} \tag{3.46}$$

$$\tau_2' = \eta(\lambda_c') + \frac{\sigma_0}{2} \tag{3.47}$$

$$\rho = \pi^2 r^2 \eta(\lambda_c)\sigma_0(4\eta^2(\lambda_c)+\sigma_0^2) \tag{3.48}$$

$$\varphi = 4\pi^2 r^2 \tau_1'^2(s+\pi^2 r^2 \tau_1'^2) \tag{3.49}$$

Performing the similar procedures as used in tunability analysis of the frequency difference control scheme in section 3.2.2, the corresponding phase mismatching error is

$$\Delta\sigma|_{\Delta f(\sigma_o',\lambda_c')=\Delta f(\sigma_o,\lambda_c)} = \sqrt{\tau_1'^2+\tau_2^2-\tau_1^2} - \tau_2' \tag{3.50}$$

Comparing equations (3.43) and (3.50), it has

$$|\Delta\sigma\,|_{\Delta s(\sigma_o',\lambda_c')=\Delta s(\sigma_o,\lambda_c)}| \le |\Delta\sigma|_{\Delta f(\sigma_o',\lambda_c')=\Delta f(\sigma_o,\lambda_c)}| \quad \text{if } s \ge 2\pi^2 r^2 \eta(\lambda_c)\sigma_o \tag{3.51}$$

This inequality shows theoretically that if proper strains are applied on the AO in-

teractions, the composite transmission profile obtained by using the strain difference control scheme has a better tunability than that obtained by using the frequency difference control scheme.

3.3.3 Proof of the Inequality (3.51)

For the sake of easy reference, a new denotation $z = \eta_c\sigma_0(4\eta_c^2 + \sigma_0^2)$ is introduced. The phase mismatch errors $\Delta\sigma$ for the strain difference control and the frequency scheme can be expressed as

$$\Delta\sigma\,|_{\Delta s'=\Delta s} = \frac{\sqrt{2}\tau_2\tau_1'\sqrt{s+\pi^2r^2\tau_1'^2}}{\sqrt{s\tau_1^2-\pi^2r^2z+\sqrt{4\pi^2r^2\tau_1'^2(s+\pi^2r^2\tau_1'^2)\tau_2^4+(s\tau_1^2-\pi^2r^2z)^2}}} - \tau_2' \tag{3.52}$$

$$\Delta\sigma|_{\Delta f'=\Delta f} = \sqrt{\tau_1'^2+2\eta_c\sigma_0}-\tau_2' \tag{3.53}$$

where $\Delta s' = \Delta s(\sigma_o', \lambda_c')$, $\Delta s = \Delta s(\sigma_o, \lambda_c)$, $\Delta f' = \Delta f(\sigma_o', \lambda_c')$ and $\Delta f = \Delta f(\sigma_o, \lambda_c)$. In order to prove inequality (3.51), the following two equations are used:

$$\begin{aligned} & 16\pi^4r^4\tau_2^4\eta_c^2\sigma_0^2 + 16\pi^4r^4\tau_2^4\tau_1'^2\eta_c\sigma_0 - 4\pi^4r^4z\tau_2^2(\tau_1'^2+2\eta_c\sigma_0) \\ = \;& 16\pi^4r^4\tau_2^2\eta_c^2\sigma_0^2(\tau_1'^2-\tau_1^2) \end{aligned} \tag{3.54}$$

$$\begin{aligned} & 4\pi^2r^2\tau_1'^2\tau_2^4 - 4\tau_1^2\pi^2r^2\tau_2^2(\tau_1'^2+2\eta_c\sigma_0) \\ = \;& 8\pi^2r^2\tau_2^2\eta_c\sigma_0(\tau_1'^2-\tau_1^2) \end{aligned} \tag{3.55}$$

It shows that (3.54) and (3.55) have the same sign. If $\tau_1' = \eta(\lambda_c') - \frac{\sigma_0}{2} \le \tau_1 = \eta(\lambda_c) - \frac{\sigma_0}{2}$, it is clear from (3.54) and (3.55) that

$$16\pi^4r^4\tau_2^4\eta_c^2\sigma_0^2 + 16\pi^4r^4\tau_2^4\tau_1'^2\eta_c\sigma_0 - 4\pi^4r^4z\tau_2^2(\tau_1'^2+2\eta_c\sigma_0) \le 0 \tag{3.56}$$

$$4\pi^2r^2\tau_1'^2\tau_2^4 - 4\tau_1^2\pi^2r^2\tau_2^2(\tau_1'^2+2\eta_c\sigma_0) \le 0 \tag{3.57}$$

Similarly, if $\tau_1' = \eta(\lambda_c') - \frac{\sigma_0}{2} \geq \tau_1 = \eta(\lambda_c) - \frac{\sigma_0}{2}$, it is clear from (3.54) and (3.55) that

$$16\pi^4 r^4 \tau_2^4 \eta_c^2 \sigma_0^2 + 16\pi^4 r^4 \tau_2^4 \tau_1'^2 \eta_c \sigma_0 - 4\pi^4 r^4 z \tau_2^2 (\tau_1'^2 + 2\eta_c \sigma_0) \geq 0 \quad (3.58)$$

$$4\pi^2 r^2 \tau_1'^2 \tau_2^4 - 4\tau_1^2 \pi^2 r^2 \tau_2^2 (\tau_1'^2 + 2\eta_c \sigma_0) \geq 0 \quad (3.59)$$

Therefore, if $s \geq 2\pi^2 r^2 \eta_c \sigma_o$, we have

$$\begin{aligned} s &\geq 2\pi^2 r^2 \eta_c \sigma_0 \\ &\geq \frac{16\pi^4 r^4 \tau_2^4 \eta_c^2 \sigma_0^2 + 16\pi^4 r^4 \tau_2^4 \tau_1'^2 \eta_c \sigma_0 - 4\pi^4 r^4 z \tau_2^2 (\tau_1'^2 + 2\eta_c \sigma_0)}{4\pi^2 r^2 \tau_1'^2 \tau_2^4 - 4\tau_1^2 \pi^2 r^2 \tau_2^2 (\tau_1'^2 + 2\eta_c \sigma_0)} \end{aligned} \quad (3.60)$$

When $\tau_1' = \eta(\lambda_c') - \frac{\sigma_0}{2} \leq \tau_1 = \eta(\lambda_c) - \frac{\sigma_0}{2}$, using (3.57), the above inequality is re-arranged as

$$\begin{aligned} s(4\pi^2 r^2 \tau_1'^2 \tau_2^4 - 4\tau_1^2 \pi^2 r^2 \tau_2^2 (\tau_1'^2 + 2\eta_c \sigma_0)) \leq\ & 16\pi^4 r^4 \tau_2^4 \eta_c^2 \sigma_0^2 + 16\pi^4 r^4 \tau_2^4 \tau_1'^2 \eta_c \sigma_0 \\ & -4\pi^4 r^4 z \tau_2^2 (\tau_1'^2 + 2\eta_c \sigma_0) \end{aligned} \quad (3.61)$$

From which, it follows that

$$\begin{aligned} 4\pi^2 r^2 \tau_1'^2 (s + \pi^2 r^2 \tau_1'^2) \tau_2^4 + (s\tau_1^2 - \pi^2 r^2 z)^2 \leq\ & 2\pi^2 r^2 \tau_2^2 (\tau_1'^2 + 2\eta_c \sigma_0) \\ & + (s\tau_1^2 - \pi^2 r^2 z))^2 \end{aligned} \quad (3.62)$$

Following equations are deduced

$$\begin{aligned} &\sqrt{\sqrt{4\pi^2 r^2 \tau_1'^2 (s + \pi^2 r^2 \tau_1'^2) \tau_2^4 + (s\tau_1^2 - \pi^2 r^2 z)^2} - (s\tau_1^2 - \pi^2 r^2 z)} \\ &\qquad \leq \sqrt{2}\pi r \tau_2 \sqrt{\tau_1'^2 + 2\eta_c \sigma_0} \end{aligned} \quad (3.63)$$

On the other hand, it follows from (3.52) that

$$\begin{aligned}\Delta\sigma\,|_{\Delta s(\sigma_o',\lambda_c')=\Delta s(\sigma_o,\lambda_c)} &= \frac{\sqrt{2}y\tau_1'\sqrt{s+\pi^2r^2\tau_1'^2}}{\sqrt{s\tau_1^2-\pi^2r^2z+\sqrt{4\pi^2r^2\tau_1'^2(s+\pi^2r^2\tau_1'^2)\tau_2^4+(s\tau_1^2-\pi^2r^2z)^2}}}-\tau_2' \\ &= \frac{\sqrt{2}\sqrt{\sqrt{4\pi^2r^2\tau_1'^2(s+\pi^2r^2\tau_1'^2)\tau_2^4+(s\tau_1^2-\pi^2r^2z)^2}-(s\tau_1^2-\pi^2r^2z)}}{2\pi r\tau_2}-\tau_2'\end{aligned} \tag{3.64}$$

Combining (3.53) and (3.63) gives

$$\Delta\sigma\,|_{\Delta s(\sigma_o',\lambda_c')=\Delta s(\sigma_o,\lambda_c)} \le \sqrt{\tau_1'^2+2\eta_c\sigma_0}-\tau_2' = \Delta\sigma|_{\Delta f(\sigma_o',\lambda_c')=\Delta f(\sigma_o,\lambda_c)} \tag{3.65}$$

which confirms inequality (3.51). In a special case when an enhanced notch transmission is considered, $\sigma_o = 0$, $\Delta\sigma\,|_{\Delta s(\sigma_o',\lambda_c')=\Delta s(\sigma_o,\lambda_c)} = 0$, and $\Delta\sigma|_{\Delta f(\sigma_o',\lambda_c')=\Delta f(\sigma_o,\lambda_c)} = 0$. Therefore, the equality in (3.51) holds for $s \ge 0$.

When $\tau_1' = \eta(\lambda_c') - \frac{\sigma_0}{2} \ge \tau_1 = \eta(\lambda_c) - \frac{\sigma_0}{2}$, using (3.59), the inequality (3.60) is re-arranged as

$$\begin{aligned}s(4\pi^2r^2\tau_1'^2\tau_2^4-4\tau_1^2\pi^2r^2\tau_2^2(\tau_1'^2+2\eta_c\sigma_0)) \;\ge\; & 16\pi^4r^4\tau_2^4\eta_c^2\sigma_0^2+16\pi^4r^4\tau_2^4\tau_1'^2\eta_c\sigma_0 \\ & -4\pi^4r^4z\tau_2^2(\tau_1'^2+2\eta_c\sigma_0)\end{aligned} \tag{3.66}$$

With the similar derivation, following equation can be obtained

$$\Delta\sigma\,|_{\Delta s(\sigma_o',\lambda_c')=\Delta s(\sigma_o,\lambda_c)} \ge \sqrt{\tau_1'^2+2\eta_c\sigma_0}-\tau_2' = \Delta\sigma|_{\Delta f(\sigma_o',\lambda_c')=\Delta f(\sigma_o,\lambda_c)} \tag{3.67}$$

But at this time, $\Delta\sigma\,|_{\Delta s(\sigma_o',\lambda_c')=\Delta s(\sigma_o,\lambda_c)}$ and $\Delta\sigma|_{\Delta f(\sigma_o',\lambda_c')=\Delta f(\sigma_o,\lambda_c)}$ are negative. Thus,

the conclusion is drawn that when $s \geq 2\pi^2 r^2 \eta_c \sigma_o$,

$$|\Delta\sigma|_{\Delta s(\sigma_o',\lambda_c')=\Delta s(\sigma_o,\lambda_c)}| \leq = |\Delta\sigma|_{\Delta f(\sigma_o',\lambda_c')=\Delta f(\sigma_o,\lambda_c)}|. \tag{3.68}$$

3.3.4 Simulation Studies

To see the above analysis more intuitively, we compare the tunability of the maximally flat stopband tunable filter respectively implemented by using the strain difference control scheme and the frequency difference control scheme in simulation. In the first simulation, the stopband transmission is designed at the initial central wavelength $\lambda_c = 1500nm$ and tuned to $\lambda_{c'} = 1600nm$.

In the second simulation, the stopband transmission is designed at the central wavelength $\lambda_c = 1600nm$ and tuned to $\lambda_{c'} = 1500nm$ in the opposite direction. The applied parameters C and L are chosen as 1.48 and $60cm$, respectively. As discussed in the last section, the corresponding optimal phase mismatching difference σ_o is 3.0631026371. With those parameters, the minimum strain required in (3.51) is obtained as $2\pi^2 r^2 \eta(\lambda_c)\sigma_o = 0.000337521$ and 0.000258264 for maximally flat stopband designed at $1500nm$ and $1600nm$, respectively. Thus, the strains on the fiber are controlled to $s = 0.05$ in the simulation.

The stopband transmission is tuned from $1500nm$ to $1600nm$. The corresponding transmissions of the strain difference control scheme are shown in Fig.3.5. Firstly the composite transmission profile is designed at $\lambda_c = 1500nm$ and maximally flat stop bands as specified are obtained via both the strain difference control and frequency difference control. Fig.3.5.1 shows the stopband transmission designed at $1500nm$ subject to strain difference control. Fig.3.5.3 shows the stopband transmission designed at $1500nm$ subject to frequency difference control. Fig.3.5.2 and Fig.3.5.4 respectively show the results of the stopband transmission profile designed

by the strain difference control and frequency difference control being tuned to the central wavelengths at $1600nm$.

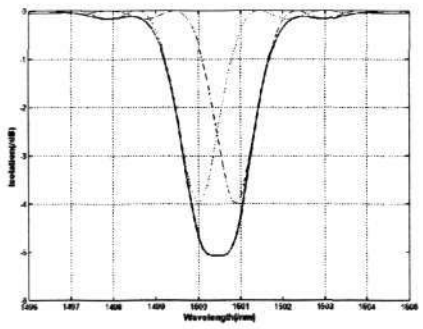

3.5.1: Stopband transmission profile designed at $\lambda_c = 1500nm$ subject to strain difference control.

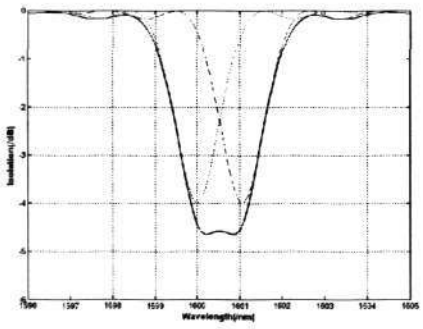

3.5.2: Transmission profile in Fig.3.5.1 tuned to $\lambda_c' = 1600nm$.

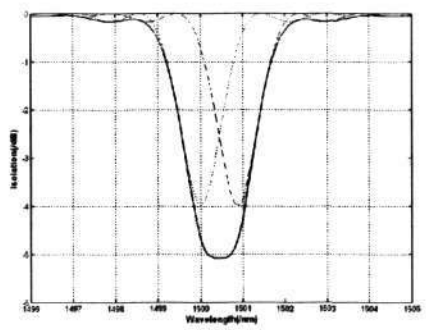

3.5.3: Stopband transmission profile designed at $\lambda_c = 1500nm$ subject to frequency difference control.

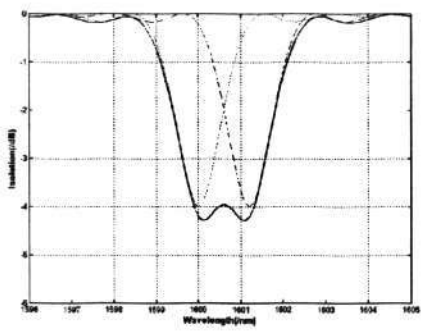

3.5.4: Transmission profile in Fig.3.5.3 tuned to $\lambda_c' = 1600nm$.

Figure 3.5: Composite transmission profile of two-stage AF-AOTF subject to strain difference control and frequency difference control (initially designed at $1500nm$).

Fig.3.6 shows the stopband transmission designed at $1600nm$ and tuned to $1500nm$. Fig.3.6.1 and Fig.3.6.2 show the transmissions obtained by using strain difference control scheme. The corresponding transmissions by using the frequency difference control scheme are shown in Fig.3.6.3 and Fig.3.6.4, respectively. In both cases no matter, which direction is tuned to, the composite transmission distortions are

obviously suppressed by using the strain difference control scheme. These curves again confirm that the strain difference control scheme is capable of achieving better tunability of the composite transmission profile than the frequency difference control scheme.

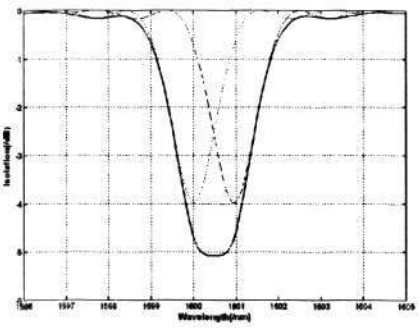

3.6.1: Stopband transmission profile designed at $\lambda_c = 1600nm$ subject to strain difference control.

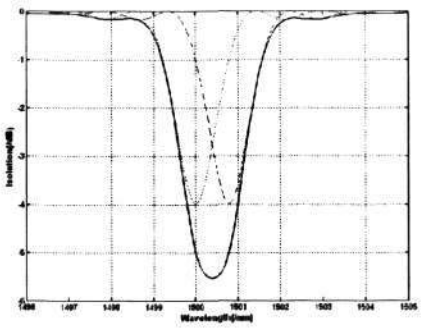

3.6.2: Transmission profile in Fig.3.6.1 tuned to $\lambda_c' = 1500nm$.

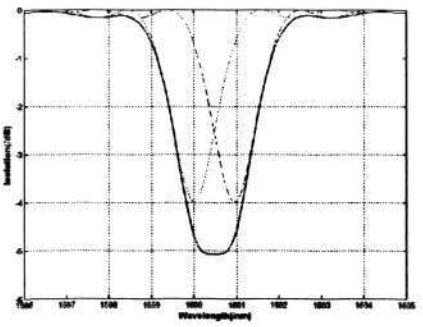

3.6.3: Stopband transmission profile designed at $\lambda_c = 1600nm$ subject to frequency difference control.

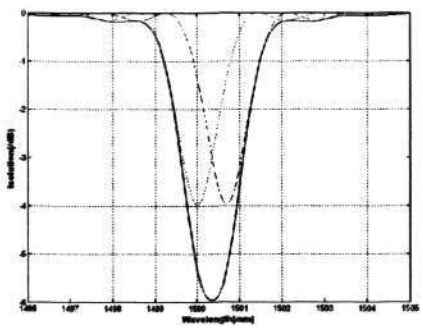

3.6.4: Transmission profile in Fig.3.6.3 tuned to $\lambda_c' = 1500nm$.

Figure 3.6: Composite transmission profile of two-stage AF-AOTF subject to strain difference control and frequency difference control (initially designed at $1600nm$).

3.3.5 PZT Nonlinearity Effect on the Transmission Deformation

In above discussion, we focused on the tuning mechanisms of multi-stage AF-AOTF while assuming that the all employed PZTs can provide strong AO coupling efficiency. Under this assumption, we have $C_1 = C_2$ in the whole tuning range. But, this assumption is not always hold for the AF-AOTFs using un-etched single mode fiber due to the relative weak coupling between the fundamental mode and cladding mode. For this kind of AF-AOTF devices, the acoustic bandwidth limitation of PZT strongly affect the performance of AF-AOTF and necessary to be considered.

In theory, the model of PZT is very complicated. It has many resonance frequencies and antiresonance frequencies. However, in the neighborhood of resonance frequency of main mode of vibration, a simple lumped element lossy circuit can be used to qualitative analysis the characteristics of PZT [84]. The corresponding AO coupling coefficient C in a small acoustic bandwidth near a resonance frequency of PZT is approximately described as

$$C(f) = \frac{\tau V/(4\pi^2)}{\sqrt{(f^2 - F^2)^2 + f^2 k^2}} \tag{3.69}$$

$$k = \frac{R}{2\pi L} \tag{3.70}$$

where L is the motional inductance, R is the motional resistance, V and F are the driving electric voltage and resonance frequency of the PZT respectively. τ is the conversion ratio between the mechanical vibration amplitude and AO coupling coefficient. Substitute (3.69) into (2.1), the transmission of a single-stage AF-AOTF

by considering the nonlinearity of the PZT is obtained as

$$\begin{aligned} G(\lambda, f) &= 10\log\frac{P_{out}}{P_{in}} \\ &= 10\log(1 - \frac{(\frac{\tau V/(4\pi^2)}{\sqrt{(f^2-F^2)^2+f^2k^2}})^2}{(\frac{\tau V/(4\pi^2)}{\sqrt{(f^2-F^2)^2+f^2k^2}})^2 + \delta(\lambda,f)^2} \\ &\quad \sin^2 L\left(\sqrt{\frac{\tau^2V^2/(16\pi^4)}{(f^2-F^2)^2+f^2k^2} + \delta(\lambda,f)^2}\right)) \\ &= 10\log(1 - \frac{\tau^2V^2\sin^2 L\left(\sqrt{\frac{\tau^2V^2/(16\pi^4)}{(f^2-F^2)^2+f^2k^2} + \delta(\lambda,f)^2}\right)}{\tau^2V^2 + 16\pi^4\delta^2(\lambda,f)((f^2-F^2)^2+f^2k^2)}) \end{aligned} \quad (3.71)$$

Thus, the transmission resulting from cascading several AF-AOTFs with considering the nonlinearity of all the PZTs are obtained by.

$$\begin{aligned} G(\lambda, f_i, V_i) &= 10\log\left(\prod_{i=1}^{N}\left(1 - \frac{C_i^2}{C_i^2+\delta_i^2}\sin^2\left(L\sqrt{C_i^2+\delta_i^2}\right)\right)\right) \\ &= 10\log\left(\prod_{i=1}^{N}\left(1 - \frac{\tau^2V_i^2\sin^2 L\left(\sqrt{\frac{\tau^2V_i^2/(16\pi^4)}{(f_i^2-F^2)^2+f_i^2k^2} + \delta_i(\lambda,f_i)^2}\right)}{\tau^2V_i^2 + 16\pi^4\delta_i^2(\lambda,f_i)((f_i^2-F^2)^2+f_i^2k^2)}\right)\right) \end{aligned} \quad (3.72)$$

In the above model, f_i, V_i and F are the driven RF signal frequency, driving electric voltage and resonance frequency of the ith PZT. For the case of cascading two AF-AOTFs, the desired transmission $G(\lambda)$ can be implemented through carefully setting values of f_1, f_2, V_1, V_2. But, the relationships between these design parameters and the operating position of the filter are nonlinear. Hence, when the designed transmission is tuned to a new position by adding an identical increment Δf to both f_1 and f_2, the transmission will deviate from its initially designed shape.

To build a flat stopband filter by two AF-AOTFs, the two AO coupling coefficients

must be kept matching.

$$C_1(f_1, V_1) = C_2(f_2, V_2) = C \tag{3.73}$$

Apply (3.69) to (3.73), we can obtain that

$$\begin{cases} V_2 = \frac{V_1\sqrt{(f_2^2-F^2)^2+f_2^2k^2}}{\sqrt{(f_1^2-F^2)^2+f_1^2k^2}} \\ f_1 = C_{ext}(\eta(\lambda_0) - \frac{\sigma_0}{2})\sqrt{s_1 + \pi^2r^2(\eta(\lambda_c) - \frac{\sigma_0}{2})^2} \\ f_2 = C_{ext}(\eta(\lambda_0) + \frac{\sigma_0}{2})\sqrt{s_2 + \pi^2r^2(\eta(\lambda_c) + \frac{\sigma_0}{2})^2} \end{cases} \tag{3.74}$$

For the frequency difference control scheme with strain applied, it is set that $s_1 = s_2$. When the transmission shift to a new position by the tuning of the acoustic frequency to $f_1 + \Delta f$ and $f_2 + \Delta f$, we obtain the corresponding acoustic coupling coefficients denoted by $\hat{C}_i$ are

$$\begin{cases} \hat{C}_1 = \frac{\tau V_1/(4\pi^2)}{\sqrt{((f_1+\Delta f)^2-F^2)^2+(f_1+\Delta f)^2k^2}} \\ \hat{C}_2 = \frac{\tau V_1/(4\pi^2)\sqrt{((f_1+\nu)^2-F^2)^2+(f_1+\nu)^2k^2}}{\sqrt{(f_1^2-F^2)^2+f_1^2k^2}\sqrt{((f_1+\Delta f+\nu)^2-F^2)^2+(f_1+\Delta f+\nu)^2k^2}} \end{cases} \tag{3.75}$$

The mismatch of AO coupling efficiency mismatch after and before transmission operating position shifting can be obtained by

$$\begin{aligned} \Delta C_{s_1=s_2} &= \frac{\tau V_1/(4\pi^2)}{\sqrt{((f_1+\Delta f)^2 - F^2)^2 + (f_1+\Delta f)^2k^2}} \\ &- \frac{\tau V_1/(4\pi^2)\sqrt{((f_1+\nu)^2 - F^2)^2 + (f_1+\nu)^2k^2}}{\sqrt{(f_1^2 - F^2)^2 + f_1^2k^2}\sqrt{((f_1+\Delta f+\nu)^2 - F^2)^2 + (f_1+\Delta f+\nu)^2k^2}} \end{aligned} \tag{3.76}$$

where $\nu > 0$ is the required frequency difference to generate the desired optimal phase mismatch. Obviously, when the composite transmission is shifted away from its initial design position along the wavelength, we have$|\Delta C_{s_1=s_2=s}| \neq 0$. This mismatch thus contributes transmission deformation.

For the case of strain difference control scheme, without loss of generality, we assume that $s_1 = s$. According to the strain difference control scheme, the applied RF signals on two AF-AOTFs have equal frequency.

$$f_1 = f_2 \tag{3.77}$$

Thus, the optimized strain difference is

$$\triangle s = s_2 - s_1 = -\frac{2\eta(\lambda_0)\sigma_0}{(\eta(\lambda_0) + \frac{\sigma_0}{2})^2} s \tag{3.78}$$

And from the initialization condition (3.74), it can be easily derived that

$$V_1 = V_2 \tag{3.79}$$

Obviously, the corresponding amplitude mismatch after and before transmission operating position shifting is

$$\Delta C_{s_1=s, s_2=s+\triangle s} = 0 \tag{3.80}$$

Thus we can conclude now that: the transmission distortion caused by the AO coupling efficiency variation due to the PZT nonlinearity effect can also be suppressed by strain difference control scheme.

To see the overall effect of the strain on the tunability of AF-AOTF, by considering both the phase mismatch and the PZT nonlinearity, simulation studies are conducted to verify the theoretical analysis.

In the simulation,we choose the parameters respectively as $C_1 = C_2 = 0.9327$, $L_1 = L_2 = 1m$ and $F_1 = F_2 = 2.3084Mhz$. The obtained transmission is well consistent with the experimental results. The performance of the designed filter is investigated when the transmission is designed at $\lambda_c = 1543nm$ and tuned to $\lambda_c' = 1546nm$.

We compare the performance of the designed filter subject to frequency difference control and subject to strain difference control.

Fig. 3.7.1 shows the simulation results where the flat stopband transmission profile that is initially designed at the optical wavelength $\lambda_c = 1543nm$ and tuned to $\lambda_c = 1546nm$ subject to frequency difference control. The initial flat stopband transmission profile is implemented by setting the frequency of the RF signal of the second PZT lower by $0.0063Mhz$ than that of the first PZT, which has the value of $2.3047Mhz$.

In the case of using strain difference control scheme, both two RF signals take the same frequency of $f = 2.3047Mhz$. The flatness of the stopband is guaranteed through the axial strain difference control with $s_1 = 0.01$ and $s_2 = 0.01047$. Fig. 3.7.2 shows the corresponding transmission profile when the center wavelength shifts from $1543nm$ to $1546nm$ by tuning the RF signal frequency f.

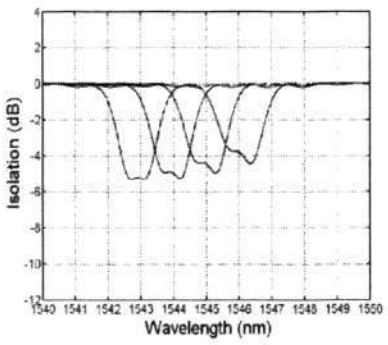

3.7.1: Composite transmission profile deformation subject to frequency difference control.

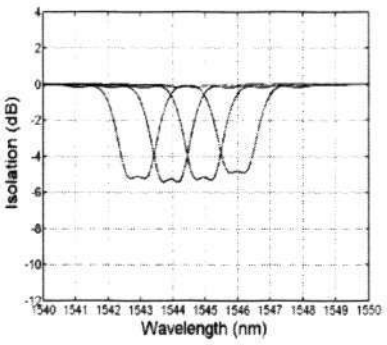

3.7.2: Composite transmission profile deformation subject to strain difference control.

Figure 3.7: Composite spectral responses of a two-stage cascading AF-AOTF subject to frequency difference and strain difference control schemes with consideration of the PZT nonlinearity.

From the simulation results, it is clear that compared with the frequency design scheme, strain difference control scheme can much more sufficiently suppress the

transmission deformations due to both the phase mismatch difference variation the PZT frequency response nonlinearity.

3.3.6 Experimental Results

This section reports experimental results of the tunability comparison of composite transmission obtained respectively by the strain difference control scheme and the frequency difference control scheme. To this end, the maximally flat stop band transmission is implemented by using different schemes with two AO interaction stages.

First, a two-stage AF-AOTF subject to strain difference control scheme is considered. The AF-AOTF is fabricated using a 4m long standard SMF-28 single mode fiber. The two stripped sections are obtained with roughly the same length of $60cm$. In the experiment, a C-band light source is used to provide a broadband light input to the filter. The transmission profile of the filter is observed by an optical spectrum analyzer (OSA).

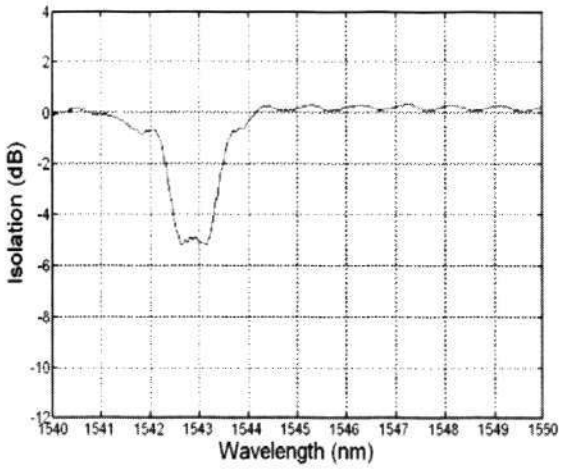

Figure 3.8: Composite transmission profile of two-stage AF-AOTF subject to strain difference control at the calibrated wavelength ($\lambda_c = 1543nm$)

To obtain the maximally flat stop band transmission, the system is calibrated by the following procedures. Firstly, the RF frequency is tuned to $2.348MHz$ and amplitudes of the RF signal are maintained at $300mV$. In this case, OSA prompts two shifted notch spectra. Then, with the RF frequency fixed, strain is applied on each stripped sections by moving the damper stages. The strain adjustment is carried on until the two notch responses overlap with each other and form a flat stopband transmission. After the calibration is done, a flat stopband transmission profile as shown in Fig.3.8 is obtained. To examine the tunability of the stopband transmission, the RF signal is tuned from $2.348MHz$ to $2.327MHz$ with all other setting parameters fixed. The transmission profile in response to RF signal frequencies of $2.341MHz$, $2.334MHz$ and $2.327MHz$ are shown in curves 2, 3 and 4 in Fig.3.9, respectively.

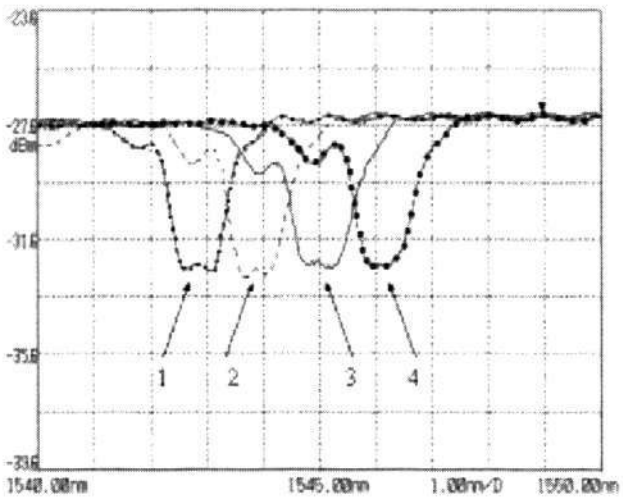

Figure 3.9: Composite transmission profile of two-stage AF-AOTF subject to strain difference control at different central wavelengths (curve 1: f=2.348Mhz; curve 2: f=2.341MHz; curve 3: f=2.334MHz; curve 4: f=2.327MHz).

Next, the implementation of the maximally flat stop band transmission by using two-stage AF-AOTF subject to frequency difference control is considered. Both AO interaction stages are have the same AO length with that used in the strain difference control, but they are controlled only by radio frequencies (RF) signal f_i $(i = 1, 2)$

without applying strain. Similarly, the system is first calibrated by tuning the RF frequency f_1 and f_2 to $2.360MHz$ and $2.364MHz$, respectively. So a flat stop band transmission as in Fig.3.8 is obtained at the central wavelength $1543nm$. Then, for sake of comparison, the stop band transmission is tuned respectively to have the same central wavelengths as those of curves 2, 3 and 4 in Fig.3.9 by tuning the frequencies f_1 and f_2 while maintaining a constant difference as $f_1 - f_2 = 0.004MHz$. The corresponding responses are displayed in Fig.3.10. Comparing the responses in Fig.3.10 and Fig.3.9, it is clear that the multi-stage AF-AOTF with the strain difference control has less transmission deformation than the cascading structure AF-AOTF subject to the frequency difference control. The experiment results are in reasonable agreement with the simulation results. As shown in Fig.3.7, the PZT nonlinearity can introduce additional distortion on the system transmission profile. It justifies the theoretical conclusion in above two sections that the strain difference control can produce a desired composite transmission profile without the synchronization problem suffered by existing all-fiber AOTF filters subject to the frequency difference control.

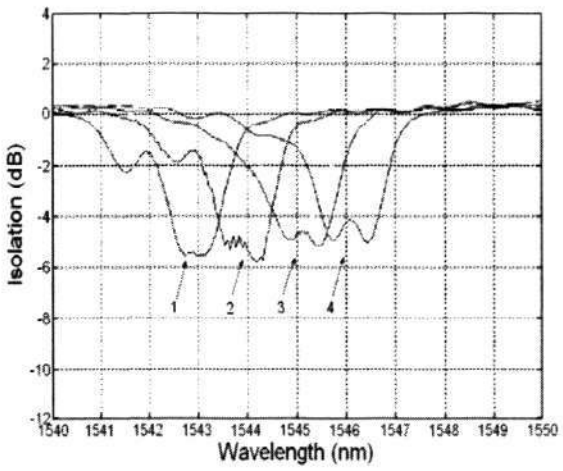

Figure 3.10: Composite transmission profile of two-stage AF-AOTF subject to frequency difference control (curve 1: f_1/f_2 = 2.360Mhz/2.364Mhz; curve 2: f_1/f_2 = 2.355Mhz/2.359Mhz; curve 3: f_1/f_2 = 2.350Mhz/2.354Mhz; curve 4: f_1/f_2 = 2.345Mhz/2.349Mhz).

3.4 Conclusions

In this chapter, strain control schemes to improve the system tunability of multi-stage AF-AOTF are studied. Firstly, in the traditional multi-stage AF-AOTF where all participant AF-AOTFs are controlled by different frequency RF signals, the strain effect on the transmission tunability is theoretically studied for the first time. It is proven analytically that applying strong axial strain on each acousto-optical interaction fiber can improve the tunability of the multi-stage AF-AOTF subject to frequency difference control.

Secondly, a novel strain difference control scheme to achieve the desired tunable complex transmission is proposed. In the proposed scheme, all AO interaction stages are driven by the RF signals with same frequency. The realization of the complex transmission profile is achieved by applying different and constant strains on the fiber in each AO interaction stage. Besides the tunability improvement, the tuning of the multi-stage AF-AOTF is implemented through tuning the single RF signal frequency just like one AF-AOTF. Theoretical analysis shows this design scheme can effective suppress the transmission profile distortion due to both the AF-AOTF principle nonlinearity and the PZT performance limitation. As a result, the system tunability is improved by using the proposed design scheme. The theoretical conclusions are verified by the simulation and experimental results.

Chapter 4

Loop Structure AF-AOTF

4.1 Introduction

In this chapter, we address the effect of the acoustic bandwidth which is the key implementation issue of multi-stage AF-AOTF. It is found the acoustic bandwidth is the key factor limiting the further improvement of the tunability of the composite transmission no matter which improved control schemes in the last chapter are applied. To solve the problem, a loop structure AF-AOTF is proposed and demonstrated. This AF-AOTF structure accommodating multiple AO interactions can utilize the full range of the acoustic bandwidth. It thus can provide better tunability working with the improved control schemes.

To see the effect of the acoustic bandwidth on the tunability, we first consider two traditional multi-stage AF-AOTFs in section 4.2. One is the cascading AF-AOTFs and the other is the multi-frequency AF-AOTF which applies multiple RF frequencies on single PZT to drive an AO interaction. Then, in section 4.3, we present the results of using loop structure AF-AOTF to deliver enhanced notch transmission by the strain difference control scheme. In section 4.4, the performance

of the loop structure AF-AOTF is compared with the traditional structures of multi-stage AF-AOTF in terms of implementation issues including the applicability of the improved control schemes, the transmission modulation agility, the practical tuning range, the tuning time, the tunability of the transmission, and the system costs.

4.2 Acoustic Bandwidth Limitation of Traditional Multi-stage AF-AOTFs

As shown in Chapter 3, a multi-stage AF-AOTF is the most efficient method to function as an optical tunable filter with complex transmission. The tuning of the obtained complex transmission is achieved by controlling all participant AF-AOTFs simultaneously. Conventionally, there are two structures of multi-stage AF-AOTF. One is the cascading structure and the other is the multi-frequency AF-AOTF. The control schemes of multi-stage AF-AOTF have been analyzed in the last chapters. Now we examine an implementation issues, acoustic bandwidth, with these multi-stage AF-AOTFs.

4.2.1 Cascading Structure AF-AOTF

The most familiar multi-stage AF-AOTF is cascading AF-AOTF. A cascading structure multi-stage AF-AOTF is shown in Fig.4.1.

The cascading structure AF-AOTF is fabricated on n pieces of fiber whose coatings are stripped off. Each piece of bare fiber is adhered to the tip of an isolate taper shape horn. The bottom of these horns are attached to n axial mode piezoelectric transducers (PZT) individually. Each PZT is driven by an isolate RF signal generator. Between any two neighboring AO interaction stages, optical mode striper, acoustic damper and several meters fiber with polymer coating are employed to

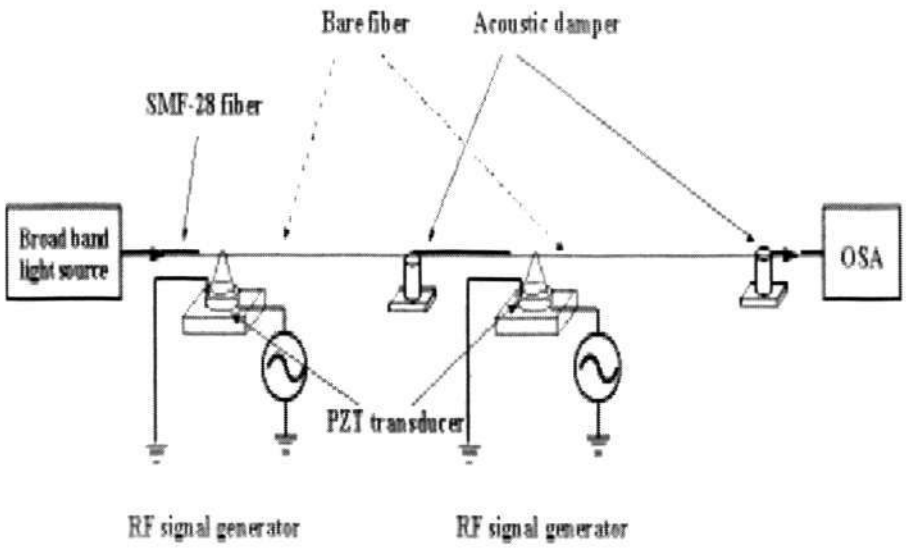

Figure 4.1: Schematic diagram of cascading structure AF-AOTF. PZT–Piezoelectric transducer. OSA–Optical spectrum analyzer.

filter out the unwanted resultant acoustic wave and optical power in the high order mode. For the un-polarized light source, polarization controller or polarizer is inserted between two neighbor AO interaction stages to avoid the polarization effect.

For the cascading structure AF-AOTF, the AO interactions perform on different pieces of isolate bare fiber. Each AO interaction stage has its own individual acoustic signal control system. Therefore, the control of the acoustic wave frequency, amplitude and the axial strain of certain AO interaction stage are independent with that of other AO interaction stages. Furthermore, the fiber diameter, AO interaction length and even the fiber material of each AO interaction stage can be separately adjusted without any side-effects on other parts of the system. As shown in Chapter 2, through varying above parameters, the optical isolation, center wavelength, notch bandwidth and roll-off factor of a single-stage AF-AOTF can be fully controlled. Among different multi-stage AF-AOTFs, cascading structure multi-stage AF-AOTF has most available control variables. Hence, cascading AF-AOTF has the most excellent flexibility on the complex transmission profile modulation. Compared with

other multi-stage AF-AOTF structures, more complex transmission profiles can be achieved in relative simpler manners by using cascading AF-AOTF .

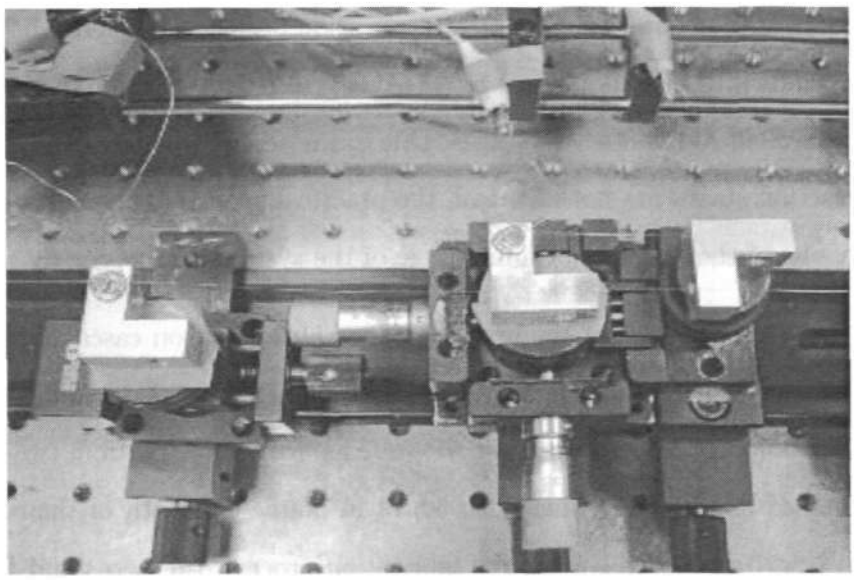

Figure 4.2: Experimental setup of cascading structure AF-AOTF.

However, in practice, the tunability of the complex transmission produced by the cascading structure AF-AOTF is not excellent. AF-AOTF can only provide strong AO interaction in certain acoustic frequency range. This acoustic frequency range is denoted as the acoustic bandwidth of AF-AOTF. It has been recognized as the primary factor that restricts the tuning range of AF-AOTF [56]. For a single-stage AF-AOTF, the acoustic bandwidth of the system is determined by the piezoelectric ceramic material, fabrication of AF-AOTF, horn shape and many other mechanical factors. For a cascading multi-stage AF-AOTF, there are more than one acoustic transducers exist in the system. Because the limitations on the material homogeneousness and fabrication accuracy, it is difficult and expensive to assure that all acoustic transducers of different AO interaction stages have identical acoustic properties. Thus, in practice, mismatches between the acoustic bandwidths of different AO interaction stages are inevitable. Acoustic bandwidth mismatches between different AO interaction stages will result in reduction of the practical tuning range

of the multi-stage AF-AOTF. In the whole tuning range of multi-stage AF-AOTF, the acoustic transducers of all AO interaction stages are required to provide strong acoustic power to maintain the overall transmission profile. Therefore, the practical acoustic bandwidth of the multi-stage AF-AOTF is the intersection of the acoustic bandwidths of all AO interaction stages. Due to the acoustic bandwidths of different AO interaction stages are not identical, the practical acoustic bandwidth is narrow than any one of them and the tuning range of the system can be greatly reduced.

Fig.4.3 shows an example of the acoustic bandwidth effect on cascading structure multi-stage AF-AOTF. Two single-stage AF-AOTFs are cascaded to deliver a band-stop transmission. These single-stage AF-AOTFs are fabricated from two pieces of equally etched single mode fiber with $50\mu m$ in diameter. Both of them have interaction length of $10cm$. During the fabrication process, the horns and PZTs are carefully chosen to reduce the acoustic bandwidth mismatch between the acoustic transducers of these two AO stages as much as possible under the current facility condition. The frequency difference control scheme is applied on this two-stage AF-AOTF and its transmission is tuned in the range of $[1566nm, 1580nm]$. From Fig.4.3, it shows that when the transmission is tuned to the edge of the system bandwidth, one of the two participant notch transmissions will become very weak, while the other one still have strong AO coupling efficiency. The acoustic bandwidth mismatch between two AO interaction stages greatly reduces the practical bandwidth of the system.

Therefore, the acoustic bandwidth mismatch between different AO interaction stages introduces difficulties into the control of cascading structure AF-AOTF. To obtain desired AO coupling efficiency at certain wavelength, each AO interaction stage needs an individual RF signal control module. During the tuning process of the multi-stage AF-AOTF, all these RF signals need to be recalculated and synchronized with each other. The calculation workload of the device is thus big, which in turn

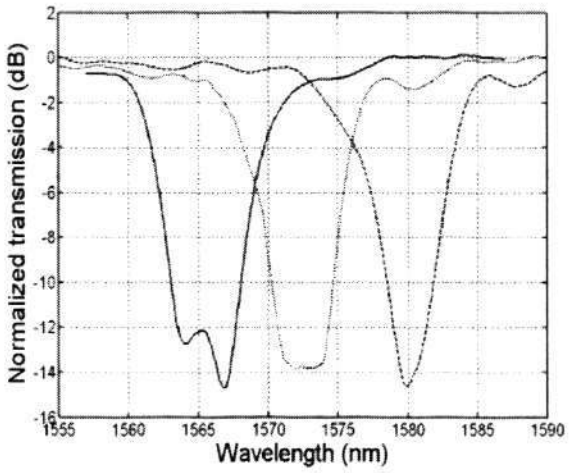

Figure 4.3: The optical tuning range limitation of cascading AF-AOTF.

limits the system response speed.

Furthermore, for the cascading structure AF-AOTF, each AO interaction stage needs a complete setup including PZT, horn and RF signal control module. The number of accessory components make the system is often troubled by high costs, massive volume and excessive power requirement. Especially when the device has many AO interaction stages, these problems will become more serious.

For the cascading structure AF-AOTF, both the frequency difference control scheme and the strain difference control scheme can be applied to implement complex transmission because the strain and the acoustic frequency on each AO interaction stage can be controlled individually.

4.2.2 Multi-Frequency AF-AOTF

Another structure of multi-stage AF-AOTF is multi-frequency AF-AOTF as shown in Fig.4.4.

An acoustic signal containing multiple frequency components can be applied on an

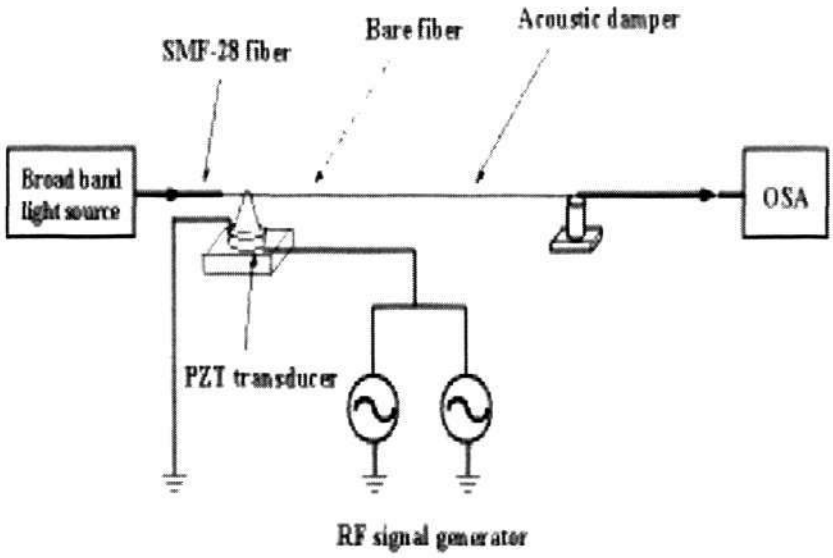

Figure 4.4: Schematic diagram of multi-frequency AF-AOTF.

single AO interaction stage to produce various transmissions. For a multi-frequency AF-AOTF, different acoustic waves share a set of AO interaction stage that consists of one-piece bare fiber, PZT, horn, mode stripper and acoustic damper. Each acoustic wave is produced by a RF signal at certain frequency and produces a notch transmission. The isolation and central wavelength of the notch transmission can be individually controlled through modulating the amplitude of a frequency component RF signal. An AF-AOTF driven by a RF signal with n different frequency components is equivalent to an optical filter with n effective AO interaction stages, while all AO interaction stages share the same acoustic medium and producer.

Multi-frequency AF-AOTF greatly simplifies the device configuration. Only one set of PZT, horn, mode stripper and acoustic damper are required. It leads to some advantages such as small volume and low cost.

For multi-frequency AF-AOTF, if the applied RF signal frequencies are close to each other, coherent crosstalk between different acoustic waves will happen and disturb the desired transmission. To show this phenomena, an experiment is carried out,

where a multiple-frequency AF-AOTF is used to deliver the stopband transmission. Fig.4.5.1 shows the experimental results where the AO interaction length is chosen as $60cm$ and two RF frequencies are applied on the same PZT. When the frequencies of these two RF signals are tuned to $2.360MHz$ and $2.370MHz$, respectively, a clear interference spectrum pattern is observed on OSA. Further reducing the difference between the frequencies of these two RF signals will enhance the interference pattern as shown in Fig.4.5.2.

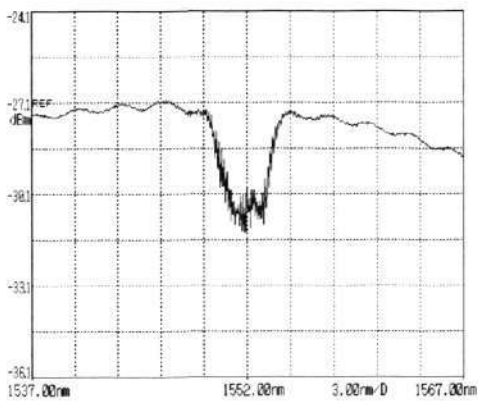

4.5.1: Two-stage Multiple-frequency AF-AOTF ($f_1 = 2.360MHz$ and $f_2 = 2.370MHz$).

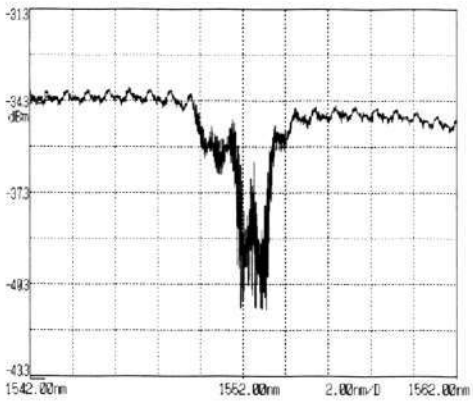

4.5.2: Two-stage Multiple-frequency AF-AOTF ($f_1 = 2.360MHz$ and $f_2 = 2.365MHz$).

Figure 4.5: Coherent cross talk between different frequency acoustic waves in the multi-frequency AF-AOTF.

To avoid the cross talk problem, the RF frequencies are spaced enough with each other. The notch transmissions used to form a complex transmission is actually contributed by different mode coupling. However, the number of available evacuation optical modes for AO coupling process is limited. Currently, there are not more than four cladding modes observed in experiment. Thus, the number of AO interactions for multi-frequency AF-AOTF is limited and may not satisfy the requirement of some applications.

Furthermore, because the light power in the fundamental mode is coupled into differ-

ent cladding modes, the required frequency difference between different RF driving signals is large, about $0.3MHz - 0.8MHz$. To obtain the desired isolation, the frequencies of all these driving signals must be guaranteed in the acoustic bandwidth of the PZT. Therefore, for multi-frequency AF-AOTF, the PZT acoustic bandwidth limitation has more serious effect on the device tuning range in practice. For example, assuming the PZT acoustic bandwidth is given from $2.5MHz$ to $3MHz$. Then, for the AO coupling between Lp_{01} and Lp_{11}^{cl}, the corresponding optical wavelength can be tuned from $1650nm$ to $1550nm$. But for the AO coupling between Lp_{01} and Lp_{12}^{cl} modes, the corresponding optical tuning range can only be tuned from $1600nm$ to $1500nm$. Thus, to build a bandstop transmission, the available optical tuning range of the system is from $1550nm$ to $1600nm$. The tuning range of the system is reduced from $100nm$ to $50nm$ by the mismatch between the optical bandwidth of the AO coupling between different modes.

Finally, the optical beatlength L_B between different pairs of optical modes have different relationships with the optical wavelength. For example, assuming that $L_B|_{01,11}$ is the optical beatlength between Lp_{01} mode and Lp_{11}^{cl} mode; $L_B|_{01,12}$ is the optical beatlength between the Lp_{01} mode and Lp_{12}^{cl} mode. The corresponding RF driving signals are f_1 and f_2, respectively. When the central wavelength of the notch shifts from λ_0 to λ_1, the required variation of $L_B|_{01,12}$ and $L_B|_{01,11}$ are $\Delta L_B|_{01,11}(\lambda_0 \rightarrow \lambda_1)$ and $\Delta L_B|_{01,12}(\lambda_0 \rightarrow \lambda_1)$, respectively. We always have that

$$\Delta L_B|_{01,11}(\lambda_0 \rightarrow \lambda_1) \neq \Delta L_B|_{01,12}(\lambda_0 \rightarrow \lambda_1) \tag{4.1}$$

The required acoustic frequency variation for different AO interaction stages are different $\Delta f_1 \neq \Delta f_2$. To maintain the overall transmission in the whole tuning range of the device, separated control modules are required for the RF signals f_1 and f_2. When many acoustic waves are applied on the fiber, the control of all the RF signals will be quite complicated and possibly offset the benefit from the simplicity

of the configuration.

In multi-frequency AF-AOTF, all AO interaction stages share the same AO interaction medium. Thus, the mechanical parameters such as AO interaction length, fiber diameter and axial strain of all AO interaction stages are same. As a result, the optical properties such as bandwidth and roll-factor of all notch spectra are correlated with each other. This causes some limitation on the overall transmission design.

Only the frequency difference control scheme can be applied in the design of multi-frequency AF-AOTF. The transmission deformation of the system is worse than other structures which can accommodate both the strain control and the frequency control. To overcome this problem, additional frequency composite control with a careful design is required to suppress the phase mismatch error during the center wavelength tuning process.

4.3 Loop Structure AF-AOTF

To overcome the limitations of the traditional multi-stage AF-AOTF, a loop structure of multi-stage AF-AOTF is proposed to implement the optical tunable filter to deliver complex transmissions. This structure can accommodate the proposed tunability improve schemes. The schematic diagram of loop structure AF-AOTF is shown in Fig.4.6.

The filter is fabricated by folding a piece of fiber to form a loop. Several sections of the fiber in the loop are stripped off their coating. One end of each of these sections is placed in parallel and attached to the tip of same horn, which is adhered to an axial mode PZT. The other ends of the stripped sections inside the loop are respectively fixed at several moving acoustic damper stages, respectively. When a radio frequency

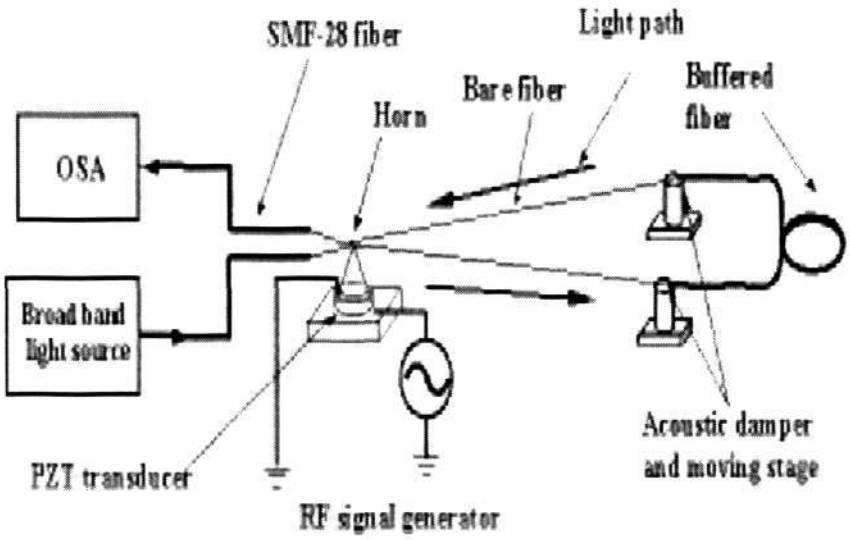

Figure 4.6: Schematic diagram of loop structure AF-AOTF.

(RF) voltage is applied to the PZT, an acoustic field is formed and amplified at the tip of the metal horn. The resultant flexural acoustic waves propagate along each pieces of stripped fiber and produce micro bends along them. In turn, the AO coupling happens on each piece of fiber. Therefore, each piece of stripped sections forms an AO interaction stages. As they are driven by a single acoustic excitation source, the acoustic wave frequency on each piece of bare fiber is the same and the center wavelengths of all notches exist at the same optical wavelength. By individually controlling the strain on different piece of bare fiber, the position of each notch profile is shifted to the desired position. The overall transmission of these notches exactly meets the desired complex transmission. The strains applied on each piece of bare fiber are fixed. The centerwavelength of obtained transmission is controlled by the frequency of the RF signal only. The process of the system centerwavelength tuning is simple and naturally synchronous just like that of a single-stage AF-AOTF.

The loop structure is free from the synchronizing of different AO interaction stages, which results in many attractive features. The most attractive feature is that loop

structure can efficiently make use of the acoustic bandwidth PZT and has large tuning range. For loop structure, the optical power in the fundamental mode is coupled to the same cladding mode. But unlike the multi-frequency AF-AOTF, there is no coherent cross-talk problem for the loop structure AF-AOTF. This is because all AO couplings happen on individual AO interaction regions. On each piece of bare fiber, there is only one acoustic wave exist. In combination with the fact that all AO interaction stage are driven by the same RF signal through same acoustic generator, the optical tuning range for all AO interaction stages are identical. The whole acoustic bandwidth of PZT is available for the system, which means large tuning range.

Secondly, because in all AO interaction stages the optical power in the fundamental mode is coupled to the same cladding mode, the relationship between the acoustic frequency and corresponding optical center wavelength are the same. All notches are synchronically shifted along the optical wavelength when the driving RF signal frequency changes. It greatly simplifies the control scheme design of the system. The required calculation time is greatly reduced, which leads to fast tuning speed. Thirdly, because each AO interaction stage has an individual AO coupling medium, the bandwidth of each notch profile can be modulated through varying the fiber diameters individually. Therefore, the modulation agility on transmission of loop structure AF-AOTF is worse than that of cascading structure AF-AOTF but better than multi-frequency AF-AOTF. Finally, for loop structure, only one acoustic generator is required. The corresponding acoustic signal control system design is also greatly simplified as mentioned above. Because during the tuning process, the strain difference is fixed and it can be obtained during the calibration process, no complex strain control components are required. Compared with other structures, the loop structure is the most economic solution of the optical tunable filter with complex transmission.

In the following parts of this section, we use two examples to show the advantages of loop structure. In first case, loop structure is used to solve the weak AO coupling efficiency problem for single mode fiber based AF-AOTF. In the second case, loop structure is used to deliver bandstop transmission. By comparing with the experimental results obtained by using cascading structure AF-AOTF and multi-frequency AF-AOTF, it shows that loop structure AF-AOTF is less affected by the acoustic bandwidth limitation and has superiority on the system tunability.

Single mode fiber is the standard optical link in most optical networks currently. As a result, AF-AOTF based on single mode fiber is an attractive component for optical communication because it can be simply employed in most optical networks without any modifications. However, the AO coupling efficiency of the single mode fiber based AF-AOTF is low due to the weak overlap of acoustic and optical field in the single mode fiber. Although enhancing the power of the acoustic field is a straightforward way to generate strong AO coupling in single mode fiber, the acoustic power in the fiber is limited by the power utilization efficiency of the acoustic transducer and acoustic attenuation along the fiber[85]. This greatly limits the application of single mode fiber based AF-AOTFs. Several schemes have been proposed to improve the AO coupling efficiency. They include the one of applying AO interaction on tapers and couplers [65],[56], the one of using longitudinally coupling acoustic flexural waves [58], and the one of reducing the cladding diameter by chemically etching fiber[80, 81]. These schemes have been shown to be able to improve the AO interaction even though with some limitations, but they need special treatment of fiber and their improvement is still limited. Actually, a simple way to obtain an enhanced notch transmission is to use a multi-stage AF-AOTF. By tuning the acoustic frequencies of all cascaded AOTFs, the notch transmissions of AOTFs can be made to superpose at the same central wavelength, and in turn a composite enhanced notch transmission can be achieved. However, a synchronous tuning of all the frequencies is required to maintain an acceptable superposition result when the

composite transmission is being tuned from one central wavelength to another. It is quite difficult for the conventional cascading structure AF-AOTF. By using loop structure, the difficulty in synchronous tuning is naturally avoided.

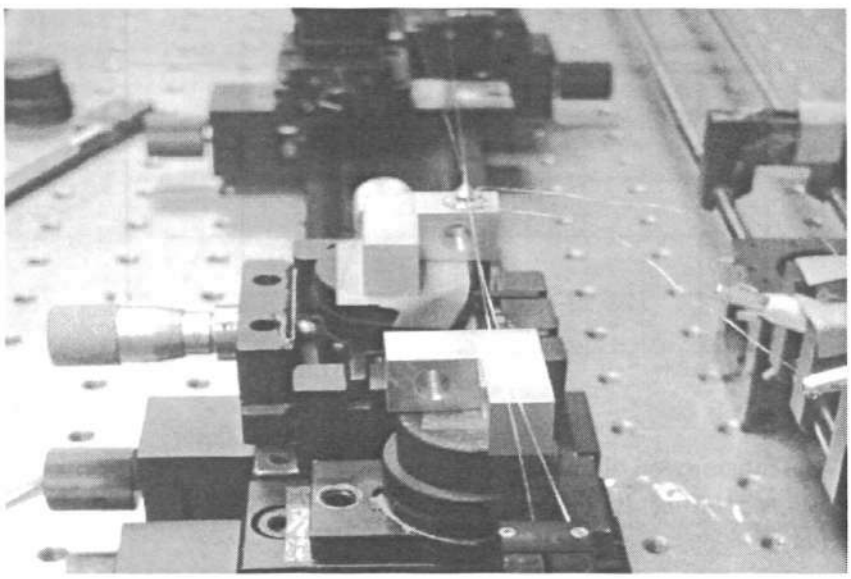

Figure 4.7: Experimental setup of loop structure AF-AOTF.

A two-stage loop structure AF-AOTF based on single mode fiber is built up to implement an enhanced tunable notch filter according to the configuration in Fig.4.7. In the experimental setup, both AO interaction stages have the same AO interaction length of 60cm. The buffered fiber between two AO interaction stages is left with 1m long, and the driving power applied to the PZT is maintained at $130mW$. In the experiment, a C-band SLED light source is used to provide a broadband light input to the filter. The transmission of the filter is observed by an optical spectrum analyzer (OSA). To obtain an enhanced notch transmission, the AOTF is calibrated by the following procedures. First, the RF frequency is tuned to 2.38MHz. In this case, the OSA shows two shifted notch spectra. Then, with the RF frequency fixed, strain is applied respectively on each stripped section by moving the damper stages. The strain adjustment is carried on until the two notch responses totally overlap. After the calibration is done, a single notch transmission is obtained as shown by curve

2 in Fig.4.8. The RF signal is varied to examine the tunability of loop structure

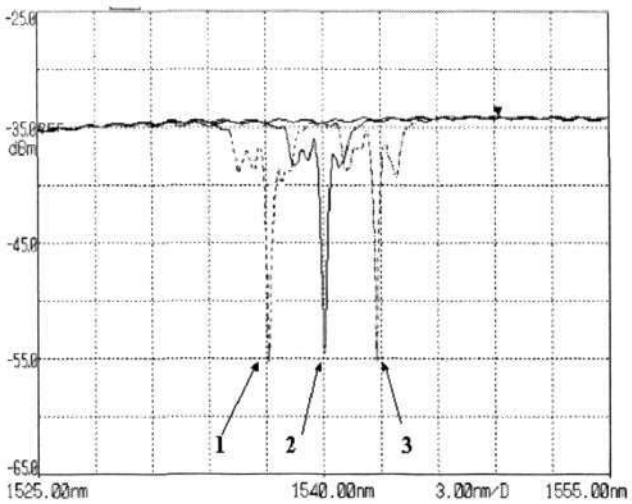

Figure 4.8: Transmission of enhanced notch filter based on loop structure AF-AOTF in response to tuning RF signal frequency (1–f=2.390MHz;2–f=2.380MHz;3–f=2.370MHz).

AF-AOTF with all other setting parameters fixed. Fig.4.8 shows the output spectra in response to RF frequencies 2.39MHz, 2.38MHz and 2.37MHz, respectively. By continuously tuning the RF frequency, identical notch responses are observed at other wavelengths over the whole C-band. This result shows that the notch transmission can be shifted with the RF frequency, just as tuning a conventional AF-AOTF. For comparison, a conventional AF-AOTF with a single AO interaction section[86] is also built in experiment with the same settings as above, *e.g.*, 130mW RF signal power and 60cm long stripped sections. Tuned the RF frequency respectively to 2.37MHz, 2.38MHz and 2.39MHz, the notch responses are recorded in Fig.4.9. Comparing the transmissions in these two figures, it is clear that the loop structure AF-AOTF greatly enhances the notch transmission with the maximum optical isolation being increased from 9dB for the conventional AF-AOTF to 20dB. In addition, loop structure design needs only one set of accessory equipment such as RF signal generator, PZT and horn. The filter can be more easily controlled by a more economical means than the ones obtained by cascading structure AF-AOTF.

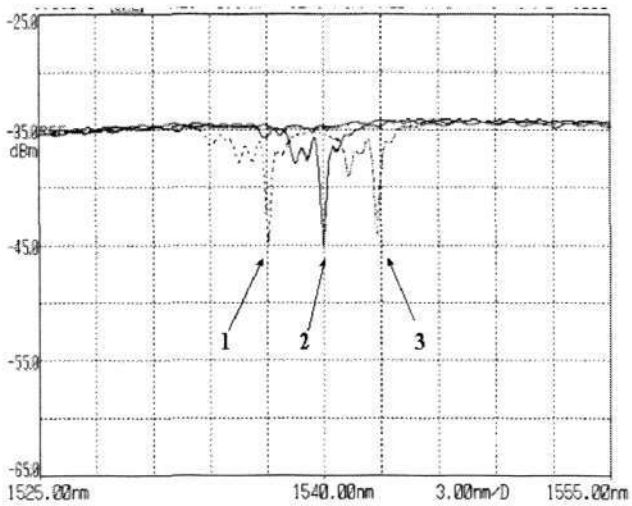

Figure 4.9: Transmission of single-stage AF-AOTF in response to tuning RF signal frequency (1–f=2.390MHz;2–f=2.380MHz;3–f=2.370MHz).

In last section, we have shown the acoustic bandwidth effect on the cascading structure AF-AOTF and multi-frequency AF-AOTF. Now we will conduct some experimental studies to exam the acoustic bandwidth effect on loop structure AF-AOTF. The experiment of on using two-stage loop AF-AOTF to deliver a bandstop transmission as shown in Fig.4.3 is conducted in first. The experimental results is shown in Fig.5.7 and more discussion can be found in next chapter where the applications of multi-stage AF-AOTF are discussed in detail.

Then, to illustrate the effect of the acoustic bandwidth of PZT on the multiple-frequency AF-AOTF and to demonstrate the performance when using multiple loops in the strain-controlled AF-AOTF, we conducted experiments by using four notches to deliver a maximally flat stop-band transmission with a wider bandwidth. A strain-controlled loop AF-AOTF with four loops is fabricated by using a $SMF-28$ fiber as shown in Fig.4.10 where only one arm of each loop is used as an AO interaction stage. The length of any AO interaction stage is chosen as $20cm$. A maximally flat stop-band transmission is first calibrated at $1570nm$ by applying an acoustic frequency of $2.711MHz$ and tuning the strain of each arm. The calibrated

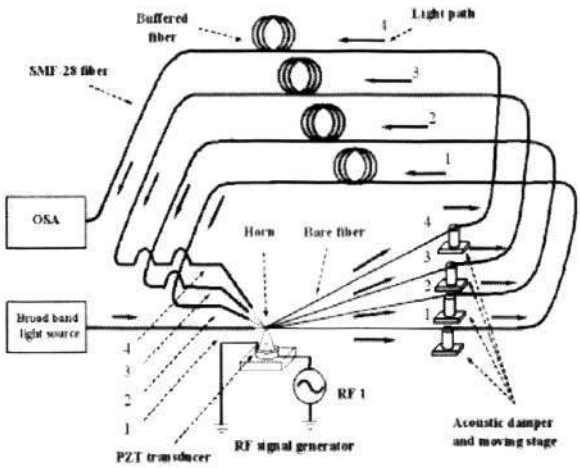

Figure 4.10: Experimental setup of a four-loop strain-controlled AF-AOTF

stop-band is shown by curve 2 in Fig.4.11.1. After the calibration, we tune the frequencies to $2.733MHz$ and $2.689MHz$, respectively. The corresponding stopband transmissions are shown by curve 1 and 3 in Fig.4.11.1 respectively. The results demonstrate that multiple loops can be implemented in the loop structure AF-AOTF to generate a more complex transmission profile. It is also noted from the experimental results that the AO coupling efficiency would be limited if too many loops are used. For the multiple-frequency AF-AOTF, it is fabricated as shown in Fig.4.11.2, where the AO length is chosen as 20cm and four RF frequencies are applied on the PZT. To achieve the same flat stopband transmission at $1570nm$ as the one displayed by curve 2 in Fig.4.11.1, four frequencies are chosen as $1.940MHz$, $2.240MHz$, $2.692MHz$, and $3.341MHz$ so that the notches resulting from mode-coupling $Lp_{01} - Lp_{11}^{cl}$, $Lp_{01} - Lp_{12}^{cl}$, $Lp_{01} - Lp_{13}^{cl}$ and $Lp_{01} - Lp_{14}^{cl}$ are obtained and superposed. By tuning the acoustic amplitudes of each notch, a flat stop-band transmission is calibrated at $1570nm$ and it is shown in curve2 of Fig.4.11.2. The maximum isolation of the bandstop transmission is limited by the mode coupling efficiency of $Lp_{01} - Lp_{14}^{cl}$. Then, we tune the composite stopband by the same tuning method as that used in the loop structure AF-AOTF. In the method, all the

acoustic frequencies are tuned with the same incremental value while the acoustic amplitudes remain the same as calibrated. The stopband transmission is tuned to the same central wavelengths as in Fig.4.11.1. The results are shown in curves 1 and 3 of Fig.4.11.2, respectively. Compare to the curves in Fig.4.11.1, it is observed that the stopbands resulting from the multiple-frequency AF-AOTF have severe distortion. This can be understood by examining the frequency responses of the PZT with respect to different mode coupling.

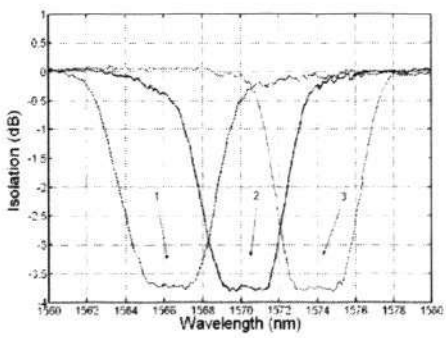

4.11.1: Four-loop Strain-controlled AF-AOTF

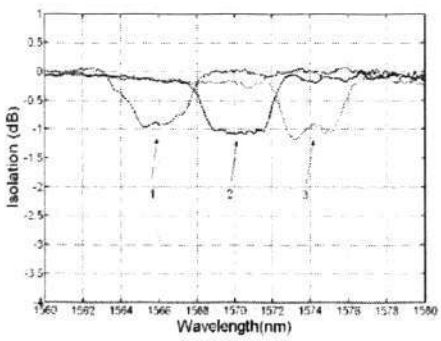

4.11.2: Multiple-frequency AF-AOTF

Figure 4.11: The bandstop responses obtained by the loop AF-AOTF and the multiple-frequency AF-AOTF

The frequency responses are measured in experiment by recording the isolation of the notch resulting from each mode-coupling while the notch is tuned within the range of $1560nm - 1580nm$ as shown in Fig.4.11.2. The measurement results are given in Fig.4.12. When the stopband transmission is tuned in the range, the four frequencies used by the multiple-frequency AF-AOTF spread in four bands denoted respectively by band 1 to band 4 in Fig.4.12, while the frequency of the strain-controlled loop AF-AOTF tunes only band 3. Clearly, since band 2 has a bigger variation than band 3, the strain-controlled loop AF-AOTF exhibits a better tunability than that of the multiple-frequency AF-AOTF.

Of course, compared to the traditional multi-stage AF-AOTFs, the loop structure

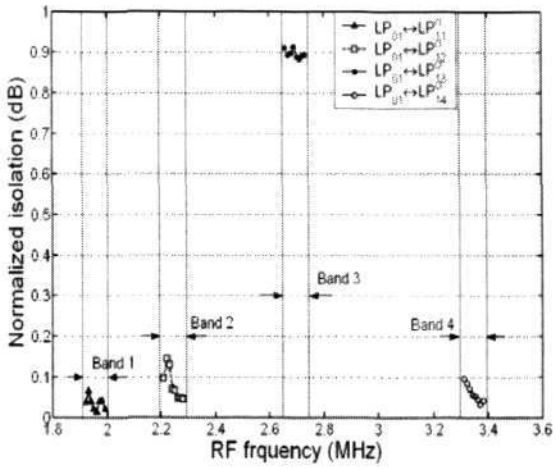

Figure 4.12: Frequency responses of PZT for different mode couplings

also has limitations in some aspects. In loop structure AF-AOTF, the sharing of the acoustic generator avoids the synchronizing problems but reduces the modulation agility on transmission. Different notches isolations are achieved through individually adjusting the AO interaction length of each AO interaction at the initial static state. During the tuning process, the isolation of the system can be modulated through adjusting the RF signal amplitude. But compared with the cascading structure AF-AOTF, it is not convenient to dynamically adjust the isolation of each notch profile individually for that dynamically modulating the acoustic interaction length is quite complicated in practice.

For the loop structure AF-AOTF, all AO interaction stages are driven by the same RF signal and only the strain difference control can be applied. Because the strain is fixed during the tuning process, the modulation agility on transmission is less than the cascading structure AF-AOTF but better than that of the multi-frequency AF-AOTF.

4.4 Comparison of Different Integration Structures of Multi-stage AF-AOTF

In previous sections, three implementation structures of multi-stage AF-AOTF with complex transmission have been discussed. It shows that loop structure AF-AOTF has superiority on tunability. However, other structures also have some advantages in particular applications. To give a comprehensive comparison of different multi-stage AF-AOTF structures, the performance of the loop structure AF-AOTF is compared with the traditional structures of multi-stage AF-AOTF in terms of following implementation issues:

- Applicability of the improved control schemes: The control schemes, frequency difference control and strain difference control, that can be applied on the multi-stage AF-AOTF.
- Agility on transmission profile modulation: The ability to implement what kind of transmission profiles by using multi-stage AF-AOTF.
- Tuning range: The practical tuning range of the AF-AOTF, which is primarily limited by the acoustic bandwidth limitation of the acoustic transducer.
- Tuning time: The tuning time of multi-stage AF-AOTF including the calculation time of the control parameters.
- Tunability: The transmission distortions when the transmission is tuned to a new central wavelength.
- System costs: The total cost of the system including the cost on the acoustic transducers, control components and other accessary equipments.

The comparison of different AF-AOTF structure is summarized in Table.4.1.

Table 4.1: Comparison of different integration structures for AF-AOTF

Structure	Cascading structure AF-AOTF	multi-frequency AF-AOTF	Loop Structure AF-AOTF
Configuration	Complicated	Simple	Simple
Control scheme	Frequency difference modulation scheme or strain difference modulation scheme	Frequency difference modulation scheme	Strain difference modulation scheme
Agility on transmission profile modulation	High	Low	Normal
Practical tuning range	Depends on the fabrication	Small	Large
Tuning time	Long	Long	Short
Tunability	Depends on the fabrication	Poor	Excellent
System Cost	High	Normal	Low

From Table.4.1 and discussions in previous sections, we can draw some remarks about the properties of the three structures multi-stage AF-AOTF. First, it shows that the loop structure AF-AOTF working with the strain difference control scheme can provide the best tunability and the highest cost efficiency. It is suitable to be employed in the applications where the operating wavelength is required to be shifted in large tuning range with a desired transmission. The applications include dynamic multiplexer, demultiplexer, tunable attenuator, tunable elimination filter and tunable signal modulator.

Secondly, the cascading structure AF-AOTF has the best modulation agility on the transmission. Both the strain difference control scheme and the frequency difference control scheme can be applied on this structure. But the tuning range of the cascading structure AF-AOTF is limited by the synchronization problem. The cascading structure AF-AOTF is suitable to be used in the applications where the transmission is required to be in-line modulated and the system operating wavelength is fixed or

confined in small range. For example, it can be used in the dynamic EDFA gain equalization.

Third, the multi-frequency AF-AOTF has the average performance in most characteristics. It is simple and economic compared to the cascading structure AF-AOTF. But its modulation ability on transmission is limited by the number of the available cladding modes. Only the frequency difference control scheme can be applied on the multi-frequency AF-AOTF. If the demand on the accuracy of system transmission is not critical, multi-frequency AF-AOTF may be a good choice in some applications.

4.5 Conclusion

In this chapter, the practical problems in the implementation of multi-stage AF-AOTF with complex transmission are studied. To overcome the limitations with the traditional multi-stage AF-AOTF, a novel loop structure AF-AOTF is proposed to accommodate the proposed tunability improved schemes. Its performance is compared with those of other structures. Based on the comparison results, the optimal application environments for different integration structures are addressed to provide a design guideline for implementation of the optical tunable filter with complex spectrum based on AF-AOTF technology.

Chapter 5

Applications of AF-AOTF in Optical Communications

5.1 Introduction

In early chapters, the design, optimization and physical implementation of the tunable complex transmission profile based on multi-stage AF-AOTF have been systematically developed. This chapter will illustrate several typical and important applications of the tunable complex transmission profile in the optical communication system. In all these applications, AF-AOTF plays an important role to implement the modulation of the optical signals. However, as the objectives of these applications are different, the design and control of the employed AF-AOTFs are significantly different as well. Thus, it is necessary to individually develop and discuss the design and control scheme in each application. In the following several chapters, these problems of AF-AOTF in the applications of optical Add/Drop multiplexing, EDFA gain equalization and EDFA gain clamping are studied.

5.2 Application of AF-AOTF in Optical Add/Drop Multiplexing

Optical fiber can transmit the optical signal in wide bandwidth, which can reach about $25 - 30THz$, without large transmission loss. The traditional time division multiplexing scheme usually works at the speed not more than 100GHz and cannot utilize the broad bandwidth of fiber. It is limited by the speed of the time multiplexing and demultiplexing components. To exploit more of the broad bandwidth of the fiber, wavelength division multiplexing technology (WDM) is developed. In WDM networks, the information is transmitted through multiple channels located at different wavelengths. The modulation speed of certain single wavelength is reduced, while the whole bandwidth capacity of the networks is greatly increased. One of the enabling technologies for WDM networks is dynamic Optical Wavelength Add/Drop Multiplexing (OADM) [2]. It plays a key role in the implementation of some important logic functions such as the optical routing and optical switching. To achieve the dynamic optical wavelength Add/Drop multiplexing, the optical transmission profile is required to be modulated and tuned along the optical wavelength with time. Obviously, optical tunable filter is essential for these operations. Among the available optical tunable filter technologies, AF-AOTF is promising for OADM for its attractive characteristics mentioned in Chapter 1. The idea of OADM based AF-AOTF technology has been reported in [74], where single-stage AF-AOTF was used to select out the optical channels to be added/dropped. However, the performance of the employed AF-AOTF is not optimized for OADM application. For dynamic OADM, the employed optical tunable filter should have an enough wide bandwidth and a fast roll-off factor in order to suppress the channel crosstalk and minimize the transmission profile distortion. To achieve these requirements, optimization and particular design of AF-AOTF transmission performance for the OADM application are necessary and have not been reported yet.

In this section, the realization issue of broadband optical tunable filter based on AF-AOTF technology for the dynamic OADM application is studied. Optical transmission profiles with different bandwidths and fast roll-off factor are obtained in experiment. These filters are implemented by the multi-stage AF-AOTF with a loop structure subject to strain difference control.

5.2.1 Performance Requirements of AF-AOTF for Dynamic Optical Add/Drop Multiplexing

For the dynamic optical Add/Drop multiplexing, the employed optical tunable filter is expected to have the following features.

- Firstly, since the practical optical pulses on each channel usually have certain pulse width and it is often required to add/drop multiple channels at the same time, the tunable filter should have a wide enough bandwidth with certain attenuation or gain value.

- Secondly, because that more and more transmission channels are simultaneously employed in one optical fiber, the optical channel spacing becomes smaller and smaller. As a result, the crosstalk between neighbor channels becomes serious. To avoid this problem, fast roll-off at the band edge is demanded. Usually, the roll-off factor of the designed filter is evaluated by the shape factor which is defined as the ratio between two bandwidth - the bandwidth at a specified attenuation on the roll-off curve to the corner bandwidth at its specified attenuation, usually $-3dB$. Especially, high shape factor is urgently demanded by the dense wavelength division multiplexing networks.

- Finally, because the channel switching and dynamic network reconfiguration will happen in high frequency in the dynamic optical networks, the tunable

filter for Add/Drop multiplexing must have fast response speed and simple control scheme. Therefore excellent tunability is also required.

5.2.2 Limitation of Ultra-Broadband Single-Stage AF-AOTF for Dynamic Optical Add/Drop Multiplexing

The ordinary bandwidth of signal AF-AOTF is in the range of $0.4 \sim 2nm$ at the attenuation of $-3dB$ using available standard single mode fiber. Li and Jin reported the method to control the bandwidth of AF-AOTF in [78, 75]. The ultra narrow band AF-AOTF with $-3dB$ bandwidth $0.4nm$ and ultra-broad band AF-AOTF with $-3dB$ bandwidth of $362nm$ were fabricated in experiment. However, in these demonstrations, the narrow or broad transmission bandwidth is achieved at the expense of a slow band roll-off. The transmission bandwidth at all isolation or gain value is almost equally broadened with the decreasing of the fiber diameters. Thus, the shape factor of a single-stage AF-AOTF is quite low and cannot provide the desired transmission performance.

The limitation of the shape factor of single AF-AOTF is because that the transmission profile of single AF-AOTF is a Sinc square function and its shape factor is only determined by the optical isolation. For a single-stage AF-AOTF, the transmission function is

$$G = 10\log\left(1 - \frac{C^2L^2\sin^2(L\sqrt{C^2+\delta^2})}{L^2C^2 + L^2\delta^2}\right) \tag{5.1}$$

To achieve xdB isolation, it requires that

$$\frac{\sin^2(L\sqrt{C^2+\delta^2})}{L^2C^2 + L^2\delta^2}) = \frac{1 - 10^{(-x/10)}}{(CL)^2} \tag{5.2}$$

Denoting $\sqrt{L^2C^2 + L^2\delta^2}$ as h, (5.2) become as

$$\frac{\sin^2(h)}{h^2} = \frac{1 - 10^{(-x/10)}}{(CL)^2} \tag{5.3}$$

Equation (5.3) can be numerically solved for any CL value. Denote the solution of (5.3) for the xdB isolation as h_x. Thus, the required δ for xdB isolation is

$$\delta_x = \frac{\sqrt{h_x^2 - C^2L^2}}{L} \tag{5.4}$$

Expanding δ to Taylor series and keeping the linear term $\Delta\lambda$ at the centerwavelength where $\delta = 0$ gives

$$\begin{aligned} \delta_x &= \delta_c + \frac{\partial\delta}{\partial\lambda}\frac{\Delta\lambda}{2} \\ &= \frac{\partial\delta}{\partial\lambda}\frac{\Delta\lambda}{2} \end{aligned} \tag{5.5}$$

Recalling the definition of δ in Chapter 2, following equation is deduced

$$\begin{aligned} \frac{\partial\delta}{\partial\lambda} &= \frac{\partial\left(\frac{\pi}{\Lambda} - \frac{\pi}{L_B}\right)}{\partial\lambda} \\ &= \frac{\pi}{L_B^2}\frac{\partial L_B}{\partial\lambda} \end{aligned} \tag{5.6}$$

Thus, xdB-bandwidth is

$$\begin{aligned} \Delta\lambda\,|_{xdB} &= \frac{2\sqrt{h_x^2 - (CL)^2}L_B^2}{\pi L\frac{\partial L_B}{\partial\lambda}} \\ \frac{\partial L_B}{\partial\lambda} &\neq 0; \end{aligned} \tag{5.7}$$

where C is the coupling coefficient, L is the AO interaction length, h_x (for $x =$

12 or 3) is the root of the following equation

$$\frac{\sin^2(h_x)}{h_x} = \frac{1-10^{(-x/10)}}{(CL)^2} \tag{5.8}$$

Therefore, the xdB to $-3dB$ band shape factor is given by

$$Q_x = \frac{\sqrt{{h_x}^2-(CL)^2}}{\sqrt{h_3^2-(CL)^2}} \tag{5.9}$$

For the case of the ultra-broad band AF-AOTF, $\frac{\partial L_B}{\partial \lambda} = 0$ and the xdB-bandwidth can no longer be determined by (5.7). But through expanding Q_x to Taylor series and maintaining the quadratic term $\Delta\lambda$, it can be obtained that

$$\begin{aligned} \delta_x &\approx \delta_c + \frac{\partial \delta}{\partial \lambda}\frac{\Delta\lambda}{2} + \frac{\partial^2 \delta}{\partial \lambda^2}\frac{\Delta\lambda^2}{4} \\ &\approx \frac{\partial^2 \delta}{\partial \lambda^2}\frac{\Delta\lambda^2}{4} \end{aligned} \tag{5.10}$$

With the condition that $\frac{\partial L_B}{\partial \lambda} = 0$, the second order derivatives of δ to λ can be obtained as

$$\begin{aligned} \frac{\partial^2 \delta}{\partial \lambda^2} &= \frac{\partial}{\partial \lambda}\left(\frac{\pi}{L_B^2}\frac{\partial L_B}{\partial \lambda}\right) \\ &= \frac{\pi}{L_B^2}\frac{\partial^2 L_B}{\partial \lambda^2} \end{aligned} \tag{5.11}$$

Thus, the xdB-bandwidth can be obtained as

$$\begin{aligned} \Delta\lambda\,|_{xdB} &= 2\sqrt{\frac{\delta}{\frac{\partial^2 \delta}{\partial \lambda^2}}} \\ &= 2\sqrt{\frac{\sqrt{h_x^2-(CL)^2}L_B^2}{\pi L \frac{\partial^2 L_B}{\partial \lambda^2}}} \end{aligned} \tag{5.12}$$

The corresponding xdB to $-3dB$ band shape factor is given by

$$Q_x = \frac{\sqrt[4]{h_x{}^2 - (CL)^2}}{\sqrt[4]{h_3^2 - (CL)^2}} \tag{5.13}$$

Equation (5.7) and (5.13) show that the shape factor of single-stage AF-AOTF is only determined by the AO interaction length L and AO coupling coefficient C. It is quite limited and cannot satisfy the requirement of many applications. To show this, $-12dB$ to $-3dB$ band shape factors is examined to evaluate the transmission performance of the filter. During this comparison, all filters are required to deliver a stopband of 0.4nm $-12dB$-bandwidth.

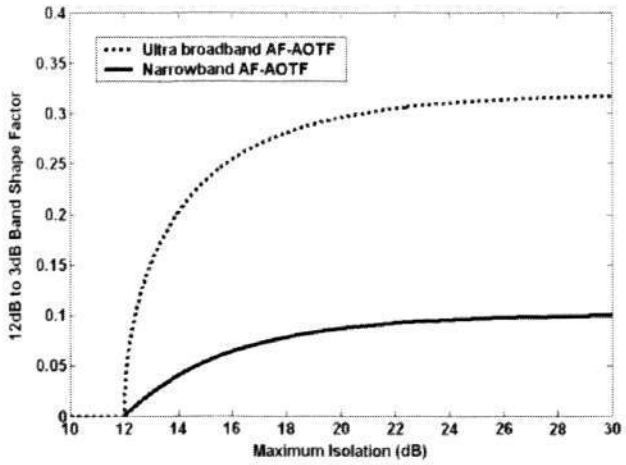

Figure 5.1: $-12dB$ to $-3dB$ band shape factors of a single-stage AF-AOTF.

Fig.5.1 depicts the values of Q_{12} corresponding to system maximum isolation, which is equal to $-20log(cos(CL))$. Q_{12} is an increasing function with respect to the optical isolation of the single AF-AOTF. To achieve high shape factor, high isolation induced by the single AF-AOTF is required. However, due to coupling efficiency limitation of PZT, high isolation is quite difficult to be implemented in wide optical wavelength range. Furthermore, even any high isolation could be obtained, the maximum value of the $-12dB$ to $-3dB$ shape factor is still quite limited, no more

than 10% for normal AF-AOTF and 30% for ultra-broad band AF-AOTF.

Actually, for the ultra-broad band AF-AOTF, as the condition $\frac{\partial \delta}{\partial \lambda} = 0$ only hold in a small wavelength band, the shape factor is much smaller than the values shown in the Fig.5.1 (for example, the ultra-broad band AF-AOTF shown in [75]).

5.2.3 Application of Broadband Multi-stage AF-AOTF in Dynamic Optical Add/Drop Multiplexing

Although the bandwidth of the filter can be greatly increased by etching the cladding diameter, the shape factor or the roll-off factor is still unsatisfactory. Thus, to implement a tunable stopband with desired bandwidth and fast roll-off or high shape factor, multi-stage AF-AOTF becomes the only practical way. The schematic diagram of dynamic optical wavelength Add/Drop multiplexing based on AF-AOTF technology is shown in Fig.5.2. The dynamic optical wavelength Add/Drop multiplexer is primarily composed of two parts, optical mode conversion part and optical mode selective routing part. The mode conversion part is based on multi-stage AF-AOTF. It splits the optical power in dropped wavelengths and transited wavelengths to different optical modes. The optical mode selective routing part is achieved through mode selective coupler [73] or null coupler [87]. These mode selective components are based on the fact that different optical mode has different field distribution along the fiber cross-section. Then, by carefully adjusting the distance between two fibers, optical field distribution are specialized in such a way that the strong overlap only happens between two cladding modes or a cladding mode and the guided fundamental mode. Through the optical mode selective routing part, optical power in cladding modes are directed to the neighboring fiber instead of being filtered out as the mode stripper does, while optical power in the fundamental mode is guided and transmitted along the original optical path.

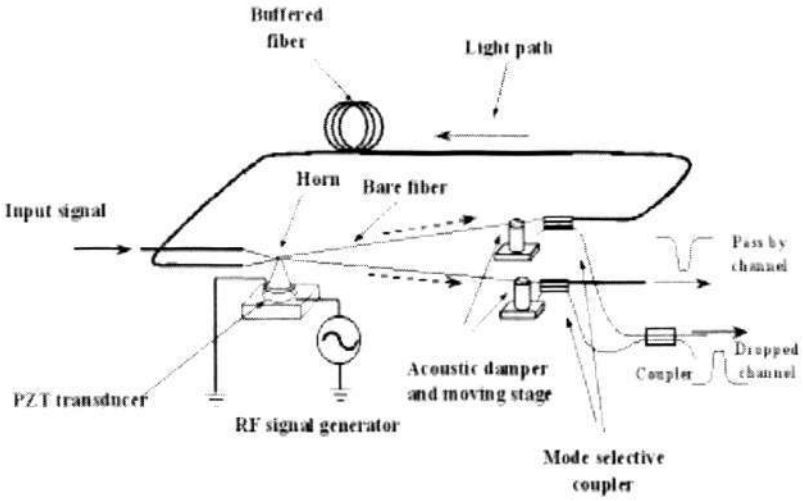

Figure 5.2: Schematic diagram of dynamic optical wavelength Add/Drop multiplexing based on loop structure AF-AOTF.

In the dynamic add/drop multiplexing, the operational wavelength is required to be tuned along optical wavelength. During this tuning process, the transmission profile deformation is undesired. Thus, the required most important ability of the system transmission profile is to be exactly maintained during the tuning process. Because the tuning speed is quite important for dynamic Add/Drop Multiplexing, the control scheme for optical tunable filter is desired to be as simple as possible to reduce the time cost on calculation. Thus, according to the discussions presented in Chapter 3 and Chapter 4, loop structure multi-stage AF-AOTF subject to the strain difference control is chosen for the application of dynamic add/drop multiplexing to obtain the best tunability. The axial strain in different fibers only need to be calibrated during the fabrication process and fixed during the tuning process. No complicated strain control is imposed on the system. In the proposed filter, all AO interaction stages are driven by one acoustic excitation source, the stopband is tuned by adjusting one acoustic frequency, just like tuning a single-stage AF-AOTF.

5.2.4 Experimental Results

The mode selective components have broad bandwidth more than several tens nanometers, which can cover whole C band in optical communication technology. The system overall transmission profile is primarily determined by the optical tunable filter involved in the system. In addition, the mode selective components are not the major objective considered in this thesis and high performance mode selective coupler has been reported in [73]. Thus, for the sake of simplicity, the discussion is focused on the design of the mode conversion part of the system. A narrow-band and a wide-band tunable stopband filter are fabricated with the structure shown in Fig.4.6.

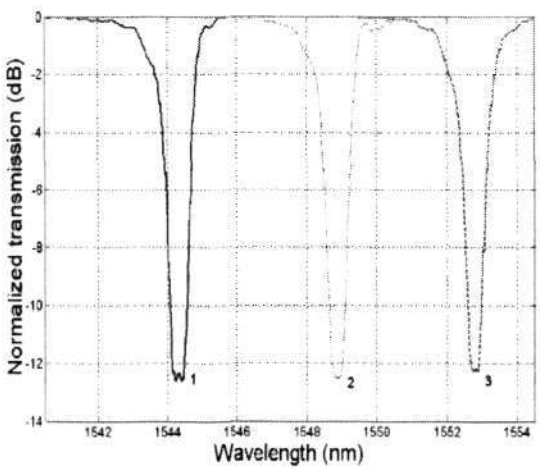

Figure 5.3: Narrow stopband transmission obtained by the loop AF-AOTF subject to strain difference control.

Firstly, a two-stage AF-AOTF is fabricated to deliver a narrow-band stopband transmission with $-12dB$ bandwidth of $0.4nm$ and $-3dB$ bandwidth of $1.0nm$. The filter uses a standard SMF-28 single mode fiber to form a loop. The two stripped sections are obtained with roughly the same length of $60cm$. In the experiment, a C-band light source is used to provide a broadband light input to the filter. The output spectral responses of the filter are observed by an optical spectrum analyzer (OSA).

The RF signal applying to the PZT is produced by a signal generator and amplified by a $37dB$ power amplifier. The filter is calibrated by the following procedures. Firstly, the RF frequency is tuned to $3.093MHz$ and the amplitude of the RF signal is maintained at $200mV$. In this case, OSA shows two shifted notch spectra with $12.5dB$ attenuation. Then, with the RF frequency and amplitude fixed, strain is applied respectively on each of the stripped sections by moving the damper stages. The strain adjustment is continued until the two notch responses overlap with each other and form a flat stop transmission at 1545nm as shown in Fig.5.3.

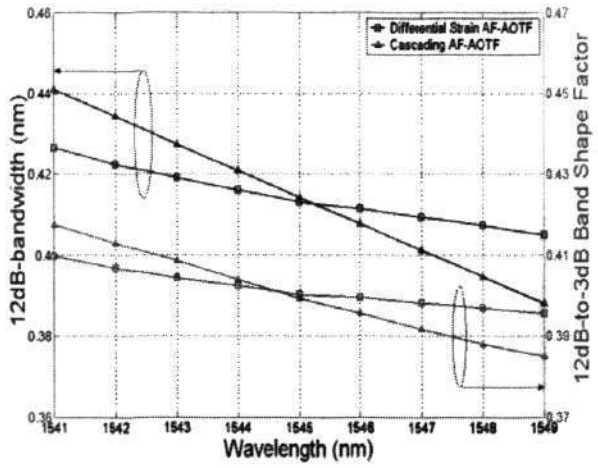

Figure 5.4: Experimental measurements of the narrow stopband transmission tunability.

To examine the tunability of the stopband transmission, the RF frequency is varied while all other setting parameters are fixed. The stopband transmission profile in response to RF frequencies of $3.115MHz$, $3.093MHz$ and $3.071MHz$ are shown as curves 1, 2 and 3 in Fig.5.3, respectively. Continuing the tuning process of the central wavelength of the stopband every $1nm$ from $1541nm$ to $1549nm$, the $-3dB$- and the $-12dB$-bandwidths are recorded. The tunability of the stopband is measured by the band shape factor which is defined as the ratio between $-12dB$ bandwidth and $-3dB$ bandwidth. The band shape factors together with the $-12dB$-bandwidths at

different central wavelengths are plotted as curves marked by squares in Fig.5.4. It is seen from the figure that the variations of the $-12dB$-bandwidths are less than $0.02nm$ and the variations of the $-12dB$ to $-3dB$ band shape factors are less than 4%.

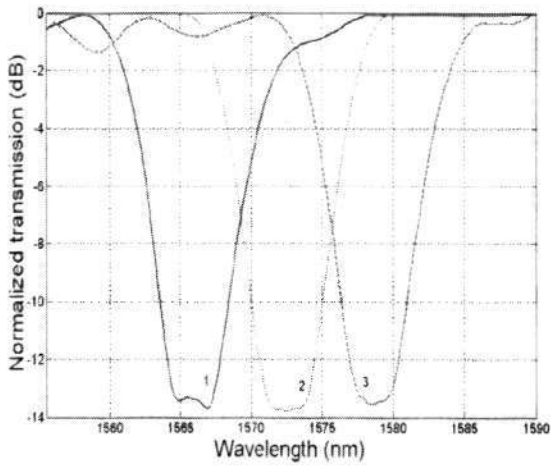

Figure 5.5: Broad stopband transmission obtained by the loop AF-AOTF subject to strain difference control ($4nm$ $-12dB$-bandwidth and $3dB/nm$ band roll-off).

As a comparison, the same transmission profile is implemented by cascading two AF-AOTFs without applying strong axial strains. Both AF-AOTFs are fabricated with the same AO length as that used in the loop structure AF-AOTF and are controlled by two RF signals with the frequencies of f_i $(i = 1, 2)$, respectively. Similarly, the two-stage cascading structure AF-AOTF is firstly calibrated by tuning the RF frequencies f_1 and f_2 respectively to $3.079MHz$ and to $3.077MHz$, so that the same stopband as shown by curve 2 in Fig.5.3 is obtained at the central wavelength of $1545nm$. Then, the stopband transmission is tuned by varying the frequencies f_1 and f_2 while maintaining a constant difference as $f_1 - f_2 = 0.002MHz$ to maintain the stopband shape. Tuning the stopband central wavelength from $1541nm$ to $1549nm$ with an increment of $1nm$ each time, the $-12dB$-bandwidths and the $-12dB$ to $-3dB$ band shape factors of the corresponding stopbands are recorded and plotted

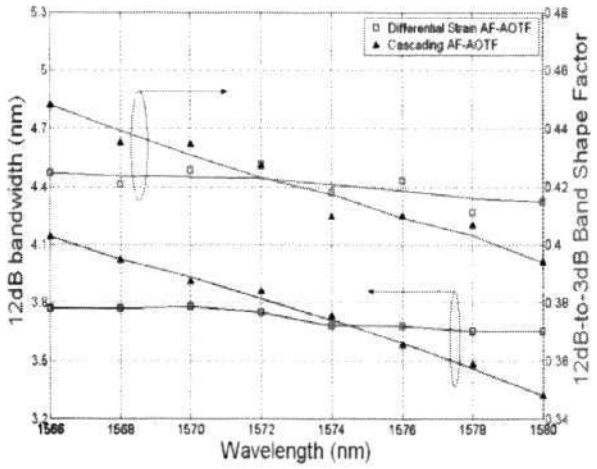

Figure 5.6: Experimental measurements of the broad stopband transmission tunability.

by the triangular-marked curves in Fig.5.4. Compared to the square-marked curves, it is obvious that the multi-stage AF-AOTF subject to strain difference control can deliver a more consistent stopband than the AF-AOTF subject to frequency difference control. The variations of the $-12dB$-bandwidth and the $-12dB$ to $-3dB$ band shape factors have been improved by one factor with the proposed AF-AOTF subject to strain difference control. If the band roll-off is defined as how fast the stopband drops from $0.1dB$ to $-12dB$, the narrow-band tunable filter has $6dB/nm$ roll-off.

Next, an multi-stage AF-AOTF subject to strain difference control as illustrated in Fig.4.6 is fabricated to deliver a broad stopband transmission with 4nm $-12dB$-bandwidth. To this end, the AO fibers are chemically etched to $50\mu m$ in diameter and the AO lengths are chosen as $10cm$. By performing the same calibration procedures mentioned above for the narrow-band filter, the desired stopband is obtained at $1572nm$ as shown by curve 2 in Fig.5.5 with the RF frequency being set at $f = 3.1MHz$. Then, the $-12dB$-bandwidth and the $-12dB$ to $-3dB$ band shape factor are examined while tuning the stopband from $1566nm$ and $1580nm$ by $2nm$.

The results are plotted as square-marked curves in Fig.5.6. Similarly, the same etched fiber is used to fabricate a two-stage cascading structure AF-AOTF without applying axial strains. The $-12dB$-bandwidths and the $-12dB$ to $-3dB$ band shape factors of the cascading structure AF-AOTF are examined over the same band of $[1566nm, 1580nm]$. The recorded results are included as triangular-marked curves in Fig.5.6. Clearly, the same conclusions as those for the narrow-band filter can be drawn for the wide-band stopband filter. Note that the proposed scheme can also be used to generate other bandwidths by etching the fiber with different diameters.

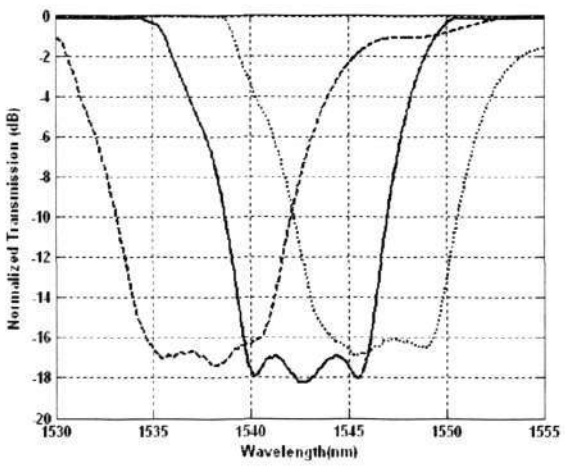

Figure 5.7: Extra-broad stopband transmission obtained by the three-stage loop AF-AOTF subject to strain difference control.

Furthermore, extra-broad stopband transmission with more than $7.5nm$ $-12dB$-bandwidth is obtained based on the loop structure three-stage AF-AOTF in experiment to show the integration ability of loop structure AF-AOTF. The employed AO fibers diameter is $45\mu m$ and the AO lengths are $10cm$. Then, through same calibration procedures mentioned above except for the fiber looped twice, the desired stopband is obtained at $1572nm$ as shown by solid curve in Fig.5.7 with the RF frequency being set at $f = 1.306Mhz$. Then, the $-12dB$-bandwidth and the $-12dB$

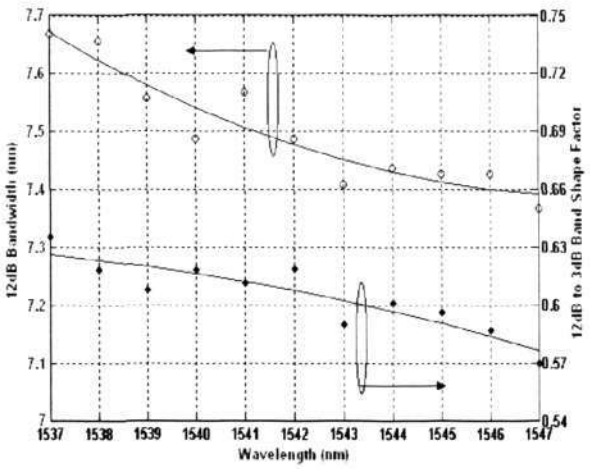

Figure 5.8: Experimental measurements of the extra-broad stopband transmission tunability.

to $-3dB$ band shape factor are examined while tuning the stopband from $1537nm$ and $1547nm$ by $1nm$ as shown in Fig.5.7. The corresponding $-12dB$ bandwidth and shape factor are shown in Fig.5.8.

In the experiments mentioned above, high $-12dB$ to $-3dB$ shape factor of 0.41, 0.38 and 0.6 are achieved. The required maximum optical isolation for any one component AF-AOTF is not more than $-12dB$. Under the same condition, the shape factor of single notch AF-AOTF is not more than 0.1 even strongly etched fiber is employed. Thus, by using the proposed multi-stage AF-AOTF, high shape factor is achieved with small RF driving power. It is also easier to be implemented in practice. Obviously, proposed multi-stage AF-AOTF is more suitable for the implementation of dynamic optical add/drop multiplexing. The optical pulse dispersion is suppressed and serious cross-talk between transited channels and modulated channels can be avoided. The required channel spacing is reduced, which means more available optical channels can be employed in the same optical link. It increases the utilization efficiency of the optical bandwidth and provides a potential solution for high performance dynamic OADM in practice.

5.3 Applications of AF-AOTF in EDFA Gain Control

As a high efficient optical amplifier, Erbium-doped fiber amplifier (EDFA) plays a key role in current long haul optical network and is indispensable for the future high speed all-optical networks [88, 89]. However, EDFA is suffered by the following technical limitations when it is employed in all-optical WDM networks.

Firstly, The EDFA gain is not uniform with respect to optical wavelength and the optical signal at about $1535nm$ is usually more strongly enhanced than those in other wavelengths. Thus, when a flat wide band optical signal passes through an EDFA, the transmission profile is not uniform with optical wavelength as shown in Fig.5.9. Furthermore, if a number of EDFAs are cascaded in a chain, which is common in long-haul optical communication networks, the power difference among these wavelengths is amplified by each amplifier. For example, just $1dB$ difference can grow to more than $10dB$ after 10 amplifiers. High power difference among the optical wavelengths results in low signal to noise ratio and lead to serious transmission errors. Therefore, the optical band around $1535nm$ cannot be used as the signal channel and the usable EDFA bandwidth is significantly limited. To solve this bandwidth limitation, static and dynamic EDFA gain equalization technologies are developed recently and have attracted more and more attention [90].

Secondly, because EDFA operates near saturation, the total output power of the amplifier is almost constant. As a result, the system input power variation directly affects the amplifier gain in all signal channels. When intensity modulated signal is incident on an EDFA, undesired time varying perturbation appears in all signal channels. More seriously, these perturbations are amplified and accumulated along the amplifier chain and cause high bit error rate at the receiver. Therefore, EDFA gain clamping is another hot research topic for optical amplifying technology.

Different kinds of tunable complex transmission profiles play key role in all EDFA gain control processes mentioned above. In the same time, as shown in the early chapters of the thesis, multi-stage AF-AOTF is an important implementation means of tunable complex transmission profile. Therefore, application of multi-stage AF-AOTF in the EDFA gain control has became an interest research topic. In the rest part of this section, we will present some pilot study results on design and control of multi-stage AF-AOTF in these applications.

5.3.1 Application of AF-AOTF in EDFA Gain Equalization

Both static and dynamic EDFA gain equalization require some optical tunable filters to generate some complex transmission profile to precisely compensate the unflatness of EDFA gain profile. It is undoubted that multi-stage AF-AOTF is an appropriate choice due to its excellent properties such as wide tuning range, high transmission profile modulation agility and simple control scheme [66, 91, 92]. However, the design and control of multi-stage AF-AOTF for these applications, especially for the dynamic EDFA gain equalization, still need to be further developed. In the rest of this section, an improved genetic algorithm is proposed to solve the nonlinear multi-variables optimization difficulty in the dynamic control of transmission profile of EDFA gain compensation filter. Theoretical analysis of proposed algorithm is analyzed and verified by simulations.

5.3.1.1 Static EDFA Gain Equalization Using AF-AOTF

As mentioned in Chapter 2, AF-AOTF has a flexible notch transmission profile. The isolation and centerwavelength of the notch transmission can be electronically modulated. By cascading several AF-AOTFs, any transmission profile can be implemented. Thus, AF-AOTF technology provides advantages in the optical transmis-

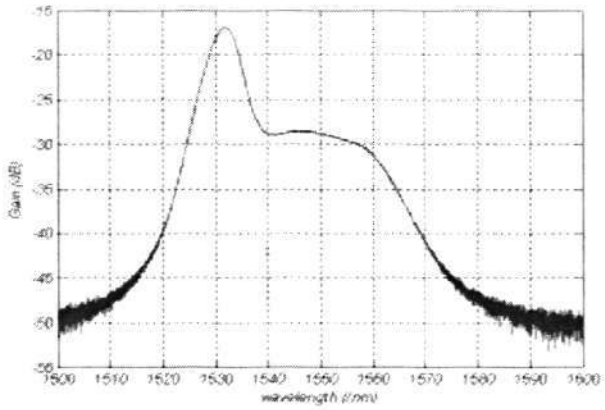

Figure 5.9: Typical gain profile of EDFA.

sion profile design and is appropriate for the application of EDFA gain equalization. Typical EDFA gain profile is shown in Fig.5.9. The available bandwidth of EDFA is about 30nm, which is within the tuning range of AF-AOTF. There is a peak with bandwidth of about $8nm$ around $1530nm$ need to be suppressed.

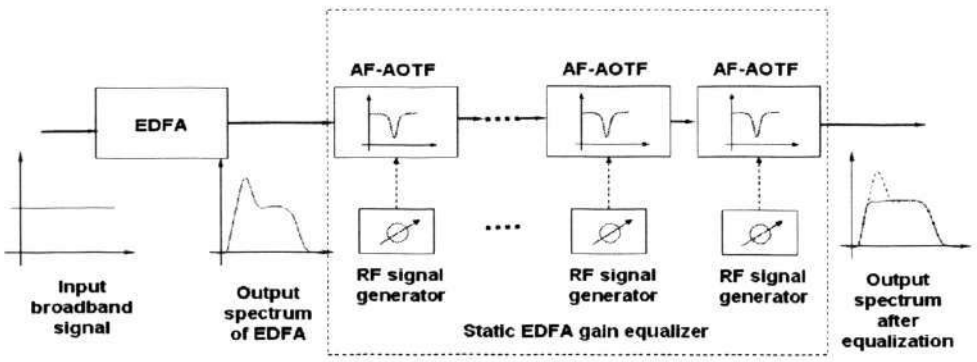

Figure 5.10: Schematic diagram of static EDFA gain equalization using AF-AOTF.

To suppress the additional peak in the EDFA gain spectrum, several AF-AOTFs are cascaded to implement the desired transmission profile for EDFA gain compensation. Because the operating position of system overall transmission is fixed, the best structure for the integration of several AF-AOTFs is the cascading structure according to the discussion in Chapter 3. A schematic of static EDFA gain equalization is

shown in Fig.5.10.

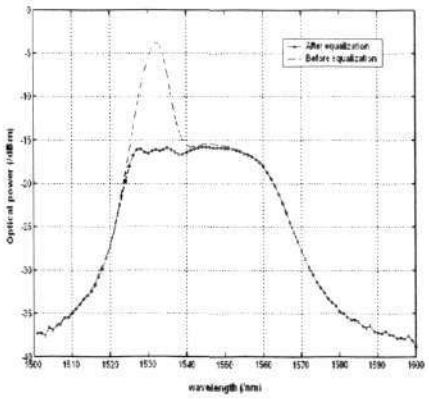

5.11.1: Overall transmission profile after static equalization.

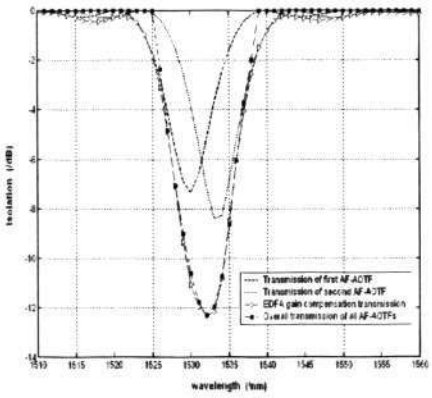

5.11.2: Transmission profile of static EDFA gain equalizer.

Figure 5.11: Static EDFA gain equalization.

Fig.5.11 shows an example where two AF-AOTFs are cascaded to suppress the effect of the peak in EDFA gain spectrum. After static gain equalizer, flat overall gain transmission profile is obtained with the maximum gain excursion of $0.56dB$. Obviously, using more AF-AOTFs can reduce the excursion of the gain profile at the cost of the system economic efficiency.

5.3.1.2 Dynamic EDFA Gain Equalization Using AF-AOTF

Compared with the static gain equalization of EDFA, dynamic EDFA gain equalization is much more useful but difficult to be implemented [93]. Because of the EDFA gain tilt effect, if the input optical power changes, the gain profile of EDFA changes as well. For different wavelengths, the corresponding gain variations are different. The gain increments of some wavelengths are larger than those of others and the gain profile leans to certain direction. This effect is denoted as the gain tilt effect of EDFA. Thus, using a fixed gain compensation filter that is designed in static EDFA gain equalization, the overall gain profile of the system cannot maintain its flatness

any more. For this kind of system, dynamic EDFA gain equalization is required to suppress the gain tilt effect.

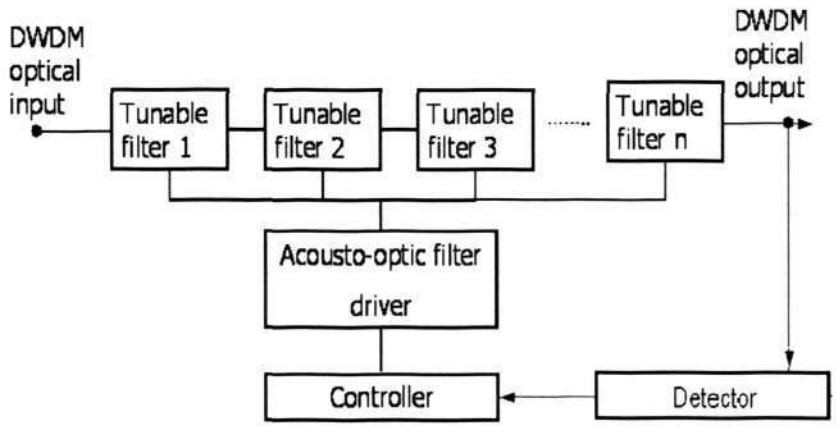

Figure 5.12: Schematic diagram of the dynamic EDFA equalizer.

The dynamic EDFA gain equalization is implemented through connecting EDFA with a dynamic EDFA compensating filter. The transmission of this filter can automatically follow the variation of EDFA transmission. The overall transmission profile of EDFA and following filter are flat in all time. Some kinds of optical filter technologies have been used to achieve dynamic EDFA gain compensation. They include Mach-Zehnder filter, fiber Bragg grating [94, 95] and some other approaches [96]. In these methods, Mach-Zehnder filter is limited by its tuning range, which cannot cover the whole bandwidth of EDFA. Fiber Bragg grating is not easily to be tuned once it has been fabricated. Compared with the methods mentioned above, the dynamic EDFA gain equalization using all-fiber acousto-optic tunable filter is a potential solution [66]. The schematic diagram of dynamic gain equalization using AF-AOTF is shown in Fig.5.12.

The EDFA gain equalizer is based on an n-stage AF-AOTF. A Multiplexer and several photo detectors are used to obtain the gain spectrum information of EDFA. Computer is used to analyze the detected EDFA gain profile and control the RF signal generators to provide appropriate AF-AOTF driving signals.

The bandwidth of EDFA is divided into n sub-bands equidistantly. Each stage is charged by one AF-AOTF, which is assumed to be fabricated from fiber taper for sake of simplicity. The driving signal frequency of each AF-AOTF can be determined as

$$f_i = \frac{C_{ext}\lambda_i^2(j_{11}^2 - j_{01}^2)^2}{64\pi^3 r^3 n_0^2} \quad \text{for} \quad i = 1, 2, 3...n \tag{5.14}$$

where λ_i is centerwavelength of ith sub-band. The cost function of this sub-band is

$$J_i = max_{\lambda_i - \lambda_{i+1}}\{(\ln P_{out}(\lambda) - \ln P_e(\lambda) - \ln F(\lambda))^2\} \tag{5.15}$$

where $P_{out}(\lambda)$ denotes the output transmission profile of the equalizer and $F(\lambda) = \frac{P_{out}(\lambda)}{P_{in}(\lambda)}$ is the transfer function of the EDFA gain compensation filter. λ_i and λ_{i+1} are the starting and the ending wavelength of ith sub-band. According to the model of multi-stage AF-AOTF (2.6) shown in Chapter 3, $F(\lambda)$ can be obtained as

$$F(\lambda) = \prod_{i=1}^{n}\left(1 - \frac{(\frac{ku_i}{f_i})^2}{(\frac{ku_i}{f_i})^2 + \delta_i^2}\sin^2\left(L_i\sqrt{(\frac{ku_i}{f_i})^2 + \delta_i^2}\right)\right) \tag{5.16}$$

$$k = \frac{8\sqrt{2}\pi^2 j_{01} j_{11} n_0(1+\chi)}{(j_{11}^2 - j_{01}^2)^2\lambda} \tag{5.17}$$

The major difficulty of dynamic EDFA gain equalization is dynamically designing and optimizing the optical filter parameters such as the RF signal frequency f_i, amplitude u_i and AO coupling length L_i of each AF-AOTF. These works make sure the overall transmission profile $F(\lambda)$ are always kept match with the desired EDFA gain compensation transmission profile at any time. This is guaranteed by minimizing the system cost function $J = \Sigma_{i=1}^{n} J_i$. The major problems in the optimization process are: The gain profile of the EDFA is a nonlinear function with respect to optical wavelengths. It depends on the absorption and emission spectra of EDFA. These parameters are measured in experiment and have no general and clear mathematical expression. The filter design is difficult to be archived by using conventional

linear optimization schemes. These optimization schemes are suffered by local minima problem and the obtained system performance is not satisfied. Thus, reliable nonlinear optimization scheme is required to solve this problem. In next section, an improved genetic algorithm is proposed to implement the EDFA gain compensation filter design.

5.3.1.3 Genetic Algorithm

Genetic algorithm is numerical technique that mimics the process of survival of the fittest. It is well-suited to do the simultaneous optimization of several features within multi-dimensional spaces. Especially, genetic algorithm does not need any differentiation operations and has no local minima problem. The algorithm is explained below

1)For each AF-AOTF, there are three parameters available to be used as the control parameters: the AO coupling length, the frequency and amplitude of the applied RF signal.

2) An initial gene group with n genes is generated using random values within the predetermined limitations. These limitations are caused by the PZT transducer coupling efficient and the operation length limitation in real applications. n is the number of the sampling of the approached curve.

3) The suitability of the solution is evaluated by its fitness. It is completed by comparing the system response with the desired response along the optical wavelength. The absolute values of the error at each sampling point are summed together as the fitness.

$$fit(i) = \Sigma_{j=1}^{n} |F_j - C_{i(j)}| \tag{5.18}$$

where F_j is the sampling value of the desired system response function, which is used as access pool. $C_{i(j)}$ is the function value produced by applying the parameters

in ith gene. Obviously, using more sampling points will obtain better optimization results. However, it causes large calculation workload.

4) The best gene, which has the minimum fitness, in the old generation, is preserved in advance. The average value of fitness is also calculated. In the next step, a new generation genes (child generation) is produced based on the gene information of the present generation genes (parent generation). It is preferred that the genes in each new generation are better than those in the old generation. Thus, the child generation genes should inherit the excellent characteristics and cast away the bad properties in the parent generation as much as possible. This is implemented through crossover possibility design. The crossover possibility $P_c(j)$ of each gene is generated based on its fitness as

$$P_c(j) = \begin{cases} \frac{0.5(fit_{max} - fit(j))}{fit_{max} - fit_{avg}} & ; \quad fit(j) > fit_{avg}. \\ 0.5 & ; \quad fit(j) \leq fit_{avg} \end{cases} \tag{5.19}$$

It is shown that the gene with better performance has lower crossover possibility. Then, a random crossover possibility P_c is produced to determine the crossover point. The genes after this point ($P_c(i) > P_c$) are exchanged according to the rule below.

$$Gene(i) = A \cdot Gene(i) + (1 - A) \cdot Gene(k) \tag{5.20}$$

where A is a random value within 0 to 1, $Gene(k)$ is a gene randomly selected from the rest genes in the parent generation.

5) To ensure that no region of the solution space becomes inaccessible to the algorithm, mutation is applied to child generation. The fitness of each gene in the child generation is calculated again and the mutation possibility is produced as

$$P_m(j) = \begin{cases} \frac{0.5(fit_{max} - fit(j))}{fit_{max} - fit_{avg}} & ; \quad fit(j) > fit_{avg}. \\ 0.5 & ; \quad fit(j) \leq fit_{avg} \end{cases} \tag{5.21}$$

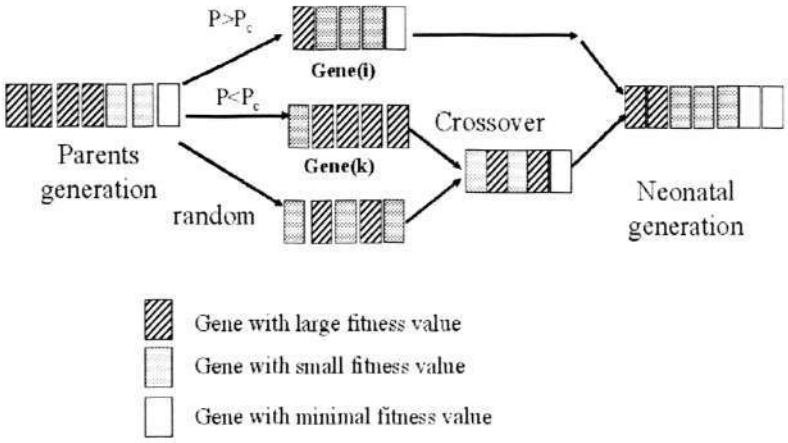

Figure 5.13: The process of crossover.

Same as the crossover process, a random mutation possibility Pm is produced to determine the mutation point. The genes after this point ($P_c(i) > P$) are exchanged according to the rule below.

$$Gene(i) = A \cdot Gene(i) + (1 - A) \cdot Gene(r) \tag{5.22}$$

where A is also a random value within 0 to 1, $Gene(r)$ is a gene randomly produced in the whole optimization space.

After mutation has been applied, the offspring constitutes the new generation. Then, the worst gene in the new generation genes is replaced by the best gene of the last generation. The purpose of this process is to ensure that the child generation genes are not worse than the parent generation genes and converge to a global optimization point. Steps $3 \sim 5$ are repeated until the specification of the approach error is met.

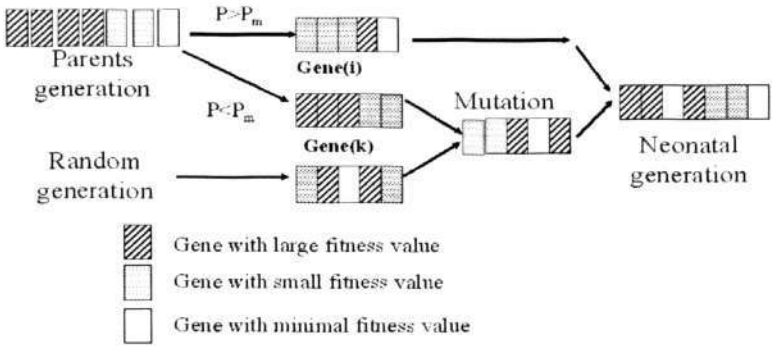

Figure 5.14: The process of mutation.

5.3.1.4 Case Study

To show the optical filter design scheme, six AF-AOTFs are used to suppress the EDFA gain profile as a case study. In this case, the desired system response is the gain transmission profile as shown by the dot dash line in Fig.5.15. It can exactly compensate the gain unflatness of EDFA. The required gain transmission profile is produced by cascading six AF-AOTFs. The available control parameters are the RF signal frequency ω_i, RF signal amplitudes u_i and the AO interaction length L_i for each AF-AOTF. Then, the best solution that includes 18 parameters for the six AF-AOTFs is generated by using the improved genetic algorithm.

The simulated response of this system with the optimized control parameters is obtained. Fig.5.15 shows the transmission combination of six AF-AOTFs. The dot dash line is the desired transmission profile that is used to suppress the EDFA gain peak around 1535nm. The solid line is the overall transmission profile of the six AF-AOTFs combination. The other dash lines show the transmission profile of each AF-AOTF. It represents the efficiency of the optimization of the system using the improved genetic algorithm. When the gain profile of EDFA is changed, previous design of EDFA gain equalizer cannot maintain the flatness of the output power

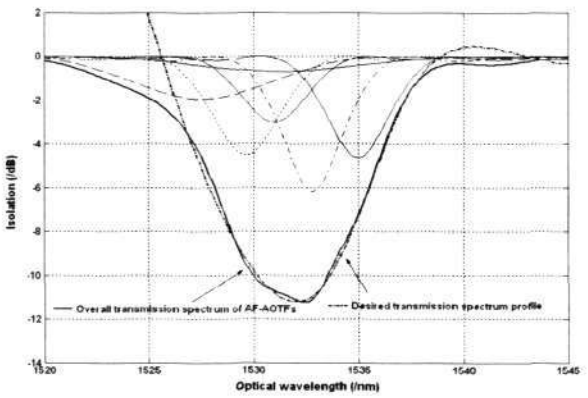

Figure 5.15: Composite transmission profile of the dynamic EDFA gain equalizer based on AF-AOTF technology and Genetic Algorithm designed at $-17.5dB$.

transmission. Then, the optical detectors detect the unflat EDFA gain profile and feed it back to the controller. The controller automatically calculates the required control parameters for all AF-AOTFs using the improved genetic algorithm. Fig.5.16 shows the redesigned transmission profile for the gain equalizer. The corresponding output power spectra of EDFA are shown in Fig.5.17. In both two cases, excellent flatness of EDFA gain profile is obtained with signal ripple less than $1dB$ over wide dynamic range covering the total EDFA bandwidth and the gain tilt effect is suppressed through dynamic design of the control signal for all AF-AOTFs.

The genetic algorithm has several further advantages over conventional analytically based techniques. First of all, there is no predetermined information or linear approximation of EDFA gain profile required in the filter design process. Thus, for any random gain profile deformation of EDFA, this scheme can always find the best group of filter design parameters. In other words, the optimization result can be adaptively adjusted in the dynamic process of the system, which is necessary for the adaptive EDFA gain control. Furthermore, in order to reduce the computing time, a look-up table approach is useful. The overall transmission profile are measured under all possible situations and used to calculate the relative control signal in ad-

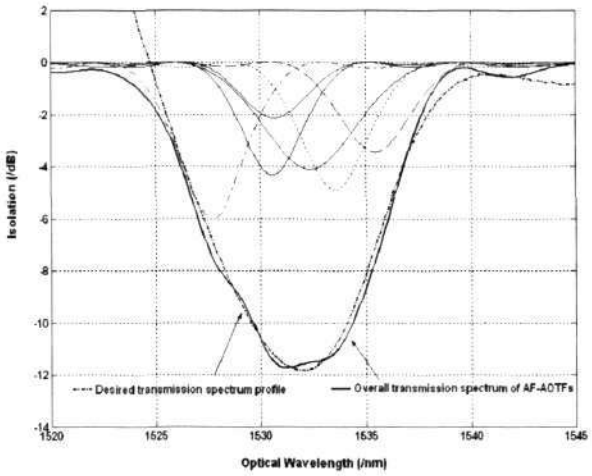

Figure 5.16: Composite transmission profile of the dynamic EDFA gain equalizer based on AF-AOTF technology and Genetic Algorithm designed at $-13.5dB$.

vance. All these information are stored in a data table. In the real applications, the required parameter values for each AF-AOTF are called up according to the on-line measurement of the transmission profile of AF-AOTF. If the computer speed is high enough, the system response time is only limited by the acoustic wave transient time of about $10\mu s$. The look-up table approach can greatly improve the tuning speed of the system.

5.3.2 Application of AF-AOTF in EDFA Gain Clamping

In most applications in WDM optical communication networks, the EDFA gain is not only required to be equal with respect to optical wavelength but also to be constant with respect to time. In last section, the solution of first requirement, dynamic EDFA gain equalization based on multi-stage AF-AOTF, has been presented and discussed. In this section, we will discuss the solution of the second requirement, which is usually denoted by EDFA gain clamping in scientific literature.

Several EDFA gain clamping technologies have been proposed. They include auto-

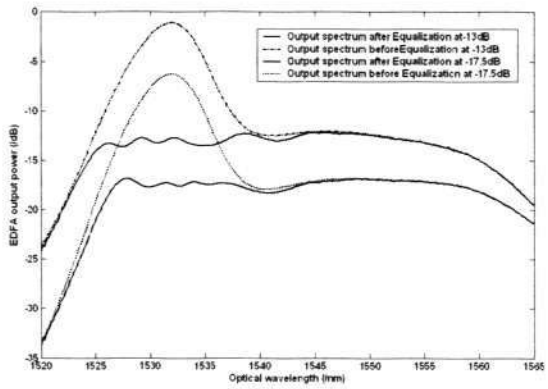

Figure 5.17: EDFA transmission profile after dynamic equalization using Genetic Algorithm.

matic EDFA gain clamping by all-optical feedback [97, 98], fast pump control [99], fast electronic feedforward [100] and fast link control [101]. Among these technologies, automatic EDFA gain clamping by all-optical feedback scheme shows great attraction for future all-optical networks. This scheme employs an all-optical feedback loop on the amplifier and forms a self-oscillating laser cavity. In the steady state, the EDFA gain exactly compensates the laser loop loss at the laser wavelength. With a constant and appropriate laser loop loss or in other word optical feedback level, the static EDFA gain is automatically clamped at desired value.

However, future dynamic all-optical network will face more critical request on the dynamic performance. The transmission routing, wavelength allocation and transmission path control will be implemented on the optical level [44, 11, 102]. The traffic and network reconfiguration will be regular and the input power variation through the EDFA employed in the network will be more frequent and violent [103, 104, 105, 106, 107, 108, 109]. As a result, when all-optical feedback gain clamping scheme is used on the EDFA employed in these dynamic optical networks, high frequency and long sustained optical signal power relaxation oscillation transient occurs in the optical transmission link [110, 111, 112, 113]. Especially for

large-scale networks, where a large number of EDFAs are employed in the chain, the power relaxation oscillation is amplified by each cascaded EDFAs and becomes more and more serious along the EDFA chain. At the end of the optical transmission link, the survival channel power transient will be too fast for the corrective action to work and the maximum excursion power in the laser wavelength will exceed the thresholds for nonlinear effects such as stimulated Brillouin scattering. As a result, strong nonlinear effect and high transmission error appear in the signal channels. Obviously, current design of all-optical gain clamped EDFA cannot meet the requirement of the future dynamic all-optical networks until the slowly decaying relaxation oscillation transient is avoided or suppressed.

The power relaxation oscillation transient in all-optical gain clamped EDFA is caused by the under-damped response of the system with respect to the abrupt variation of the EDFA input power. In current design of all-optical gain clamped EDFA, the optical feedback loop loss or in other word the optical feedback level of the ring laser is fixed at certain value to obtain desired EDFA gain in steady state, which is called static all-optical EDFA gain clamping in rest parts of this section. Dynamic performance related to system transient is not an issue for consideration. The employment of constant optical feedback level results in small system damping constant [114]. To suppress the undesired oscillatory transient, higher damping constant and strong optical feedback is expected.

Thus, we propose a novel system design with dynamic optical feedback level control using AF-AOTF to improve the dynamic performance of all-optical gain clamped EDFA, while ensuring the steady state performance in this section. In the proposed optical amplifier design, both static and dynamic performances of the system are considered by choosing appropriate poles with pole placement method. AF-AOTF instead of the optical attenuator, which is employed in the traditional static all-optical EDFA gain clamping design, is used to dynamically modulate the opti-

cal feedback level. Compared with ordinary static all-optical gain EDFA clamping scheme, dramatic improvement on the EDFA dynamic performance can be obtained with the employment of the proposed dynamic optical feedback level control design. In the following sections, a briefly discussion on current static all-optical EDFA gain clamping technology is given first. Some basic issues such as mathematical model of EDFA and operating principle of all-optical gain clamped EDFA are presented. Then, the structure of all-optical gain clamped EDFA with dynamic feedback level control is presented and the corresponding system mathematical model is derived with the consideration of AF-AOTF dynamics. Based on this model, dynamic optical feedback level control rule is designed using pole placement method. At last, the characteristics and efficiency of the proposed scheme are analyzed and verified by simulation results.

5.3.2.1 Static All-optical EDFA Gain Clamping

First of all, it is necessary to briefly present the basic principle of ordinary static all-optical EDFA gain clamping technology. This makes the illustration in the rest parts of this chapter more clear and avoid some complicated denotations, which may lead to misunderstanding. Fig.5.18 is a schematic diagram of static all-optical EDFA gain clamping. Multi-wavelength optical signal is sent to EDFA after passing through an optical coupler. After being amplified by EDFA, the optical signal is spitted into two by another optical coupler: the direct transmission signal and the feedback signal. The feedback optical signal is attenuated by the optical attenuator to certain level. A wavelength selective power splitter or an optical bandpass filter is employed in the feedback loop to make sure that only the optical power in certain wavelength can be fed back into the EDFA. The attenuation level of the attenuator can be manually tuned to certain value to obtain desired static EDFA gain in the calibration process. But during operating process of the system, the attenuation

level is fixed.

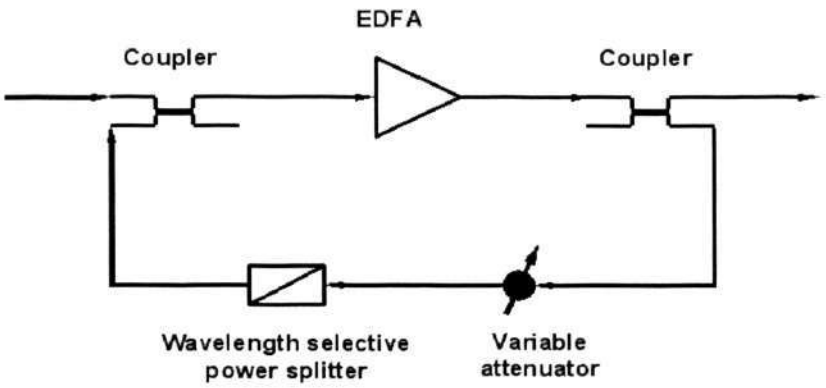

Figure 5.18: Schematic diagram of all-optical gain clamped EDFA.

It is assumed that the system is employed in ordinary WDM networks and there are $n-1$ information transmission channels passing through the EDFA. Each of these channels is assigned an appropriative optical wavelength in the EDFA passband. The EDFA pump wavelength is taken as the nth channel. Besides these n channels, an optical feedback channel is employed to form the ring laser cavity at an additional wavelength, which is named feedback laser wavelength. EDFA can be described as [115]

$$\begin{aligned} P_i^{IS}\left[\tau\frac{dG_i(t)}{dt}+G_i(t)+A_i\right] &= -\Sigma_{j=1}^{n+1}P_j^{in}(t)[e^{G_j(t)}-1] \\ A_i &= \alpha_i l \end{aligned} \tag{5.23}$$

where $P_i^{in}(t)$, P_i^{IS} and α_i are input signal power, intrinsic saturation power and absorption constant of the ith signal channel, respectively, $G_i(t)=\ln(\frac{P_i^{out}}{P_i^{in}})$ denotes the EDFA gain parameter of this signal channel and τ is the lifetime of the metastable level, l is the EDF fiber length. Equations (5.23) represents the coupled relationships between all n signal channels. Noting that the right sides of these equations

are the same, the following equations can be easily derived.

$$\begin{aligned} G_i(\infty) &= \frac{P_k^{IS}}{P_i^{IS}}(G_k(\infty) + A_k) - A_i \\ i &= 1 \cdots n \end{aligned} \tag{5.24}$$

where $G_i(\infty)$ denotes the steady state amplifier gain parameter in the ith signal channel. Equations (5.24) show that if the steady state amplifier gain of any one signal channel is obtained, the steady amplifier gains of all other channels can be determined. Furthermore, It can be easily obtained that

$$P_i^{IS}\left[\tau\frac{dG_i(t)}{dt} + G_i(t) + A_i\right] = P_k^{IS}\left[\tau\frac{dG_i(k)}{dt} + G_i(k) + A_k\right] \tag{5.25}$$

Above equation has a solution that

$$G_i(t) = \frac{P_k^{IS}}{P_i^{IS}}(G_k(t) + A_k) - A_i + (\frac{P_k^{IS}}{P_i^{IS}}(G_k(0) + A_k) - G_i(0) - A_i)\exp(-\frac{t}{\tau}) \tag{5.26}$$

If the EDFA is in steady state at $t = 0$, the last term in right side of (5.26) is zero and the transient EDFA gain parameter satisfies the following relationships.

$$\begin{aligned} G_i(t) &= \frac{P_k^{IS}}{P_i^{IS}}(G_k(t) + A_k) - A_i \\ i &= 1 \cdots n \end{aligned} \tag{5.27}$$

Thus, if the amplifier gain of certain channel e^{G_k} can be controlled, the EDFA gains in other channels are also under control. The output optical power in the $n+1$th signal channel, the feedback laser channel, P_F is selected as the single system output variable. The ring laser cavity is in steady state only when the round trip gain of the laser is equal to 1. In the steady state, EDFA gain of the laser wavelength exactly compensates the laser loop loss introduced by the couplers and the attenuator. The

corresponding gain parameter is represented as

$$G_L(\infty) = \ln\left(\frac{1}{\beta k_1 k_2}\right) \tag{5.28}$$

where $G_L(\infty)$ denotes the steady state EDFA gain parameter of the optical feedback laser channel, β is the fixed gain of the optical attenuator, k_1 and k_2 are the cross coupling ratio of two couplers respectively. For convenience of illustration, the subscript L is used to denote those variables associated with the feedback laser channel in the rest parts of this chapter. Assume that the demanded EDFA gain parameter of kth signal channel is G_k^d. According to (5.24) and (5.27), the corresponding expected value of the EDFA gain parameters at the laser wavelength can be calculated as $G_L^d = \frac{P_k^{IS}}{P_L^{IS}}(G_k^d + A_k) - A_L$. The required ring laser loop loss induced by the optical attenuator is

$$\beta = \frac{e^{G_L^d}}{k_1 k_2} \tag{5.29}$$

Usually for the static EDFA gain equalization, k is chosen as the wavelength that has the minimal gain in EDFA passband.

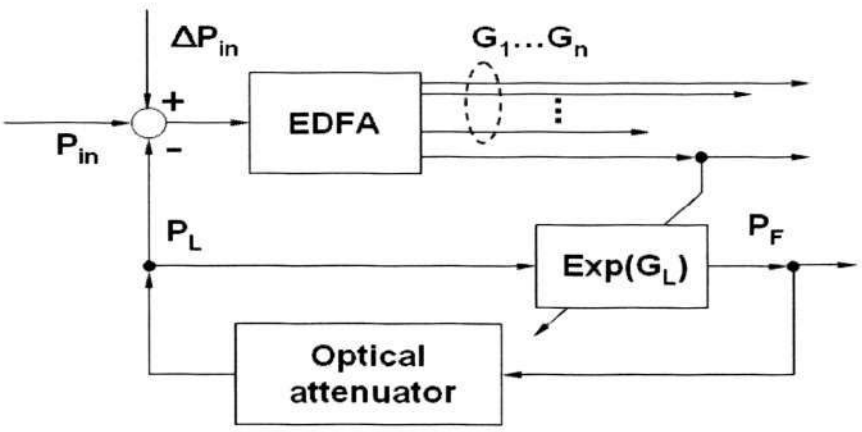

Figure 5.19: Block diagram of all-optical EDFA gain clamping.

Fig.5.19 shows the block diagram of all-optical gain clamped EDFA. The minus sign

in this figure means that the variation of the laser feedback power P_L always on the opposite direction with the input power variation $\triangle P_{in}$. If the signal input power variation is positive, the EDFA gain in the feedback laser channel e^{G_L} will reduce, while if the signal input power variation is negative, the EDFA gain will increase. As a result, the feedback laser power $P_L = P_F e^{G_L}$ always try to compensate the input power variation and maintain the total input power of EDFA constant. When appropriate laser loop loss shown in (5.29) is employed, the feedback laser power converges to its steady state value after a relaxation oscillation transient. The total input power of EDFA is maintained as its initial value, which results in constant EDFA gain as shown in (5.28).

In static all-optical EDFA gain clamping, constant optical feedback level limits the damping constant for the system and there is a high frequency relaxation oscillation transient with a large value of settling time. To suppress this undesired transient, a higher system damping constant is required. Consequently, the optical feedback level should have a value higher or lower than its steady state value when the amplifier input power reducing or increasing, respectively. At the same time, the convergence and steady state of the system must be maintained. Thus, control of the optical feedback level, named dynamic all-optical EDFA gain clamping, is demanded to simultaneously satisfy the system static and dynamic performance requirements.

5.3.2.2 Dynamic All-optical EDFA Gain Clamping Using AF-AOTF

The schematic diagram of dynamic all-optical EDFA gain clamping using AF-AOTF is shown in Fig.5.20. Here, an AF-AOTF is inserted into the ring laser cavity to modulate the optical power feedback level. The choice of AF-AOTF is because of its all-optical property, excellent electronic controllability and good dynamic performance. These properties make the computer aided dynamic optical feedback level control through electronic means is possible. At the input port of AF-AOTF, opti-

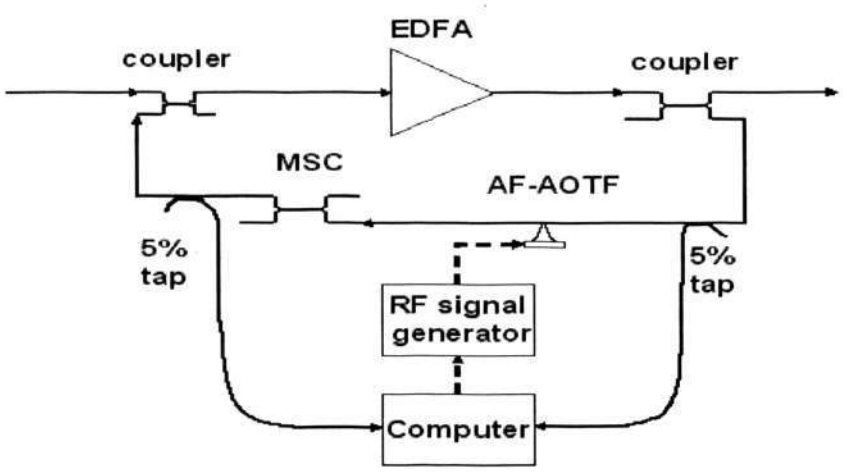

Figure 5.20: Schematic diagram of dynamic all-optical EDFA gain clamping using AF-AOTF. MSC— Mode selective coupler.

cal power in all wavelengths is guided in the fundamental mode. When they pass through AF-AOTF, a portion of optical power in a narrow band wavelength is coupled into higher order mode. Then, after passing the mode selective coupler (MSC) [59], the optical power in the high order mode is selected out and fed back to the ring laser cavity. The laser optical feedback level through AF-AOTF is indirectly controlled by the RF signal, which is used to generate the acoustic wave in the AO interaction fiber. Then, the remaining problem is how to design proper control rule for the RF signal generator to obtain excellent dynamic performance.

First of all, a mathematical model for the system is derived. The laser channel can be characterized by the linear differential equation [114].

$$\tau_{rt}\frac{dP_L(t)}{dt} = \ln[e^{G_L(t)}\beta(t)k_1k_2]\cdot\left[P_L(t) - \frac{P_{ex}(t)}{1-e^{G_L(t)}\beta(t)k_1k_2}\right] \tag{5.30}$$

where $P_{ex}(t)$ denotes the power of possible external perturbation signal, τ_{rt} is the propagation time of the light around the closed loop, $\beta(t)$ indicates the cross coupling ratio of AF-AOTF. The cross coupling ratio of MSC is assumed as 100%. Usually,

the perturbation term $P_{ex}(t) \ll P_L(t)$ and it can be neglected.

$$\tau_{rt}\frac{d\ln P_L(t)}{dt} = \ln[e^{G_L(t)}\beta(t)k_1k_2] \tag{5.31}$$

Recall the EDFA model shown in equation (5.23) and assume the AF-AOTF as a time delay system with a time constant T, the system can be represented as

$$\frac{dG_L(t)}{dt} + \frac{G_L(t)}{\tau} + \frac{A_L}{\tau} = -\frac{\Sigma_{i=1}^{n}[P_i(t)(e^{G_i(t)}-1)]}{P_L^{IS}\tau} - \frac{P_L(t)(e^{G_L(t)}-1)}{P_L^{IS}\tau} \tag{5.32}$$

$$\tau_{rt}\frac{d\ln P_L(t)}{dt} = \ln[e^{G_L(t)}\beta(t)k_1k_2] \tag{5.33}$$

$$\frac{d\beta(t)}{dt} = -\frac{\beta(t)}{T} + K_a u(t) \tag{5.34}$$

where $\beta(t)$ is the AF-AOTF transmission gain, $u(t)$ is the driving RF signal amplitude and K_a is power conversion constant of PZT. The AF-AOTF time constant T can be approximated by the acoustic wave propagation time through the AO interaction range. To increase the accuracy of the model, the amplified spontaneous emission (ASE) effect is involved into $P_i(t)$ by employing an effective bandwidth noise Δv over all EDFA spectrum [116] as: $P_i(t) = P_i^{in}(t) + hv_i\Delta v_i$. Block diagram of the system is shown in Fig.5.21. Compared with Figure.5.19, a dynamic optical feedback level control block is introduced into the system to dynamically modulate the ring laser round loop loss.

The system is nonlinear and makes the control rule design difficult. Thus, it is necessary to do some simplification and linearization. In the steady state, $\frac{G_L(t)}{dt} = 0$; $\frac{d\ln P_L(t)}{dt} = 0$; $\frac{d\beta(t)}{dt} = 0$. The steady state values of EDFA gain parameter, feedback input power and AF-AOTF transmission gain in the ring laser wavelength are denoted as $G_L(\infty)$, $P_L(\infty)$ and $\beta(\infty)$, respectively. When the input signal channel

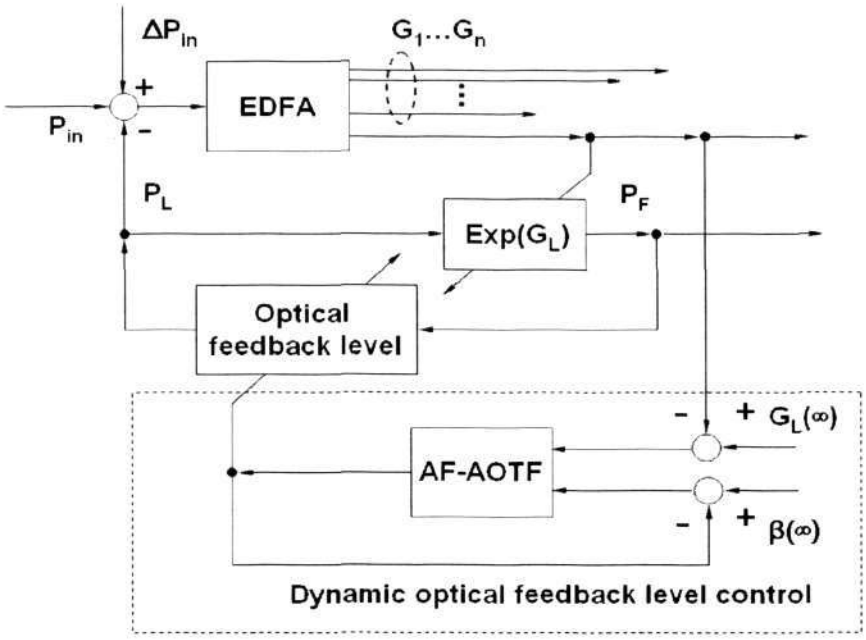

Figure 5.21: Block diagram of EDFA gain clamping with dynamic feedback level control using AF-AOTF.

number is determined, these values are constant and can be easily determined as

$$G_L(\infty) = \frac{P_k^{IS}}{P_L^{IS}}(G_k^d + A_k) - A_L \tag{5.35}$$

$$\beta(\infty) = \frac{1}{e^{G_L(\infty)}k_1k_2} \tag{5.36}$$

$$P_L(\infty) = -\frac{\Sigma_{i=1}^{n}[P_i(t)(e^{G_i(t)} - 1)] + P_L^{IS}(G_L(\infty) + A_L)}{(e^{G_L(\infty)} - 1)} \tag{5.37}$$

$$u(\infty) = \frac{\beta(\infty)}{K_aT} \tag{5.38}$$

Then, define that

$$\Delta G_L(t) = G_L(t) - G_L(\infty) \tag{5.39}$$

$$\Delta \ln P_L(t) = \ln P_L(t) - \ln P_L(\infty) \tag{5.40}$$

$$\Delta\beta(t) = \beta(t) - \beta(\infty) \tag{5.41}$$

$$\Delta u(t) = u(t) - u(\infty) \tag{5.42}$$

The gain variation (about 0.5dB) is usually small compared to the steady gain (above 20dB) and the input power variation can be approximated as

$$\begin{aligned} \Sigma_{i=1}^{n} P_i(t)(e^{G_i(t)} - 1) &\approx \Sigma_{i=1}^{n} P_i(t)(e^{G_i(\infty)} - 1) \\ &= P_v(t) + P_0 \end{aligned} \tag{5.43}$$

where $P_0 = \Sigma_{i=1}^{n} P_i(0)(e^{G_i(\infty)} - 1) + P_L(\infty)(e^{G_L}(\infty) - 1)$ is the steady signal power increment and $P_v(t)$ is the signal input power increment variation of EDFA. Then, substituting (5.39)-(5.43) into equations (5.32)-(5.34), gives

$$\begin{aligned} \frac{d\Delta G_L(t)}{dt} + \frac{\Delta G_L(t) + G_L(\infty)}{\tau} + \frac{A_L}{\tau} &= -\frac{P_v(t) + P_0 - P_L(\infty)(e^{G_L}(\infty) - 1)}{P_L^{IS}\tau} \\ &\quad - \frac{e^{(\Delta \ln P_L(t) + \ln P_L(\infty))}(e^{\Delta G_L(t) + G_L(\infty)} - 1)}{P_L^{IS}\tau} \end{aligned} \tag{5.44}$$

$$\tau_{rt}\frac{d\Delta \ln P_L(t)}{dt} = \ln[e^{(\Delta G_L(t) + G_L(\infty))} k_1 k_2 (\Delta\beta(t) + \beta(\infty))] \tag{5.45}$$

$$\frac{d\Delta\beta(t)}{dt} = -\frac{\Delta\beta(t) + \beta(\infty)}{T} + K_a(\Delta u(t) + u(\infty)) \tag{5.46}$$

The right sides of equations (5.44)-(5.46) are expanded to Taylor series with respect to $G_L(t)$, $\ln P_L(t)$ and $\beta(t)$ at the steady point $(G_L(\infty), P_L(\infty), \beta(\infty))$. Then, substituting (5.35)-(5.38) into the obtained equations and cancelling the common

terms, gives

$$\begin{aligned}\frac{d\Delta G_L(t)}{dt} &= -\frac{\Delta G_L(t)}{\tau} - \frac{P_v(t)}{P_L^{IS}\tau} - \frac{e^{G_L(\infty)}P_L(\infty)}{P_L^{IS}\tau}\Delta G_L(t) \\ &\quad -\frac{P_L(\infty)(e^{G_L(\infty)}-1)}{P_L^{IS}\tau}\Delta \ln P_L(t) + R_{\Delta G}(t) + R_{\Delta \ln p}(t) \quad (5.47)\\ \frac{d\Delta \ln P_L(t)}{dt} &= \frac{\Delta G_L(t)}{\tau_{rt}} + \frac{e^{G_L(\infty)}k_1k_2\Delta\beta(t)}{\tau_{rt}} + R_{\Delta\beta}(t) \quad (5.48)\\ \frac{d\Delta\beta(t)}{dt} &= -\frac{\Delta\beta(t)}{T} + K_a\Delta u(t) \quad (5.49)\end{aligned}$$

where $R_{\Delta G}(t)$, $R_{\Delta \ln P}(t)$ and $R_{\Delta\beta}(t)$ represent the second and higher order terms of $\Delta G_L(t)$, $\Delta \ln P_L(t)$ and $\Delta\beta(t)$, respectively. For convenience of illustration, denote $x_1 = \Delta G_L(t)$, $x_2 = \Delta \ln P_L(t)$, $x_3 = \Delta\beta(t)$ and $u' = \Delta u(t)$. A simple linear approximation model of the system is represented as follows

$$\dot{x} = Ax + Bu' + v \quad (5.50)$$

where

$$A = \begin{bmatrix} -\frac{1}{\tau} - \frac{e^{G_L(\infty)}P_L(\infty)}{P_L^{IS}\tau} & -\frac{P_L(\infty)(e^{G_L(\infty)}-1)}{P_L^{IS}\tau} & 0 \\ \frac{1}{\tau_{rt}} & 0 & \frac{e^{G_L(\infty)}k_1k_2}{\tau_{rt}} \\ 0 & 0 & -\frac{1}{T} \end{bmatrix} \quad (5.51)$$

and

$$B = \begin{bmatrix} 0 \\ 0 \\ K_a \end{bmatrix} \quad (5.52)$$

where $x = [x_1, x_2, x_3]^T$ is the state vector of the system and u' is the system feedback to be designed, $v = -\frac{P_v(t)}{P_L^{IS}\tau}$ is the temporal external disturbance.

5.3.2.3 Design of Dynamic Optical Feedback Level Control

Now the remaining problem is how to design the feedback signal u'. Here it is done through static feedback, i.e. $u' = K^T x = h_1 x_1 + h_2 x_2 + h_3 x_3$. By adjusting the state feedback gain matrix $K = [h_1, h_2, h_3]^T$, the poles of the system can be placed at any desired positions and excellent dynamic performance can be obtained. However, the measurement of x_2 is too complicated to be implemented in practice. To obtain the real time value of x_2, $P_L(\infty)$ must be predetermined. As shown in equation (5.37), the real time value of $P_L(\infty)$ depends on the randomly varied network traffic situation. Thus, to measure x_2, all signal channels must be continuously monitored with some expensive equipment such as optical spectrum analyzer. It also requires long processing time and causes failure of the control system. To avoid this problem, only x_1 and x_3 are used as the feedback signal, i.e. $h_2 = 0$. Variables x_1 and x_2 can be simply obtained by measuring the optical powers before and after EDFA in the single feedback laser wavelength, which can be done with several cheap optical detectors. Furthermore, because the feedback ring laser can be separately set at the wavelength far away from the signal channels, less noise and disturbance are introduced into the transmitted signals. With $K = [h_1, 0, h_3]^T$, the closed loop system is

$$\dot{x} = \tilde{A}x \tag{5.53}$$

where

$$\tilde{A} = \begin{bmatrix} -\frac{1}{\tau} - \frac{e^{G_L(\infty)} P_L(\infty)}{P_L^{IS}\tau} & -\frac{P_L(\infty)(e^{G_L(\infty)}-1)}{P_L^{IS}\tau} & 0 \\ \frac{1}{\tau_{rt}} & 0 & \frac{e^{G_L(\infty)} k_1 k_2}{\tau_{rt}} \\ K_a h_1 & 0 & -\frac{1}{T} + K_a h_3 \end{bmatrix} \tag{5.54}$$

Based on linear system theory, the system is stable when the real parts of all eigenvalues of $\tilde{A}$ are negative. In our case, the system is designed to have one real eigenvalue

$\lambda_1 = q$ and two conjugated complex eigenvalues $\lambda_2 = r + sj$ and $\lambda_3 = r - sj$. Then, the following relationships are deduced.

$$q + 2r = a_{11} + a_{33} \tag{5.55}$$

$$r^2 + s^2 + 2qr = a_{11}a_{33} - a_{12}a_{21} \tag{5.56}$$

$$q(r^2 + s^2) = (a_{31}a_{23} - a_{21}a_{33})a_{12} \tag{5.57}$$

where a_{ij} is the element at ith row and jth column in matrix $\tilde{A}$. The values h_1 and h_3 depend on a_{31} and a_{33}, respectively. But there are three equations and two variables a_{31} and a_{33}. This makes some limitations on the placement of system poles. (5.55) and (5.56) make a constraint on the placement of system poles position.

$$q = \frac{(a_{11} - r)^2 + s^2 + a_{12}a_{21}}{a_{11} - 2r} \tag{5.58}$$

The required h_1 and h_3 are

$$h_1 = \frac{(r^2 + s^2 - a_{11}r - a_{12}a_{21})^2 + (4a_{12}a_{21} + a_{11}^2)s^2}{K_a a_{12}a_{23}(a_{11} - 2r)} \tag{5.59}$$

$$h_3 = \frac{1}{K_a T} + \frac{2r}{K_a} + \frac{r^2 + s^2 + a_{12}a_{21}}{K_a(a_{11} - 2r)} \tag{5.60}$$

5.3.2.4 Case Study and Discussion

In this section, some simulations to evaluate the efficiency of dynamic all-optical EDFA gain clamping scheme are carried out to verify the design scheme in the previous section. In these simulations, the designed optical amplifier is employed in a WDM optical network, which involves a 16 EDFAs chain.

Firstly, transient of single EDFA using the structure shown in Fig.5.20 is examined. In the simulation, ASE effect is considered as a noise with effective bandwidth of $\Delta v_{eff} = 125GHz$ [98] over all optical spectrum of EDFA. Saturation parameter is

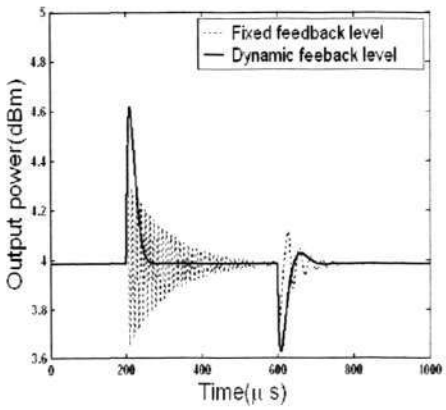

5.22.1: The survival signal channel output power response when 5 out of 8 channels are dropped and added.

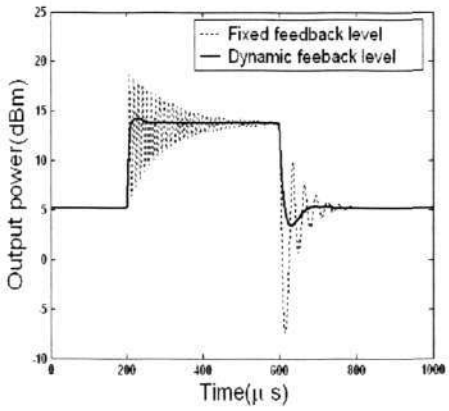

5.22.2: The compensation laser power response when 5 out of 8 channels are dropped and added.

Figure 5.22: Dynamic transient of all-optical gain clamped EDFA.

taken as $\zeta = 5.58 \times 10^{14} m^{-1} \cdot s^{-1}$. The Metastable lifetime τ, round trip time τ_{rt} and AF-AOTF time constant T are $10ms$, $0.1\mu s$ and $10\mu s$, respectively. The EDFA is pumped at $1480nm$ with laser power of $40mW$. The EDF fiber length $l = 10m$. Eight channels are employed from $1548nm$ to $1551.5nm$ with interval of $0.5nm$ and input powers of $0.025mW$/channel. The feedback laser wavelength is $1547nm$. The signal channel at the wavelength $1548nm$ is selected as the survival channel. In the simulation, it is assumed that the channels are abruptly switched and the most serious case for the network transmission power variation is that there are 5 out of 8 signal channels are added or dropped.

For comparison, static all-optical EDFA gain clamping is studied Firstly. The required attenuation gain of the attenuator is calculated as 0.0739. When 5 of 8 channels are dropped, for the static gain clamping case, the system eigenvalues are $-0.1206 \pm 1.5418i$, which leads to a damping constant of 0.078. The dynamic transients of output power and EDFA gain are shown in the dot curves in Fig.5.22.1 and Fig.5.23.1, respectively.

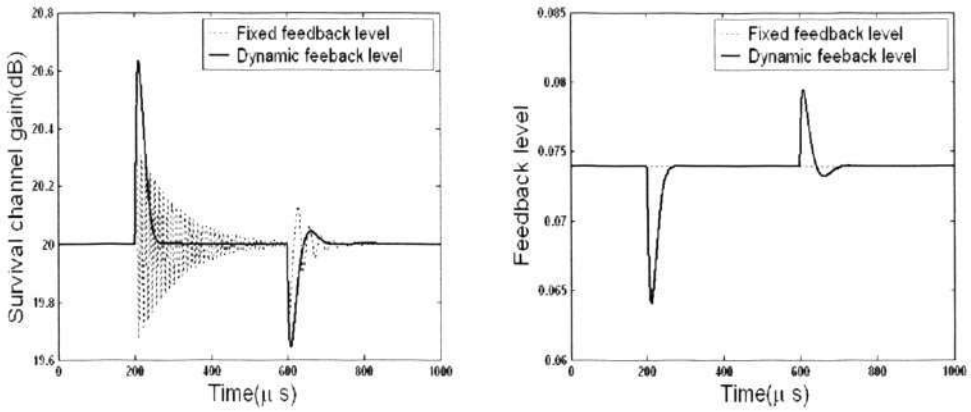

5.23.1: The survival signal channel gain response when 5 out of 8 channels are dropped and added.

5.23.2: The feedback level variation of different schemes when 5 out of 8 channels are dropped and added.

Figure 5.23: Dynamic transient of all-optical gain clamped EDFA.

Then, the AF-AOTF control rule is designed according to the method mentioned in last section. Because of the nonlinearity of the system, system dynamic performance is dominated by the real eigenvalue q only at the point very close to the steady state, where the system linearization is carried out. But at this time, the power excursion has been suppressed to a small level, which is close or below the value acceptable to the system. In most time of the transient, the system state is relative far away from the linearization point and the system dynamic performance is determined by the two complex eigenvalues. Because the principal aim is to reduce the effect the oscillation process, the absolute value of r should be selected as large as possible. However, according to equation (5.58), reducing r moves the corresponding values of q in the positive direction of the real axis. It makes the effect of the real pole q very strong and cause long convergence time. In the worst case, it can make the system unstable. Thus, there is a tradeoff problem. In the simulation, the values of r and s are set as -0.63119 and 1.46833, respectively. The corresponding value of q is -0.0811. The feedback level design parameters are $K_a h_1 = -0.0749$ and $K_a h_3 = -1$. With this design, the system stability is guaranteed firstly. Furthermore, the

two complex eigenvalues are moved away from the imaginary axis and the oscillatory effect is reduced. The selection of q makes both the laser power excursion and the system convergence speed acceptable. The power and gain transient of the system are shown in the solid curves in Fig.5.22.1 and Fig.5.23, respectively.

When 5 out of 8 channels are added, the system state matrix A is changed because of the variation of $P_L(\infty)$ and the system eigenvalues are $-0.01705 \pm 0.5773i$. Using same feedback gain matrix K designed above, the two complex system eigenvalues are $-0.0606 \pm 0.4149i$. According to equation (5.58), the corresponding value of q is -1.9121. The responding simulation results are shown in Fig.5.22 and Fig.5.23.1, respectively.

Based on the results, it can be noted that the output power oscillation in survival signal channel is very strong and need quite long time to converge to its steady state value. In the case using dynamic optical feedback level control, when the total input power of EDFA changed, the signal output power variation or the gain variation in the survival signal channel increases to its maximum value and smoothly reduces to the steady state. It is clear that the total time required for the output power and gain of the survival channel converges to its steady state, called system recovery time, is greatly reduced from $300\mu s$ to about $40\mu s$. That means much fewer transmitted bits are affected by the undesired transient. The gain oscillation frequency or in other word gain variation speed is greatly reduced by applying the dynamic feedback level control. Then, the critical correction action speed at the receiver is greatly reduced.

In the real application, the highest output power excursion is happened at the compensating laser wavelength especially when a number of channels are added or dropped [112]. It causes the nonlinear effect such as Stimulated Brillouin Scattering in the optical fiber, which introduces noise and perturbation into the transmitted information. Thus, the power excursion at the compensating laser wavelength must

be suppressed. Fig.5.22.2 shows the output power transient at the feedback laser wavelength. It is clear that the power excursion at the compensating laser channel is greatly suppressed from $5dBm$ to $0.4dBm$ through applying the dynamic feedback level control.

From above discussion, it can be concluded that the relaxation oscillation transient in the signal channel is damped and the maximum power excursion in the feedback laser wavelength is suppressed. In turn, the transmission error rate is decreased and the optical nonlinear effect in the fiber is avoided.

It must be noted that the maximum power excursion in the survival signal channel is enhanced by using the dynamic all-optical EDFA gain clamping scheme compared with that in the static all-optical EDFA gain clamping. But this negative effect on the system dynamic performance is not significant. Firstly, the power excursion in signal channel is much smaller than that of the feedback ring laser channel and cannot reach the threshold of the nonlinear optical effect. Secondly, by using dynamic optical feedback control, the relaxation oscillation effect accumulation along the EDFA chain is much slower than that of the static all-optical EDFA gain clamping case. As a result, the overall maximum power excursion in the survival signal channel slowly vanishes along the EDFA chain and has insignificant effect on the network performance. Furthermore, we found that if introduce the information of the slope of the ring laser power variation into the control signal design, this power excursion can be strongly suppressed. More research on this problem is under going.

The simulations for the cases that there are $1, 2...4$ out of 8 channels are added and dropped are also be done. In these simulations, the feedback gain matrix K is the same with that designed for the case 5 out of 8 channels are added and dropped. Similar results are obtained. From these simulation results, it is found that if the designed system is stable when the most serious input power variation happens, for any other cases, the system is always stable.

5.3.2.5 EDFA Chain Gain Clamping

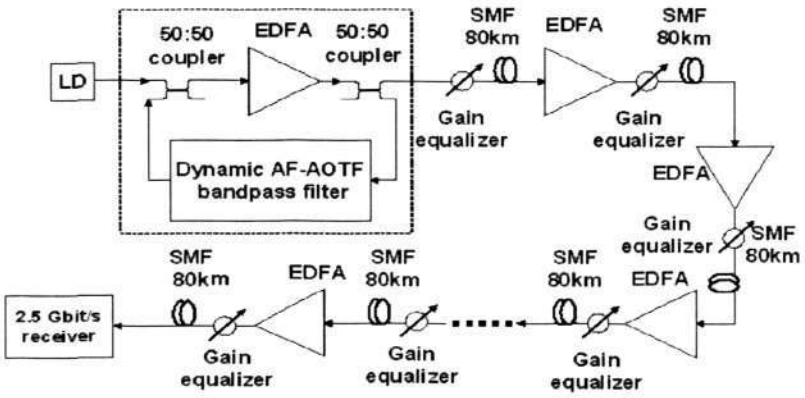

Figure 5.24: Schematic diagram of gain control of an EDFA chain using dynamic EDFA gain equalization scheme and gain clamping with dynamic feedback level control scheme.

The relaxation oscillation in any single gain clamped EDFA is not so serious to result in burst transmission error. However, it becomes serious transmission error when this unwanted transient effect is accumulated along the EDFA chain. Thus, it is necessary to examine the efficiency of proposed optical amplifier design in an optical transmission link involving long EDFA chain.

Fig.5.24 shows the schematic diagram of EDFA chain gain clamping with dynamic feedback level control. 16 EDFAs are cascaded in the chain. The first EDFA is all-optical gain clamped using the structure shown in Fig.5.20. Following each EDFA, EDFA gain equalization filter implemented by multi-stage AF-AOTF, which is discussed in last section, is employed to equalize the un-flat gain profile. The span loss between two neighboring EDFAs is $20dB$, which is equal to the desired equalized amplifier gain and $80km$ fiber span loss. The leaked ring laser power of first EDFA propagates along the EDFAs chain and acts as a compensation signal.

The transmission signals and control parameters of the system are same with that used in last simulation. Recovery time defined in [110] is one of the important indices

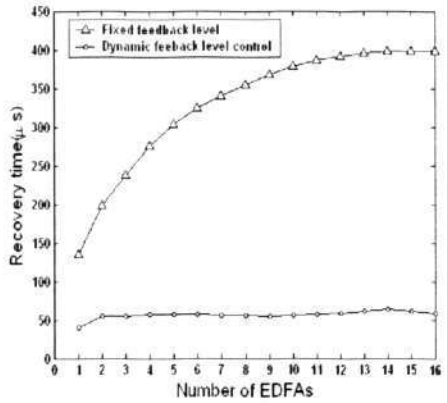

5.25.1: Recovery time for different number of EDFAs in chain when 5 out of 8 channels are dropped.

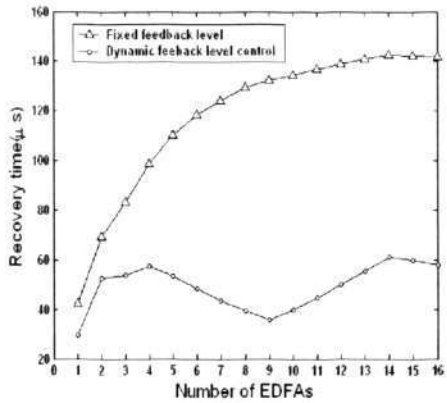

5.25.2: Recovery time for different number of EDFAs in chain when 5 out of 8 channels are added.

Figure 5.25: Recovery time of output power for a 16-EDFA chain.

used to evaluate the penalty of EDFA gain transient. Fig.5.25 shows the relationship between the system recovery time and the cascaded EDFA number when several signal channels are added and dropped. It shows that the recovery time is greatly reduced by applying the dynamic feedback level control. Furthermore, the trend that the recovery time increases with respect to the cascaded EDFA number along the EDFA chain is suppressed.

Fig.5.26, Fig.5.28 and Fig.5.27 show the power excursion and gain variation of the system for each EDFA along the chain. From Fig.5.26.1 and Fig.5.26.2, it is obvious that the power excursion in the compensating laser channel is greatly suppressed by the proposed scheme. The signal channel gain variation along the EDFA chain is shown in Fig.5.27.1 and Fig.5.27.2. With the proposed scheme, the gain variation converges more rapidly to its steady state value. When 5 out of 8 signal channels are dropped, the overall survival signal channel gain variation is smaller than that of the static all-optical EDFA gain clamping after the 6th EDFA. For the case that same signal channels are added, better overall survival signal gain variation can be

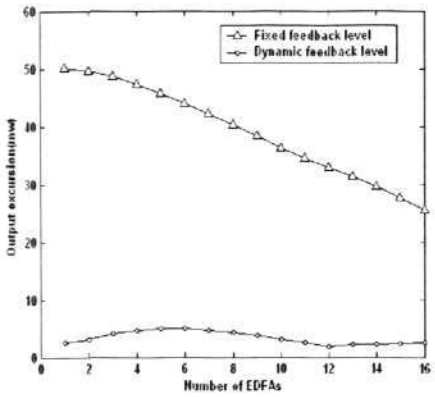

5.26.1: The compensation laser power response along the EDFA chain when 5 out of 8 channels are dropped.

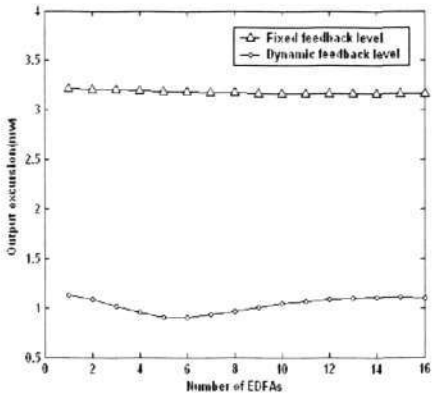

5.26.2: Power excursion of the compensating laser channel along the EDFA chain when 5 out of 8 channels are added.

Figure 5.26: Feedback laser power transient for a 16-EDFA chain.

obtained only after the second EDFA. Similar conclusion can be drawn for the power excursion of the survival signal channel as shown in Fig.5.28.1 and Fig.5.28.2. By applying dynamic feedback level control, the increase speed of the survival signal channel maximum excursion with the number of EDFAs cascaded in the chain is smaller than that of the static all-optical EDFA gain clamping. After the 13th EDFA, the overall value of the maximum excursion power is below that of the static all-optical EDFA gain clamping. Similarly, only after the second EDFA, the survival signal power excursion of the proposed scheme is smaller than that of the static all-optical EDFA gain clamping.

Above results are explained as follows: The direction of EDFA gain variation is opposite to the input power variation. Thus, the output power variation in the foregoing EDFA results in opposite direction gain variation in the followed EDFA. The gain variation of the followed EDFA diminishes the amplification effect of the excursion power. However, because EDFA has a large time constant, the opposite direction gain variation of EDFA is much slower than the variation of the input

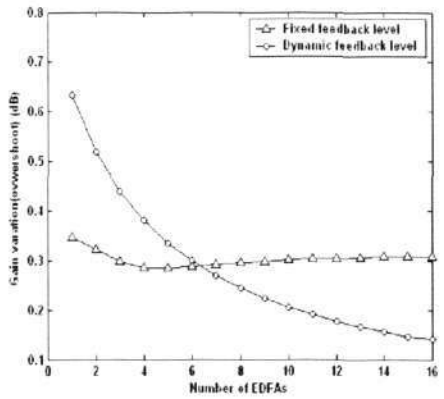

5.27.1: Gain variation of the survival channel along the EDFA chain when 5 out of 8 channels are dropped.

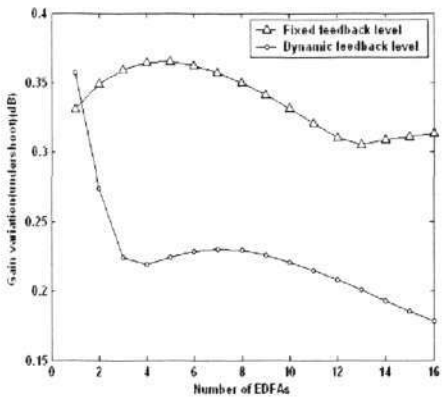

5.27.2: Gain variation of the survival channel along the EDFA chain when 5 out of 8 channels are added.

Figure 5.27: Gain transient for a 16-EDFA chain.

power. For the case of static all-optical EDFA gain clamping, the total input power excursion is very large and happened at high speed. The EDFA gain variation is not sufficient and cannot totally counteract the effect of power variation. Thus, the total output power variation is in the same direction as the input power variation and propagates to the next EDFA. The power excursion of system is amplified by each EDFA in the chain and accumulated more and more serious. For the case of the dynamic feedback level control, the power excursion in the feedback laser channel is suppressed and the power variation speed is greatly reduced. The gain variation along the EDFA chain has sufficient long time to accumulate to enough high value and dominates the slow and weak input power variation effect. As a result, the relaxation oscillation accumulation along the EDFA chain is suppressed.

Then, the application of multi-stage AF-AOTF for EDFA gain control have been discussed in this section. It shows that through combining EDFA gain equalization scheme shown in last sub-section and EDFA gain clamping scheme presented in this sub-section, the gain control problems of EDFA with respect to the optical

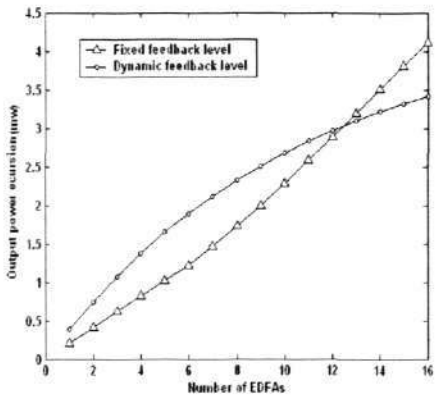

5.28.1: Power excursion of the survival channel along the EDFA chain when 5 out of 8 channels are dropped.

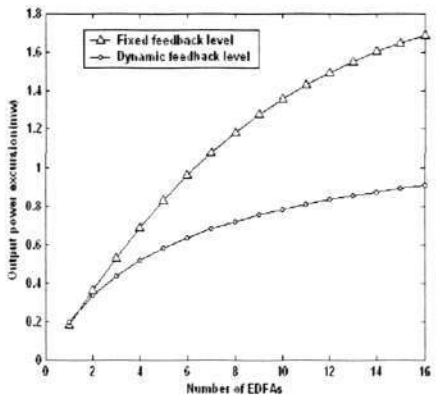

5.28.2: Power excursion of the survival channel along the EDFA chain when 5 out of 8 channels are added.

Figure 5.28: Output power transient for a 16-EDFA chain.

wavelength and time can be solved.

5.4 Conclusion

In this chapter, pilot studies on the design and control issues of particular applications of tunable complex transmission profile in optical communication networks are carried out.

Firstly, the application of multi-stage AF-AOTF in dynamic optical add/drop multiplexing is discussed. In this applications, multi-stage AF-AOTF is used to deliver the desired tunable high $-12dB$ to $-3dB$ shape factor stopband transmission profile. To obtain excellent tunability along the optical wavelength and reduce the complexity of the system, the desired transmission profile is implemented by loop structure AF-AOTF subject to strain difference control. The proposed filter is presented by experiments to deliver stopband transmission spectra with $0.4nm$, $4nm$ and $7.5nm$ $-12dB$-bandwidth, which have high $-12dB$ to $-3dB$ shape factor of

0.41, 0.38 and 0.6, respectively.

Secondly, the application of multi-stage AF-AOTF in the gain control of EDFA is discussed. Multi-stage AF-AOTF is successfully used to solve two primary issues, EDFA gain equalization and EDFA gain clamping, in the EDFA gain control. For the former issue, an improved genetic algorithm is applied to adaptively optimize the control parameters of the combined AO interaction stages. The ripple of EDFA gain profile is suppressed to a value less than 1dB. For the second issue, a novel and efficient design scheme used to suppress the relaxation oscillation in all-optical gain clamped EDFA has been proposed. By using an AF-AOTF to dynamically modulate the ring laser feedback level, both transient and steady state performance of the system can be controlled. Poles placement method is used to optimize the dynamic performance of the system. The relaxation oscillation exists in all-optical gain clamped EDFA is sufficiently suppressed. By using the proposed multi-stage AF-AOTF based dynamic EDFA gain equalization and gain clamping schemes, EDFA gain are fully controlled with respect to both optical wavelength and time. It makes EDFA can be employed in the future high speed smart all-optical networks.

Chapter 6

Conclusions and Recommendations for Further Research

6.1 Conclusions

In this thesis, the design, control and implementation of all-fiber tunable filter using multi-stage AF-AOTF technology has been systemically studied. The tuning performance improvement of multi-stage AF-AOTF with complex transmission profile is the core contribution of the thesis. For the multi-stage AF-AOTF, its key performance factor "tunability" is addressed and the quantitative measure of the tunability is given. Based on this measure, two kinds of tunability improvement schemes for multi-stage AF-AOTF are developed and their performance are demonstrated through theoretical analysis, simulation studies, and experiments. To accommodate these improved scheme, a loop structure multi-stage AF-AOTF is proposed by studying the practical limitations of the traditional multi-stage AF-AOTF struc-

tures. Furthermore, the thesis has conducted pilot studies on the applications of the obtained high performance multi-stage AF-AOTF in designing dynamic optical add/drop multiplexing filter, EDFA gain equalization and EDFA gain clamping. The major contributions of this thesis are summarized in the following aspects.

Implementation of different dynamic functions required by all-optical communication networks by using multi-stage AF-AOTF is systemically studied. Multi-stage AF-AOTF is used to realize the optical tunable optical filter with pre-specified complex transmissions. The desired complex transmission is formed by superposition of several shifted notch transmissions. Each of these notch transmissions is generated by one AO interaction stage. High performance tunable optical filter is required to maintain the pre-specified spectrum being maintained while the transmission is being tuned. In the same time, the tuning mechanism must be as simple as possible from the practical point of view. To design such a tuning mechanism with pre-specifications, the concept of tunability of a complex transmission and a quantitative measure of the tunability are for the first time formulated in the thesis. This advancement enables us to quantify the capability of a composite transmission being maintained while its position is tuned from one wavelength to another.

Using the proposed tunability measure, a strain control scheme is proposed and systematically developed to obtain tunable optical tunable filters with specified complex transmissions by using multi-stage AF-AOTFs. This scheme is first developed based on the traditional multi-stage AF-AOTF design which cascades multiple AF-AOTFs subject to frequency difference control scheme. In this design, the desired complex transmission profile is achieved by applying different frequency RF signals on each AO interaction stage where axial strain is applied as well. The tuning of the composite transmission is achieved through adding an identical increment on the RF signal frequency of all AO interaction stages. The axial strain effect on the system tunability is modelled and analyzed for the first time. It is shown in theory

that by applying a fixed axial strain on each AO fiber in the cascaded AF-AOTFs, the tunability of the resultant composite transmission can be enhanced.

To further improve the tunability of multi-stage AF-AOTF, a strain difference control scheme is proposed. In this scheme, the desired composite transmission profile is realized by introducing different but fixed strains on different AO interaction stages in the calibration stage. The driving RF signal frequency of all participant AF-AOTFs are kept identical. The overall transmission is tuned simply by tuning this single RF signal frequency as tuning a single stage of AO-AOTF. This simplicity gives advantage over the traditional frequency difference control scheme. Through theoretical analysis, it is shown that multi-stage AF-AOTF subject to strain difference control has better tunability than the multi-stage AF-AOTF subject to frequency difference scheme when they are used to deliver same complex transmission profile. The theoretical analysis is justified by both simulation and experimental studies where the desired complex transmission is simulated by a maximally flat stopband transmission.

Besides the tuning schemes, the improvement of the tunability is studied from practical perspective by addressing the implementation issues of multi-stage AF-AOTF. In traditional multi-stage AF-AOTF, each AF-AOTF is driven by individual piezoelectric transducer (PZT). The characteristics of the PZTs deviate one from the others. To avoid the synchronizing problems between different AO interaction stages in the system, a novel loop structure AF-AOTF is proposed in the thesis to avoid the system tunability degradation due to the mismatch between frequency bandwidth of different PZT in the cascading structure AF-AOTF. Enhanced notch filter using the proposed loop structure is demonstrated to solve the weak AO coupling efficiency problem of single mode fiber based AF-AOTF. Experimental results of tunable bandstop transmission by different multi-stage AF-AOTF structure are obtained and used as a case study to demonstrate the superiority of the proposed loop

structure on the different AO interaction stage synchronization. The characteristics of different AF-AOTF integration structures are compared and their advantages and disadvantages of them in different applications are also analyzed.

To demonstrate the performance improvement of multi-stage AF-AOTF and its applications in all-optical communication networks, two typical and important applications of the proposed AF-AOTFs design are investigated in the thesis as well. In the first application, a loop structure multi-stage AF-AOTF subject to strain difference control design is used to obtain a dynamic optical wavelength add/drop multiplexing filter over a broadband. As the filter can be design with high roll-off factor, the channel crosstalk and signal distortion in multiplexing is greatly reduced. In the second applications, the proposed design is used to design filters for gain control of erbium-doped fiber amplifiers in two typical applications. Two gain control applications are studied. First, an improved genetic algorithm is proposed to tune on-line the control parameters of multi-stage AF-AOTF to equalize the dynamic gain of EDFA. Second, a novel all-optical EDFA gain clamping scheme with dynamic optical feedback level control using AF-AOTF is proposed. In this design, the dynamic model taking into account the AF-AOTF dynamics is derived first, based on which poles placement method is applied to obtain the tuning rules of AF-AOTF. It is shown that the EDFA transmission penalty due to the relaxation oscillation transient is strongly suppressed by the proposed scheme.

6.2 Recommendations for Further Research

In this thesis, it has been presented that the employed PZT can directly affect the performance of AF-AOTF. The synchronization problem between different AF-AOTFs is avoided through applying loop structure design. However, there are still some challenges in the detailed study of the effect of PZT characteristics on the per-

formance of AF-AOTF. The guideline for the design and manufacturing of PZT or acoustic transducer for AF-AOTF is still underdeveloped. It is also quite interesting to theoretically analyze the acoustic wave propagating in the fiber. Especially, theoretical analysis on the acoustic field establishment and resonance effect involved in the AF-AOTF is an attractive topic since it gives guidance on the implementation and control of AF-AOTF in practice.

In this thesis, the design of AF-AOTF is based on current available fiber or simple modulation such as etching the diameter of the fiber. Since the refractive index profile of the fiber is designed for optical transmission, it induces some limitation on the performance of all-fiber acousto-optic tunable filter. For example, the minimum bandwidth of AF-AOTF is not narrow enough based on any current fiber. The special fiber index profile design for AF-AOTF is useful.

The polarization effect on the AF-AOTF is an interesting topic. Some basic research in this area has been carrying out. The obtained results show that AF-AOTF is possible to be used in PMD compensation for it is polarization dependent.

The dynamic EDFA gain equalization based on AF-AOTF technology can be further explored by applying other control methods and signal processing in the system.

In this thesis, the advantage and efficiency of loop structure AF-AOTF have been presented. It can be further explored in components design. For example, the technically design of acoustic transducer for the loop structure AF-AOTF to increasing the maximum number of integrated AO interaction stages and AO coupling efficiency maybe an interesting topic.

APPENDIX A.

Acoustic Field in AF-AOTF

There are three kinds of acoustic modes can be guided in the optical fiber: longitudinal, torsional and flexural waves. All of them can introduce periodic refractive index grating in the fiber. However, because the refractive index displacement caused by the longitudinal wave is uniform in the transverse plane, the AO coupling coefficient calculated from equation (2.4) is very weak. Therefore, the optical mode coupling excited by longitudinal wave can be neglected. The mode coupling introduced by the torsional wave is strong polarization dependent. It is only used in some special applications. But for the normal applications, flexural acoustic wave is the most common selection.

The transverse displacement of flexural acoustic wave propagates along the fiber can be described as [51, 56]

$$u(z,t) = u_0 \cos(\omega t - \kappa z) \tag{A.1}$$

where u_0 and ω are the amplitude and angular frequency of the flexural wave, respectively, κ is the acoustic wave constant. This flexural wave periodically changes the optical refractive index of the fiber. The net change of the refractive index can be described as

$$n(z,t) = n_0 + \triangle n \cos(\omega t - \kappa z) \tag{A.2}$$

where n_0 is the initial value of fiber refractive index. The refractive index change $\triangle n$ is produced from two sources. First, the mechanical micro-bending of the fiber cause the optical path length of the light transmitted through it increasing. Total optical path length change of the light in the fiber is antisymmetric along the acoustic polarization axis in the transverse plane. To quantitively calculate the optical path increasing, the fiber are divided into lot of fractions with small length of $\triangle z$. When acoustic wave propagates along the fiber, each fraction become a small corner

bending curve with radius R. Thus, the optical path change due to the geometrical micro-bending in the transverse plane of each fiber fraction is

$$\Delta l = k_0 n_0 y / R \triangle z \tag{A.3}$$

where k_0 is the propagation constant of the light. The overall optical path change of the fiber is

$$\begin{aligned} \Delta L &= \sum \Delta l \\ &= \frac{k_0 n_0 y}{R} \sum \triangle z \\ &= \frac{k_0 n_0 y z}{R} \end{aligned} \tag{A.4}$$

where z is the optical light transmission distance. The optical path change can be taken as result of the effect of refractive index variation. The effective refractive index change due to the "geometric change", here denote by Δn_g, can be given as

$$\Delta n_g = n_0 y \kappa^2 u_0 \cos(\omega t - \kappa z) \tag{A.5}$$

The derivation of above equation use the following approximation

$$\begin{aligned} \frac{1}{R} &\approx \frac{1}{\frac{d^2 u}{dz^2}} \\ &= \kappa^2 u_0 \cos(\omega t - \kappa z) \end{aligned} \tag{A.6}$$

The other primary effect cause the refractive index variation is the elasto-optic effect. Because the size of optical fiber in longitudinal dimension is much larger than that in the transverse dimension, the dominant stress in the fiber is along the z direction. When an acoustic wave described as (A.1) propagates along the fiber,

the corresponding strain components are

$$\begin{aligned} S_x &= -vy/R \\ S_y &= -vy/R \\ S_z &= y/R \end{aligned} \tag{A.7}$$

As a result, the corresponding refractive index changes in the transverse plane due to different strain components are

$$\begin{aligned} \Delta n_x &= -\frac{1}{2}n_0^3 p_{12} S_x \\ \Delta n_y &= -\frac{1}{2}n_0^3 p_{11} S_y \\ \Delta n_z &= -\frac{1}{2}n_0^3 p_{12} S_z \end{aligned} \tag{A.8}$$

where p_{ij} is the strain-optic tensor and is determined by the material and the configuration of the fiber. The total elasto-optic effect contribution to the polarization in y plane can be described as

$$\begin{aligned} \Delta n_e &= \Delta n_x + \Delta n_y + \Delta n_z \\ &= -(\frac{n_0^3}{2})\Sigma_j p_{ij} S_j \\ &= -\frac{1}{2}n_0^3(p_{12}(1-v) - vp_{11})\cos(\omega t - \kappa z) \\ &= \chi \cdot n_0 \cos(\omega t - \kappa z) \end{aligned} \tag{A.9}$$

where v is the Poisson constant. Define χ as the ratio of refractive index change. It can be represented as

$$\chi = -\frac{1}{2}n_0^2(p_{12}(1-v) - vp_{11}) \tag{A.10}$$

For silica fiber, $p_{11} = 0.12$, $p_{12} = 0.27$, $v = 0.17$, Thus, χ has a value of -0.22. It means the mechanical micro-bending and elasto-optic effect have counteractive

effect on the refractive index variation of the fiber. Thus, the overall refractive index change $\triangle n$ is given by [51]

$$\begin{aligned} \triangle n &= (\triangle n_e + \triangle n_g)/\cos(\omega t - \kappa z) \\ &= n_0(1+\chi)\kappa^2 u_0 y \\ &= \frac{4\pi^2 n_0(1+\chi)u_0 y}{\Lambda^2} \end{aligned} \tag{A.11}$$

where Λ is the acoustic wavelength in the fiber. In low frequency limit, it can be calculated as [83],

$$\Lambda = \frac{C_{ext}}{\sqrt{2}f}\sqrt{\sqrt{s^2 + \frac{4\pi^2 r^2 f^2}{C_{ext}^2}} + s} \tag{A.12}$$

where r is the radius of the cross-section of the acoustic medium, s is the axial strain on the fiber, f is the driving RF signal frequency, $C_{ext} = 5760m/s$ is the speed of extensional wave in silica.

APPENDIX B

Optical Field in AF-AOTF

AF-AOTF can be fabricated from different optical fiber and fiber-based structures. The type and number of the optical modes that possibly exist in various fiber-based structures are different. As a result, the AO couplings happen in various optical mediums have different mathematical models. Thus, to make the presentation clear and avoid any possible confusion, it is necessary to separately discuss the mathematical models of them.

In any one type of optical medium, there are more than one modes, guided modes or cladding modes, exist in the same time. AO coupling can happen between any one of them and the fundamental mode. A single frequency acoustic wave usually will generate multiple mode couplings in one time. But these resonance mode couplings happen on different wavelengths separated by tens of nanometers [58]. In the interested optical bandwidth for communication, such as C band plus L band, there is usually only one dominate mode coupling exist in one time. Furthermore, the mathematic model of all AO couplings in certain kind of optical medium has similar expression. Thus, for the sake of simplicity on the description, we only discuss one mode coupling process for each type of AO interaction medium. The obtained results can be simply extended to rest mode coupling processes.

Firstly, in single mode fiber, the fundamental mode is the only guided optical mode. Besides this guided mode, there are some cladding modes such as Lp_{11}^{cl} and Lp_{12}^{cl} mode. These cladding modes are not used for information transmission because they can not be guided by the single mode fiber in long distance. However, in the distance of tens of centimeters, these cladding modes can be weakly guided by the fiber cladding and the air. AO coupling in single mode fiber just happens between these cladding modes and the guided fundamental mode. For the fundamental mode,

the propagation constant and field distribution in the cross section are

$$\beta_0 = \sqrt{(\frac{2\pi n_{core}}{\lambda})^2 - \frac{j_{01}^2}{r_{core}^2}} \tag{B.1}$$

$$\xi_0 = \frac{1}{r_{core}\sqrt{\pi}} \frac{J_0\left(\frac{j_{01}r}{r_{core}}\right)}{J_1(j_{01})} \tag{B.2}$$

where r_{core} and n_{core} are the radius and refractive index of fiber core, J_0 and J_1 are zeroth-order and first-order Bessel function of the first kind, j_{01} is the first root of the J_0, r is radial distance from the origin, center of fiber cross-section.

The calculation of the optical field of the cladding mode is usually carried out by using some numerical method. An approximate approach to study cladding mode is to treat them as an effective discrete mode weakly guided by the fiber cladding and air. In the single mode fiber without etching, $n_{core} - n_{clad} \ll n_{clad} - n_{air}$ and $r_{clad} \gg r_{core}$, where r_{clad} and n_{clad} are the radius and refractive index of the fiber cladding, $n_{air} = 1$ is the refractive index of air. Under these conditions, the propagation constant and optical field distribution of the cladding mode, for example Lp_{11}^{cl} mode, can be approximately obtained as

$$\beta_1 = \sqrt{(\frac{2\pi n_{clad}}{\lambda})^2 - \frac{j_{11}^2}{r_{clad}^2}} \tag{B.3}$$

$$\xi_1 = -\frac{2}{r_{clad}\sqrt{\pi}} \frac{J_1\left(\frac{j_{11}r}{r_{clad}}\right)}{J_0(j_{11})} \cos(\phi) \tag{B.4}$$

where j_{11} are the first root of the J_1, ϕ is polar angle. Thus, the mode beatlength between the fundamental mode and lowest Lp_{11}^{cl} cladding mode can be approximately calculated as follows

$$L_B = \frac{2\pi}{\sqrt{(\frac{2\pi n_{core}}{\lambda})^2 - \frac{j_{01}^2}{r_{core}^2}} - \sqrt{(\frac{2\pi n_{clad}}{\lambda})^2 - \frac{j_{11}^2}{r_{clad}^2}}} \tag{B.5}$$

In the multi-mode fiber, there are multiple guided optical modes and cladding modes. However, for the optical structure with normalized frequency above the cutoff for the LP_{11} mode, the AO coupling between the fundamental mode and cladding modes are very weak [51]. Therefore, for multi-mode structure, usually only the AO couplings between the guided modes are considered. In multi-mode fiber structure, the propagation and field of fundamental mode have same expression with that of single mode fiber as equations (B.1) and (B.2).

The propagation constant and optical field distribution of the higher order guided mode, for example Lp_{11} mode, is

$$\beta_1 = \sqrt{(\frac{2\pi n_{core}}{\lambda})^2 - \frac{j_{11}^2}{r_{core}^2}} \tag{B.6}$$

$$\xi_1 = -\frac{2}{r_{core}\sqrt{\pi}} \frac{J_1\left(\frac{j_{11}r}{r_{core}}\right)}{J_0(j_{11})} \cos(\phi) \tag{B.7}$$

The optical beatlength between the fundamental Lp_{01} mode and second lowest Lp_{11} mode is

$$L_B = \frac{8\pi^2}{j_{11}^2 - j_{01}^2} \frac{r_{core}^2 n_{core}}{\lambda} \tag{B.8}$$

In the optical coupler structure, the residual fiber cores in the waist of coupler are very small and can be neglected. The light is guided by the melt cladding and air in this part. The waist usually is a multi-mode waveguide. Therefore, similar results with the multi-mode fiber case can be obtained for the AO interaction between guided optical modes in the coupler waist. The only change is n_{core} and r_{core} in

those equations are replaced by n_{waist} and r_{waist} respectively.

$$\beta_0 = \sqrt{(\frac{2\pi n_{waist}}{\lambda})^2 - \frac{j_{01}^2}{r_{waist}^2}} \tag{B.9}$$

$$\beta_1 = \sqrt{(\frac{2\pi n_{waist}}{\lambda})^2 - \frac{j_{11}^2}{r_{waist}^2}} \tag{B.10}$$

$$\xi_0 = \frac{1}{r_{waist}\sqrt{\pi}} \frac{J_0\left(\frac{j_{01}r}{r_{waist}}\right)}{J_1(j_{01})} \tag{B.11}$$

$$\xi_1 = -\frac{2}{r_{waist}\sqrt{\pi}} \frac{J_1\left(\frac{j_{11}r}{r_{waist}}\right)}{J_0(j_{11})} \cos(\phi) \tag{B.12}$$

$$L_B = \frac{8\pi^2}{j_{11}^2 - j_{01}^2} \frac{r_{waist}^2 n_{waist}}{\lambda} \tag{B.13}$$

where r_{waist} is the radius of the coupler waist, n_{waist} is the refractive index of the coupler waist.

APPENDIX C

Tuning of Single-stage AF-AOTF

By substituting equations (B.1) to (B.13) and (A.12) into (2.3) and (2.4), the phase mismatch coefficient δ and AO coupling efficient C for most AO coupling processes. From these results, several basic and important properties of AF-AOTF can be derived.

Firstly, the AO coupling only happens between the fundamental mode and some antisymmetric optical modes. It is because the field distribution of fundamental mode in the cross-section of fiber is circle symmetric while the refractive index modulation Δn is antisymmetric. If the other participant optical mode distribution is also symmetric, the integration of the refractive index variation and participant optical mode fields in (2.4) will be zero, which means no mode coupling at all.

Secondly, the AO coupling is in positive proportional with the acoustic amplitude u_0 with almost constant ratio. For the AF-AOTF fabricated from multi-mode fiber, the value of C for the mode coupling between Lp_{01} and Lp_{11} can be approximately evaluated as follows[56]:

$$C = 8\sqrt{2}\pi^2 \frac{j_{01} j_{11}}{(j_{11}^2 - j_{01}^2)^2} \frac{n_{core}(1+\chi)}{C_{ext}} \frac{f}{\lambda} u_0 \tag{C.1}$$

For AO interaction in coupler, the AO coupling coefficient is the same with (C.1) except replacing n_{core} with n_{waist}. in the optical bandwidth for communication, the dependence of C on optical wavelength $\frac{\partial C}{\partial \lambda}$ is very weak, less than 1/1000000 per nanometer. The required acoustic frequency used for AF-AOTF is in the range of several or tens of megahertz. When the optical transmission is tuned in the range of tens nanometers, the acoustic frequency variation is tens of kilohertz. The acoustic frequency variation is quite limit compared with its operation value. Thus, the primary control parameter for C is the acoustic amplitude. In the ordinary optical

wavelength bandwidth for communication, the AO coupling coefficient can be taken as in positive proportion to the acoustic amplitude.

For an AF-AOTF fabricated from single mode fiber, the AO coupling coefficient C for the mode coupling between the cladding mode Lp_{11}^{cl} and fundamental mode is

$$\begin{aligned} C &= \frac{\pi}{\lambda}\int_A \xi_0 \triangle n \xi_1 r dr d\phi \\ &= -\frac{8\pi^2 n_0(1+\chi)}{\lambda r_{core} r_{clad} \Lambda^2}\int_A \\ &\quad \frac{J_0\left(\frac{j_{01}r}{r_{core}}\right) J_1\left(\frac{j_{11}r}{r_{clad}}\right)}{J_1(j_{01})J_0(j_{11})} \sin(\phi)\cos(\phi) r^2 dr d\phi u_0 \\ &= K(f,\lambda)u_0 \end{aligned} \tag{C.2}$$

where n_0 is the initial refractive index profile in the cross-section of the single mode fiber without micro-bending. Above integration usually is carried out by using numerical method.

Hence, the acoustic wave amplitude modulation is proportional to the power of the driving RF signal. As a result, electronic modulation the RF driving signal power is the common method to control the isolation of AF-AOTF.

An example that the optical isolation of AF-AOTF modulation by change the applied RF signal power is shown in Fig.1. In this experiment, the AF-AOTF is fabricated from SMF-28 single mode fiber with the AO coupling length of $60cm$. The applied RF signal voltage varies form $80mv$ to $160mv$.

The center wavelength of the filter can be simply tuned to any optical wavelength by modulating the applied RF signal frequency. For certain desired operating centerwavelength λ_c, the required RF signal frequencies are different for mode coupling between different optical guide modes or cladding modes. However, all of them can be determined by solving the phase matching condition (2.5). For example, considering the mode coupling between Lp_{01} and Lp_{11}^{cl} in a single mode fiber. For sake

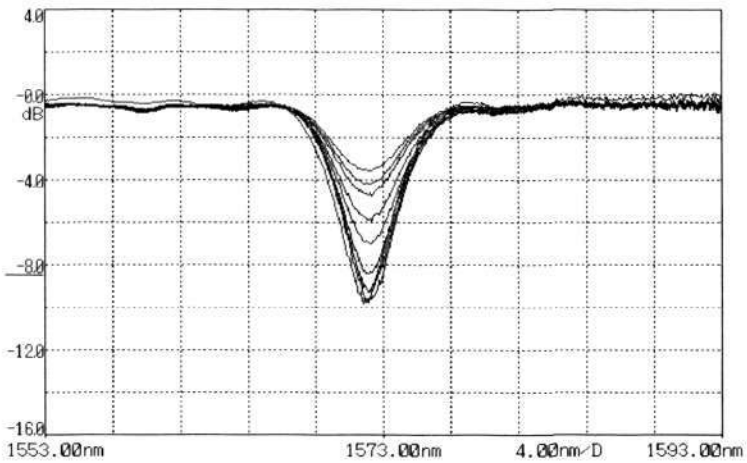

Figure 1: The effect of the applied electric power on the transmission of AF-AOTF.

of simplicity, we assume the strain in the fiber is zero. Then, to generate a notch transmission with center wavelength λ, the required acoustic frequency is

$$f = \frac{C_{ext}\left(\sqrt{(\frac{2\pi n_0}{\lambda_c})^2 - \frac{j_{01}^2}{r_{core}^2}} - \sqrt{(\frac{2\pi n_1}{\lambda_c})^2 - \frac{j_{1i}^2}{r_{clad}^2}}\right)^2 r_{clad}}{4\pi} \tag{C.3}$$

Similarly, for the mode coupling between the fundamental mode and the Lp_{11} mode in multi-mode fiber, the required acoustic frequency is

$$f = \frac{C_{ext}\lambda_c^2(j_{1i}^2 - j_{01}^2)^2}{64\pi^3 r_{waist}^3 n_0^2} \tag{C.4}$$

For the same case in coupler waist, the required acoustic frequency is

$$f = \frac{C_{ext}\lambda_c^2(j_{1i}^2 - j_{01}^2)^2 r_{clad}}{64\pi^3 r_{core}^4 n_0^2} \tag{C.5}$$

Fig.2 shows an example that the notch centerwavelength ($Lp_{01} \rightleftarrows Lp_{11}^d$) changes with the variation of the driving RF signal frequency in the range from 2.23MHz to 2.095MHz in experiment. The phenomenon that notch profile varies with the

wavelength is attributed to the nonlinear characteristics of the PZT that is used to couple acoustic wave into the fiber. The natural resonance of the PZT and the acoustic resonance between the horn and the fiber limit the available frequency tuning range of the system. The former can be solved by using high performance piezoelectric material, while the later by using a horn made of some material that has the same acoustic impedance as the fiber such as glass.

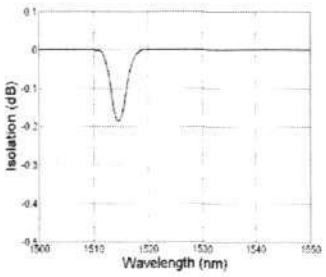

2.1: f=2.23MHz.

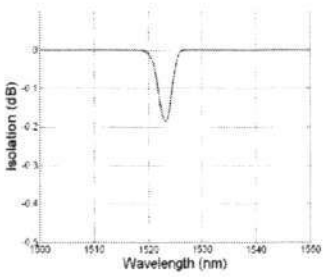

2.2: f=2.185MHz.

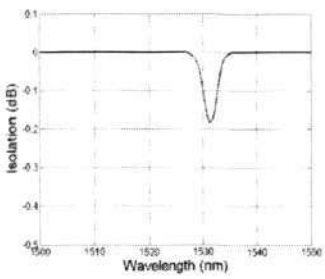

2.3: f=2.14MHz.

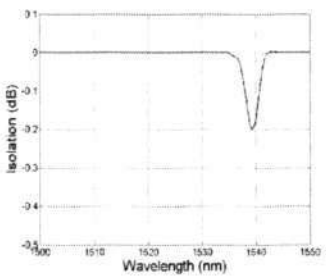

2.4: f=2.095MHz.

Figure 2: Transmission spectra of AF-AOTFs with the RF signal frequency vary from 2.23MHz to 2.095MHz.

Chemical fiber cladding etching is a common technical process used in single mode AF-AOTF manufacturing. The variation in the fiber cladding diameter will result in three primary effects on the characteristics of AF-AOTF.

Firstly, it will affect the slope of mode beatlength with respect to optical wavelength $\frac{\partial L_B}{\partial \lambda}$. It will result in increment on the bandwidth of the transmission of AF-AOTF, either notch or peak. This property can be used to realize ultra-broad optical tunable

filter [75].

Secondly, the relationship between the center operation wavelength and driving RF frequency will be shifted. Fig.3 shows the relationships between the notch centerwavelength with respect to the applied acoustic wave frequency for AF-AOTFs fabricated from different cladding diameter. Strongly etching the cladding of single mode fiber may change the sign of frequency-centerwavelength relation. For example, in the AF-AOTF made from standard single mode fiber such as SMF-28 fiber without etching, increasing the driving RF signal frequency shifts the notch centerwavelength to smaller wavelength. If the cladding diameter of this fiber is reduced below about $20\mu m$ by chemical etching, increasing the driving RF signal frequency shifts the notch centerwavelength to larger wavelength. This is because the monotonicity of optical mode beatlength with respect to optical wavelength have been changed by cladding etching.

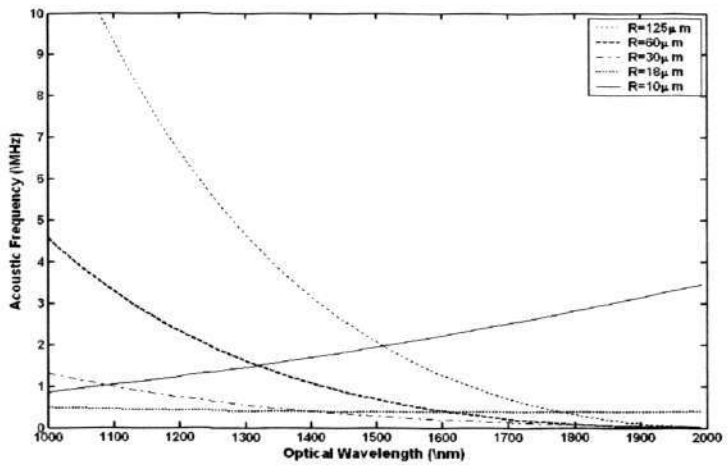

Figure 3: Relationships between the optical centerwavelength and applied RF signal frequency for the mode coupling between fundamental mode and Lp_{11}^{cl} cladding mode in the single mode fibers with different cladding diameters R .

Finally, etching fiber cladding can enhance the AO coupling efficiency. To achieve full rejection of the light at the resonance optical wavelength, the AO coupling

coefficient C must have a value large enough to satisfy the condition $CL = \pi/2 + k\pi$, where k is integer. In multi-mode fiber structure, all participant optical modes of AO interaction are guided in the same area. The field overlap of these modes are strong and the implementation of large C is not difficult. For the AO coupling in single mode fiber, the fundamental mode is distributed in the small core area while the cladding mode is distributed in the much larger cladding area. As a result, the utilizing efficiency of acoustic power K in equation (C.2) is very small. To obtain high AO coupling coefficient, large acoustic amplitude u_0, which means high RF signal power, is required. However, the acoustic amplitude u_0 coupled into the fiber is limit due to the saturation effect of acoustic transducer and acoustic attenuation in the fiber and horn. The weak AO coupling efficiency greatly limit the application of single mode fiber based AF-AOTF. An optional choice to enhance the AO coupling efficiency is to reduce fiber cladding diameter by hydrofluoric acid etching. Reducing r_{clad} will compress the optical field cladding mode and result in increasing of K in (C.2) [76, 81].

The side-effect of AO coupling enhancement by cladding etching method is it will make the system fragile. Furthermore, the bandwidth increment by using this method is not desired in some applications. Therefore, weak coupling efficiency is still a not completely solved issue for single-mode based AF-AOTF.

Author's publication

(1) Hao Li, Ying Zhang, Changyun Wen and Yeng Chai Soh, "Design of Tunable Composite Spectra using All-fiber Acousto-optical Filters Subject to Strain Control", J. Lightwave Technol. Vol. 24, No 4, April, 2006, In Press.

(2) Hao Li, Ying Zhang, Changyun Wen and Yeng Chai Soh, "Tunable Stopband Filter by Using Differential Strains in All-fiber Acousto-optical Filter", IEEE Photon. Lett. Vol. 17, No. 3, pp.609-611 March 2005.

(3) Hao Li, Ying Zhang, Changyun Wen, Yeng Chai Soh, "Strain Effect on the Tunability of Cascading All-Fiber Acoustic-optical Tunable Filters", Optics Communications, Vol. 247, No. 1-3, pp. 65-84, 2005.

(4) Hao Li, Ying Zhang, Tong Liu, Changyun Wen and Yeng Chai Soh, "All-fiber acousto-optical tunable filter with loop structure", Optical Engineering, Vol. 42, No. 12 pp. 3409-3410 2003.

(5) Hao Li, Ying Zhang, Changyun Wen, Yeng Chai Soh, "Enhance performance of acoustic-optical tunable filters by using spectral servo", Proceedings of the SPIE, Volume 5181, pp. 56-61 (2003). Wave Optics and Photonic Devices for Optical Information Processing II. Edited by Ambs, Pierre; Beyette, Fred R., Jr.

(6) Hao Li, Hong Bo Bi, Ying Zhang, Changyun Wen and Yeng Chai Soh, "EDFA spectrum equalization by using a genetic algorithm", Proceedings of the 5th EPTC 10-12 December 2003, pp 638-640, 2003.

(7) Hao Li, Ying Zhang, Changyun Wen and Yeng Chai Soh, "Relaxation oscillation suppression of all-optical gain clamped EDFA using dynamic compensating laser control using AF-AOTF", 2004, (Submitted to Photonics Technology Letters).

Bibliography

[1] P. Bonenfant and A. Rodriguez-Moral, "Optical data networking," *IEEE Communications Magazine*, vol. 38, no. 3, pp. 63–70, 2000.

[2] M. I. Irshid, "A fully transparent fiber-optic ring architecture for WDM networks," *J. Lightwave Technol.*, vol. 10, no. 1, pp. 101–108, 1992.

[3] J. Wang and B. Chen, "Dynamic wavelength assignment for multicast in all-optical WDM networks to maximize the network capacity," *IEEE Journal on Selected Areas in Communications*, vol. 21, no. 8, pp. 1274–1284, 2003.

[4] M. W. Chbat, E. Grard, L. Berthelon, A. Jourdan, and P. A. P. et al., "Toward wide-scale all-optical transparent networking: The ACTS optical pan-european network (open) project," *IEEE Journal on Selected Areas in Communications*, vol. 16, no. 7, pp. 1226–1244, 1998.

[5] P. Leisching, H. Bock, A. Richter, D. Stoll, and G. Fischer, "Reconfigurable all-optical networking at terabit transmission rates," *Conference on Optical Fiber Communication, Technical Digest Series*, vol. 1, no. 1, pp. 240–242, 2000.

[6] A. Kocyigit, D. Gokisik, and S. Bilgen, "All-optical networking," *Turk. J. Electr. Eng. Comput. Sci.*, vol. 9, no. 2, pp. 69–121, 2001.

[7] C. A. Brackett, "Dense wavelength division multiplexing networks: Principles and Applications," *IEEE Journal on Selected Areas in Communications*, vol. 8, no. 6, pp. 948–964, 1990.

[8] L. N. Binh and H. C. Chong, "Dense wavelength division multiplexing packet switching networks: a review," *Journal of Electrical and Electronics Engineering, Australia*, vol. 14, no. 3, pp. 178–195, 1994.

[9] A. Mokhtar and M. Azizoglu, "Dynamic route selection and wavelength assignment in all-optical networks," *Conference Proceedings - Lasers and Electro-Optics Society Annual Meeting-LEOS*, vol. 1, pp. 220–221, 1995.

[10] I. Saeki, S. Nishi, and K. Murakami, "All-optical code division multiplexing switching network based on self-routing principle," *IEICE Transactions on Electronics*, vol. E82-C, no. 2, pp. 187–193, 1999.

[11] N. Ghani, S. Dixit, and T.-S. Wang, "On IP over WDM integration," *IEEE Communications Magazine*, vol. 38, no. 3, pp. 72–84, 2000.

[12] M. Misono, N. Shimosaka, T. Shiozawa, M. Murakami, and M. Fujiwara, "Practical demonstration of WD/TD optical network for broadcasting station," *European Conference on Optical Communication, ECOC*, vol. Tu.B.1.6, pp. 247–250, 1995.

[13] T. Numai, "1.5-μ m two-section Fabry-Perot wavelength tunable optical filter," *J. Lightwave Technol.*, vol. 10, no. 11, pp. 1590–1596, 1992.

[14] B. Ortega, J. Capmany, D. Pastor, and R. I. Laming, "Experimental demonstration of an ultraselective and tunable optical bandpass filter using a fiber grating and a Fabry-Perot," *Electron. Lett.*, vol. 33, no. 8, pp. 669–671, 1997.

[15] B. Ortega, J. Capmany, and J. L. Cruz, "Wavelength division multiplexing all-fiber hybrid devices based on Fabry-Perot's and gratings," *J. Lightwave Technol.*, vol. 17, no. 7, pp. 1241–1247, 1999.

[16] M. Stefan and A. Markus-Christian, "Tuning performance and spectral selectivity of widely tunable vertical mach-zehnder lasers," *IEEE Journal of Quantum Electronics*, vol. 36, no. 2, pp. 192–197, 2000.

[17] Arizona, "All-optical mach-zehnder-interferometer-based demultiplexer - a computer simulation study," *IEEE Photon. Technol. Lett.*, vol. 15, no. 1, pp. 78–80, 2003.

[18] M. Abe, Y. Hibino, T. Tanaka, M. Itoh, A. Himeno, and Y. Ohmori, "Mach-zehnder interferometer and arrayed-waveguide-grating integrated multi/demultiplexer with photosensitive wavelength tuning," *Electron. Lett.*, vol. 37, no. 6, pp. 376–377, 2001.

[19] L. Xu, B. C. Wang, V. Baby, I. Glesk, and P. R. Prucnal, "All-optical data format conversion between RZ and NRZ based on a mach-zehnder interferometric wavelength converter," *IEEE Photon. Technol. Lett.*, vol. 15, no. 2, pp. 308–310, 2003.

[20] X. Z. Lin, Y. zhang, H. L. An, and H. D. Liu, "Electrically tunable single mode fiber bragg grating reflective filter," *Electron. Lett.*, vol. 30, no. 11, pp. 887–888, 1994.

[21] K. O. Hill, F. Bilodeau, B. Malo, S. Theriault, D. C. Johnson, and J. Albert, "Chirped in fiber bragg gratings for compensation of fiber dispersion," *Opt. Lett.*, vol. 19, no. 17, pp. 1314–1316, 1994.

[22] C. R. Giles, "Lightwave applications of fiber bragg gratings," *J. Lightwave Technol.*, vol. 15, no. 8, pp. 1391–1404, 1997.

[23] A. Iocco, H. G. Limberger, and R. P. Salathe, "Bragg grating fast tunable filter," *Electron. Lett.*, vol. 33, no. 25, pp. 2147–2148, 1997.

[24] Y. Li and R. E. Joshua, "FBG-based widely tunable multi-channel chromatic dispersion compensation for DWDM communications systems," *Proceedings of SPIE - The International Society for Optical Engineering*, vol. 4653, pp. 1–10, 2002.

[25] I. C. Chang, "Collinear beam acousto-optic tunable filters," *Electron. Lett.*, vol. 28, no. 13, pp. 1255–1256, 1992.

[26] A. Kar-Roy and C. S. Tsai, "Low-sidelobe weighted-coupled integrated acoustooptic tunable filter using focused surface acoustic waves," *IEEE Photon. Technol. Lett.*, vol. 4, no. 10, pp. 1132–1135, 1992.

[27] C. S. Tsai and Z. Y. Cheng, "Baseband integrated acousto-optic frequency shifter/modulator module for fiber optic at 1.3μm," *IEEE Transactions on Ultrasonics, Ferroelectrics and Frequency Control*, vol. 40, no. 4, pp. 407–410, 1993.

[28] I. Hinkow, V. Hinkov, and E. Wagner, "Low power integrated acousto-optical tunable filters in first telecommunication window," *Electron. Lett.*, vol. 30, no. 22, pp. 1884–1885, 1994.

[29] J. L. Jackel, J. E. Baran, A. Alessandro, and D. A. Smith, "A passband-flattened acousto-optic filter," *IEEE Photon. Technol. Lett.*, vol. 7, no. 3, pp. 318–320, 1995.

[30] L. Petti, L. Sirleto, P. Mormile, G. C. Righini, and G. Abbate, "Fast integrated electro-optical switch and beam deflector based on nematic liquid crystal waveguides," *Fiber and Integrated Optics*, vol. 21, no. 6, pp. 435–449, 2002.

[31] H. Ren, L. Liu, Z. Song, J. Zhang, and D. Liu, "Single LiNbO3 slab integrated electro-optic switch," *Proceedings of SPIE - The International Society for Optical Engineering*, vol. 5201, pp. 180–189, 2003.

[32] H. Chen, T. Huang, W. Shen, H. Li, and P. Gu, "Tunable optical filter based on liquid crystal Fabry-Perot etalon," *Proceedings of SPIE - The International Society for Optical Engineering, APOC 2003*, vol. 5280, pp. 408–412, 2003.

[33] E. Fluck, F. Horst, B. J. Offrein, R. Germann, H. W. M. Salemink, and G. L. Bona, "Compact versatile thermooptical space switch based on beam steering by a waveguide array," *IEEE Photon. Technol. Lett.*, vol. 11, no. 11, pp. 1399–1401, 1999.

[34] H. Ishii, M. Kohtoku, and Y. Yoshikuni, "Semiconductor arrayed-waveguide-grating (AWG) and its applications," *Pacific Rim Conference on Lasers and Electro-Optics, CLEO - Technical Digest*, vol. 1, no. 1, pp. I262–I263, 2001.

[35] M. Eric, "Optical MEMS and MOEMS for telecommunications," *Proceedings of SPIE - The International Society for Optical Engineering*, vol. 4945, pp. 1–8, 2002.

[36] L. Sirleto, G. C. Righini, L. Ciaccheri, M. A. Rishand, and F. Simoni, "Thermo-optical effects and fiber optic sensing device based on polymer dispersed liquid crystals," *Proceedings of SPIE - The International Society for Optical Engineering*, vol. 4277, pp. 403–410, 2001.

[37] S. Toyoda, N. Ooba, T. Kitoh, T. Kurihara, and T. Maruno, "Thermo-optic switch and wavelength tunable filter using polymer waveguides," *Proceedings of SPIE - The International Society for Optical Engineering*, vol. 4532, pp. 62–72, 2001.

[38] T. T. Larsen, J. Broeng, D. S. Hermann, and A. Bjarklev, "Thermo-optic switching in liquid crystal infiltrated photonic bandgap fibres," *Electron. Lett.*, vol. 39, no. 24, pp. 1719–1720, 2003.

[39] Y. H. Chew, T. T. Tjhung, and F. V. C. Mendis, "Performance of single- and double-ring resonators using 3x3 optical fiber coupler," *J. Lightwave Technol.*, vol. 11, no. 12, pp. 1998–2008, 1993.

[40] J. Zhang and J. W. Y. Lit, "All-fiber compound ring resonator with a ring filter," *J. Lightwave Technol.*, vol. 12, no. 7, pp. 1256–1262, 1994.

[41] F. Schliep, D. Garus, and R. Hereth, "Improved method for automatic evaluation of parameters of single-mode fiber-optic ring resonators," *IEEE Photon. Technol. Lett.*, vol. 8, no. 1, pp. 107–109, 1996.

[42] C. V. zquez, S. Vargas, J. M. S. Pena, and P. Corredera, "Tunable optical filters using compound ring resonators for dwdm," *IEEE Photon. Technol. Lett.*, vol. 15, no. 8, pp. 1085–1087, 2003.

[43] L. G. Kazovsky, M. Stern, S. G. Menocal, and C. Zah, "DBR active optical filters: Transfer function and noise characteristics," *J. Lightwave Technol.*, vol. 8, no. 10, pp. 1441–1451, 1990.

[44] D. Sadot and E. Boimovich, "Tunable optical filter for dense WDM networks," *IEEE Communications Magazine*, vol. 36, no. 12, pp. 50–55, 1998.

[45] W. I. Way, D. A. S. J. J. Johnson, and H. Izadpanah, "A self-routing WDM high-capacity SONET ring network," *IEEE Photon. Technol. Lett.*, vol. 4, no. 4, pp. 402–405, 1992.

[46] K. W. Cheung, "Acoustooptic tunable filter in narrowband WDM networks: System issues and network applications," *IEEE J. Select. Areas. Commun.*, vol. 8, no. 6, pp. 1015–1025, 1990.

[47] D. A. Smith, J. E. Baran, J. J. Johnson, and K. W. Cheung, "Integrated optic acoustically tunable filter for WDM networks," *IEEE J. Select. Areas. Commun.*, vol. 8, no. 6, pp. 1151–1159, 1990.

[48] M. Fukutoku, K. Oda, and H. Toba, "Wavelength division multiplexing add/drop multiplexer employing a novel polarization independent acousto-optic tunable filter," *Electron. Lett.*, vol. 29, no. 10, pp. 905–907, 1993.

[49] E. Tony and S. K. Chaudhuri, "Acousto-optic filters," *IEEE Potentials*, vol. 13, no. 4, pp. 19–22, 1994.

[50] C. N. Pannell, B. F. Wacogne, and I. Abdulhalim, "In-fiber and fiber-compatible acoustooptic components," *J. Lightwave Technol.*, vol. 13, no. 7, pp. 1429–1434, 1995.

[51] H. F. Taylor, "Bending effects in optical fibers," *J. Lightwave Technol.*, vol. 1,LT-2, no. 5, pp. 617–628, 1984.

[52] K. Nosu, H. F. Taylor, S. C. Rashleigh, and J. F. Weller, "Acousto-optic phase modulator for single-mode fibers," *Electron. Lett.*, vol. 19, no. 16, pp. 605–607, 1983.

[53] K. Nosu, S. C. Rashleigh, H. F. Taylor, and J. F. Weller, "Acousto-optic frequency shifter for single-mode fibers," *Electron. Lett.*, vol. 19, no. 20, pp. 816–818, 1983.

[54] W. P. Risk, R. C. Youngquist, G. S. Kino, and H. J. Shaw, "Acoustooptic frequency shifting in birefringent fiber," *Opt. Lett.*, vol. 9, no. 7, pp. 309–311, 1984.

[55] B. Y. Kim, J. N. Blake, H. E. Engan, and H. J. Shaw, "All-fiber acoustooptic frequency shifter," *Opt. Lett.*, vol. 11, no. 6, pp. 389–391, 1986.

[56] T. A. Birks, P. S. J. Russell, and D. O. Culverhouse, "The acousto-optic effect in single-mode fiber tapers and couplers," *J. Lightwave Technol.*, vol. 14, no. 11, pp. 2519–2529, 1996.

[57] S. H. Yun, S. Hyun, I. K. Kwang, and B. Y. Kim, "All-fiber tunable filter and laser based on two-mode fiber," *Opt. Lett.*, vol. 21, no. 1, pp. 27–29, 1996.

[58] S. H. Yun, S. Hyun, I. K. Kwang, and B. Y. Kim, "All-fiber acousto-optic tunable notch filter with electronically controllable spectral profile," *Opt. Lett.*, vol. 22, no. 19, pp. 1476–1478, 1997.

[59] H. S. Park, K. Y. Song, S. H. Yun, and B. Y. Kim, "All-fiber wavelength-tunable acoustooptic switches based on intermodal coupling in fibers," *J. Lightwave Technol.*, vol. 20, no. 10, pp. 1864–1868, 2002.

[60] T. A. Birks, D. O. Culverhouse, S. G. Farwell, and P. S. J. Russell, "All-fiber polarizer based on a null taper coupler," *Opt. Lett.*, vol. 20, no. 12, pp. 1371–1373, 1995.

[61] T. E. Dimmick, D. A.Satorius, and G. L. Burdge, "All-fiber acousto-optic tunable bandpass filter," *Conference on optical fiber communication, technical digest series*, vol. 54, no. 3, pp. WJ3/1–WJ3/3, 2001.

[62] S. H. Yun, B. K. Kim, H. J. Jeong, and B. Y. Kim, "Suppression of polarization dependence in a two-mode fiber acousto-optic device," *Opt. Lett.*, vol. 21, no. 12, pp. 908–910, 1996.

[63] M. Misono, N. Henmi, T. Hosoi, and M. Fujiwara, "High-speed wavelength switching and stabilization of an acoustooptic tunable filter for WDM network in broadcasting stations," *IEEE Photon. Technol. Lett.*, vol. 8, no. 4, pp. 572–574, 1996.

[64] M. Jeon, H. K. Lee, K. H. Kim, E. Lee, S. H. Yun, B. Y. Kim, and Y. W. Koh, "An electronically wavelength-tunable mode-locked fiber laser using an all-fiber acoustooptic tunable filter," *IEEE Photon. Technol. Lett.*, vol. 8, no. 12, pp. 1618–1620, 1996.

[65] A. S. Kewitsch, G. A. Rakuljic, P. A. Willems, and A. Yariv, "All-fiber zero-insertion-loss add-drop filter for wavelength-division multiplexing," *Opt. Lett.*, vol. 23, no. 2, pp. 106–108, 1998.

[66] S. H. Yun, B. W. Lee, H. K. Kim, and B. Y. Kim, "Dynamic erbium-doped fiber amplifier based on active gain flattening with fiber acoustooptic tunable filters," *IEEE Photon. Technol. Lett.*, vol. 11, no. 10, pp. 1229–1231, 1999.

[67] J. L. Jackel, M. S. Goodman, J. E. Baran, and W. J. Tomlinson, "Acousto-optic tunable filters (AOTF's) for multiwavelength optical cross-connects: Crosstalk considerations," *J. Lightwave Technol.*, vol. 14, no. 6, pp. 1056–1066, 1996.

[68] W. F. Liu, P. S. J. Russell, and L. Dong, "100% efficient narrow-band acoustooptic tunable reflector using fiber bragg grating," *J. Lightwave Technol.*, vol. 16, no. 11, pp. 2006–2009, 1998.

[69] Q. Li, X. Liu, J. Peng, B. Zhou, and H. Lee, "Demonstration of a fast all-fiber acousto-optic tunable filter based variable optical attenuator," *Conference Proceedings - Lasers and Electro-Optics Society Annual Meeting-LEOS*, vol. 2, no. 2, pp. 845–846, 2001.

[70] Q. Li, A. Au, C. Lin, I. Tomov, and H. Lee, "An all-fiber WDM channel monitor based on acousto-optic tunable filter with built-in on-fiber detector,"

Conference on Optical Fiber Communication, Technical Digest Series, vol. 86, pp. 574–575, 2003.

[71] Q. Li, A. A. Au, C. H. Lin, E. R. Lyons, C. S. Tsai, and H. P. Lee, "Demonstration of an all-fiber acousto-optic tunable filter based spectrometer," *Conference Proceedings - Lasers and Electro-Optics Society Annual Meeting-LEOS*, vol. 4989, pp. 155–160, 2003.

[72] D. O. Culverhouse, S. H. Yun, D. J. Richardson, T. A. Birks, S. G. Farwell, and P. S. J. Russell, "Low-loss all-fiber acousto-optic tunable filter," *Opt. Lett.*, vol. 22, no. 2, pp. 96–98, 1997.

[73] K. Y. Song, I. K. Hwang, S. H. Yun, and B. Y. Kim, "High performance fused-type mode-selective coupler using elliptical core two-mode fiber at 1550 nm," *IEEE Photon. Technol. Lett.*, vol. 14, no. 4, pp. 501–503, 2002.

[74] H. S. Park, S. H. Yun, I. K. Hwang, S. B. Lee, and B. Y. Kim, "All-fiber add-drop wavelength-division multiplexer based on intermodal coupling," *IEEE Photon. Technol. Lett.*, vol. 13, no. 5, pp. 460–462, 2001.

[75] T. Jin, Q. Li, J. Zhao, K. Cheng, and X. Liu, "Ultra-broad-band AOTF based on cladding etched single-mode fiber," *IEEE Photon. Tech. Lett.*, vol. 14, no. 8, pp. 1133–1135, 2002.

[76] T. A. Birks, S. G. Farwell, P. S. J. Russell, and C. N. Pannell, "Four-port fiber frequency shifter with a null taper coupler," *Opt. Lett.*, vol. 19, no. 23, pp. 1964–1966, 1994.

[77] A. Diez, T. Birks, W. Reeves, B. Mangan, and P. Russell, "Excitation of cladding modes in photonic crystal fibers by flexural acoustic waves," *Opt. Lett.*, vol. 25, no. 20, pp. 1499–1501, 2000.

[78] Q. Li, X. Liu, and H. P. Lee, "Demonstration of narrow-band acoustooptic tunable filters on dispersion-enhanced single-mode fibers," *IEEE Photon. Tech. Lett.*, vol. 14, no. 11, pp. 1551–1553, 2002.

[79] S. S. Lee, H. S. Kim, I. K. Hwang, and S. H. Yun, "Highly-efficient broadband acoustic transducer for all-fibre acousto-optic devices," *Electron. Lett.*, vol. 39, no. 18, pp. 1309–1310, 2003.

[80] C. Alegria, R. Feced, M. N. Zervas, R. I. Laming, and S. G. Farwell, "Acousto-optic filters based on multi-tapered fiber structures," *Electron. Lett.*, vol. 35, no. 12, pp. 1006–1007, 1999.

[81] Q. Li, X. Liu, J. Peng, B. Zhou, E.R.Lyons, and H.P.Lee, "Highly efficient acoustooptic tunable filter based on cladding etched single-mode fiber," *IEEE Photon. Technol. Lett.*, vol. 14, no. 3, pp. 337–339, 2002.

[82] C. Alegria, R. Feced, M. N. Zervas, R. I. Laming, and S. G. Farwell, "Low power acousto-optic device based on a tapered singe-mode fiber," *IEEE Photon. Technol. Lett.*, vol. 6, no. 6, pp. 725–727, 1994.

[83] A. Diez, G. Kakarantzas, T. A. Birks, and P. S. J. Russell, "High strain-induced wavelength tunability in tapered fibre acousto-optic filters," *Electron. Lett.*, vol. 36, no. 14, pp. 1187–1188, 2000.

[84] T. Kanda, T. Morita, M. K. Kurosawa, and T. Higuchi, "A flat type touch probe sensor using pzt thin film vibrator," *Sens.Actuators A*, vol. 83, no. 1, pp. 67–75, 2000.

[85] Q. Li, X. Liu, T. Li, and T. Jin, "Influence of acoustic wave attenuation on the properties of fiber aotf," *Chinese J. Lasers*, vol. 28, no. 5, pp. 463–466, 2001.

[86] J. P. Goure and I. Verrier, *Optical Fiber Devices*. UK: Bristol, 2002.

[87] J. N. Blake, B. Y. Kim, H. E. Engan, and H. J. Shaw, "Analysis of intermodal coupling in a two-mode fiber with periodic microbends," *Opt. Lett.*, vol. 12, no. 4, pp. 281–283, 1987.

[88] R. Giles and T. Li, "Optical amplifiers transform long-distance lightwave telecommunications," *Proceedings of the IEEE.*, vol. 84, no. 6, pp. 870–883, 1996.

[89] A. R. Chraplyvy, J. M. Delavaux, R. M. Derosier, G. A. F. D. A. Fishman, C. R. Giles, J. A. Nagel, and B. M. Nyman, "1420-km transmission of sixteen 2.5-gb/s channels using silica-fiber-based EDFA repeaters," *IEEE Photon. Technol. Lett.*, vol. 6, no. 11, pp. 1371–1373, 1994.

[90] A. Lindstrom, "Gain flattening drives the evolution to agile networks," *FibreSystems Europe*, pp. 21–23, April 2002.

[91] F. Kirk, H. Hongtao, and S. Wayne, "Overview of dynamic gain-flattening technologies," *Lightwave*, vol. 19, no. 3, pp. 160–169, 2002.

[92] H. S. Chung, H. B. Choi, M. S. Lee, D. Lee, N. Park, and S. J. Ahn, "Demonstration of 52-nm gain bandwidth over 2400 km (540 db loss) with gain-equalized low-noise wide-band EDFAs," *IEEE Photon. Technol. Lett.*, vol. 12, no. 3, pp. 329–331, 2000.

[93] K. Kikushima and H. Yoshinaga, "Distortion due to gain tilt of erbium-doped fiber amplifiers," *IEEE Photon. Technol. Lett.*, vol. 3, no. 10, pp. 945–947, 1991.

[94] M. Rochette, M. Guy, S. LaRochelle, J. Lauzon, and F. Trepanier, "Gain equalization of EDFA's with bragg gratings," *IEEE Photon. Technol. Lett.*, vol. 11, no. 5, 1999.

[95] S. K. Liaw, K. P. Ho, and S. Chi, "Dynamic power-equalized EDFA module based on strain tunable fiber bragg gratings," *IEEE Photon. Technol. Lett.*, vol. 11, no. 7, 1999.

[96] J. X. Cai, K. M. Feng, X. P. Chen, and A. E. Willner, "Equalization of nonuniform EDFA gain using a fiber-loop mirror," *IEEE Photon. Technol. Lett.*, vol. 9, no. 7, 1997.

[97] Y. Sun, G. Luo, J. L. Zyskind, M. A. A. M. Saleh, A. K. Srivastava, and J. W. Sulhoff, "Gain control in erbium-doped fiber amplifiers by an all-optical feedback loop," *Electron. lett.*, vol. 27, no. 7, 1991.

[98] D. H. Richards, J. L. Jackel, and M. A. Ali, "A theoretical investigation of dynamic all-optical automatic gain control in multichannel EDFA's and EDFA cascades," *IEEE Journal of Selected Topics In Quantum Electronics*, vol. 3, no. 4, 1997.

[99] L. T. Cevski, L. A. Rusch, and A. Bononi, "Gain control in EDFA's by pump compensation," *IEEE Photon. Technol. Lett.*, vol. 10, no. 9, pp. 1313–1315, 1998.

[100] H. S. Chung, H. H. Lee, J. C. Lee, M. J. Chu, and J. H. Lee, "Reduction of relaxation oscillations in optical automatic gain clamped EDFA using fast electronic feedforward," *Electron. lett.*, vol. 38, no. 5, pp. 215–217, 2002.

[101] A. K. Srivastava, J. L. Zyskind, Y. Sun, J. Ellson, G. Newsome, R. W. T. A. R. Chraplyvy, J. W. Sulhoff, T. A. Strasser, C. Wolf, and J. R. Pedrazzani, "Fast-link control protection of surviving channels in multiwavelength optical networks," *IEEE Photon. Technol. lett.*, vol. 9, no. 12, 1997.

[102] S. K. Liu, "Challenges of all-optical network evolution," *Conference Proceedings - Lasers and Electro-Optics Society Annual Meeting-LEOS*, vol. 1, pp. 182–183, 1998.

[103] W. S. Wong, H.-S. Tsai, hien Jen Chen, H. K. Lee, and M.-C. Ho, "Novel time-resolved measurement of bit-error-rate and optical-signal-to-noise-ratio degradations due to EDFA gain dynamics in a WDM network," *Optical Fiber Communictions Conference*, vol. 1, no. 1, pp. 515–516, 2002.

[104] M. I. Hayee, "EDFA power transients and their effects in high speed optical networks," *Conference Proceedings - Lasers and Electro-Optics Society Annual Meeting-LEOS*, vol. 2, 1999.

[105] M. Karsek, A. Bononi, L. A. Rusch, and M. Menif, "Gain stabilization in gain clamped EDFA cascades fed by WDM burst-mode packet traffic," *J. Lightwave Technol.*, vol. 18, no. 3, 2000.

[106] C. R. Giles, E. Dessurvire, and J. R. Simploson, "Transient gain and cross talk in erbium-doped fiber amplifier," *Opt. Lett.*, vol. 14, no. 16, pp. 880–882, 1989.

[107] Karasek, M. Menif, and A. Rush, "Output power excursions in a cascade of edfas fed by multichannel burst-mode packet traffic: Experimentation and modelling," *J. Lightwave Technol.*, vol. 19, no. 7, pp. 933–940, 2001.

[108] J. Freeman and J. Conradi, "Gain modulation response of erbium doped fiber amplifiers," *IEEE Photon. Technol. Lett.*, vol. 5, no. 2, pp. 224–226, 1993.

[109] A. K. Srivastava, Y. Sun, J. L. Zyskind, and J. W. Sulhoff, "EDFA transient response to channel loss in WDM transmission system," *IEEE Photon. Technol. Lett.*, vol. 9, no. 3, pp. 386–388, 1997.

[110] G. Luo, J. L. Zyskind, J. A. Nagel, and M. A. Ali, "Experimental and theoretical analysis of relaxation-oscillations and spectral hole burning effects in all-optical gain-clamped EDFA's for WDM networks," *J. Lightwave Technol.*, vol. 16, no. 4, 1998.

[111] G. Luo, J. L. Zyskind, Y. Sun, A. K. Srivastava, J. W. Sulhoff, C. Wolf, and M. A. Ali, "Performance degradation of all-optical gain-clamped EDFA's due to relaxation-oscillations and spectral-hole burning in amplified WDM networks," *IEEE Photon. Technol. Lett.*, vol. 9, no. 10, pp. 1346–1348, 1997.

[112] Y. Chen, L. Zhang, Z. Jiang, Q. Yu, and C. Fan, "Suppression of stimulated brillouin scattering induced by the compensating signal in all-optical gain clamped EDFA," *2000 International Conference on Communication Technologies (ICCT2000)Optical Systems and Networking*, vol. 1, no. 1, 2000.

[113] J. Chung and S. Y. Kim, "Dynamic performance of the all-optical gain-controlled EDFA cascade in multi-wavelength add/drop networks," *Electron. Lett.*, vol. 33, no. 17, pp. 1475–1477, 1997.

[114] Q. Yu and C. Fan, "Simple dynamic model of all-optical gain-clamped erbium-doped fiber amplifiers," *J. Lightwave Technol.*, vol. 17, no. 7, 1999.

[115] Y. Sun, G. Luo, J. L. Zyskind, M. A. A. M. Saleh, A. K. Srivastava, and J. W. Sulhoff, "Model for gain dynamics in erbium-doped fibre amplifiers," *Electron. lett.*, vol. 32, no. 16, 1996.

[116] C. R. Giles and E. Desurvire, "Modeling erbium-doped fiber amplifiers," *J. Lightwave Technol.*, vol. 9, no. 2, 1991.